Understanding the Impact of a Serrated Trailing Edge on the Unsteady Hydrodynamic Field

Stefan Letica[1] and W. Nathan Alexander[2]

[1]Research Aerospace Engineer, NASA Langley Research Center, Aeroacoustics Branch (Mail Stop 461), 2 North Dryden St., Building 1208, Rm. 214, Hampton, VA 23681-2199, Email: stefan.j.letica@nasa.gov

[2]Assistant Professor, Kevin T. Crofton Department of Aerospace and Ocean Engineering, Virginia Tech, Randolph Hall, Rm. 215, 460 Old Turner St., Blacksburg, VA 24061-0203, Email: alexande@vt.edu

ABSTRACT

Trailing edge noise is a common noise source in aerodynamic applications. Many prior experiments have shown that trailing edge serrations can reduce this noise, but the mechanism by which serrations reduce noise and their aerodynamic impact near the edge is not fully understood. Previous theoretical models have assumed that the turbulence convecting past a serrated trailing edge is unchanged by the presence of the serrations, but experiments have shown that this is not accurate. This work attempts to further understanding of the unsteady surface pressure fluctuations on sawtooth serrations. Experiments were performed in an anechoic wall jet wind tunnel on an undercut trailing edge with a straight and serrated edge configuration. The magnitude of unsteady surface pressure fluctuations was found to increase near the tips of the serrations for Strouhal numbers near 0.5 based on edge thickness. Spanwise coherence was increased on a single serration, while coherence across the root of adjacent serrations was similar to results across a straight trailing edge at similar spanwise separation distance.

INTRODUCTION

Trailing edge noise is produced when acoustic sources in a turbulent boundary layer are convected past a sharp trailing edge. The sharp trailing edge radiates the sound produced directly by the turbulence to the far field much more efficiently than it would in an otherwise free field environment. From the work of Curle (1955), Ffowcs Williams and Hall (1970) derived an analytical solution for the noise produced by the scattering of turbulent acoustic sources by a semi-infinite half plane with a sharp trailing edge. This method, however, requires highly resolved knowledge of the three-dimensional turbulence field, and a more practical method was desired. This was provided by Amiet (1976), who solved the scattering problem by using the surface pressure generated by the turbulent boundary layer on the plate as the input to an equation that gives the sound radiated to the far field. The turbulence is assumed to be unaffected by the presence of the trailing edge.

The most common method to reduce this noise source is through the use of trailing edge serrations. Howe (1991a) performed a theoretical study of the noise reduction produced by sinusoidal serrations showing that the edge becomes an inefficient scatterer of convected turbulent acoustic sources when it is at an angle of less than 45° to the mean flow. Like Amiet, this analysis assumed that the turbulence was unaffected by the presence of the serrations. Howe concluded that for a sinusoidal serration shape, while the total arc length along the trailing edge is increased, the effective wetted length, or the length of the edge which radiates efficiently, is reduced. From this conclusion, it was logical to assume that further reduction could be obtained by making all edges of the serrations inefficient scatterers by using a sawtooth configuration with sharp tips and roots. Howe (1991b) analyzed this configuration as well, and found that it was indeed much more effective than a sinusoidal configuration. The noise reduction was found to be heavily dependent on the serration geometry, in particular on the ratio h/λ, which is defined in Figure 1. Howe predicted that the expected noise reduction by a sawtooth trailing edge was $10\log_{10}\left(1+(4h/\lambda)^2\right)$ dB. This translates to a reduction of approximately 18 dB for $h/\lambda = 2$ and 30 dB for $h/\lambda = 8$, conditions corresponding to angles of 7.13° and 1.79° between the flow direction and edge, respectively. Additionally, Howe predicted that the sound reduction would only be effective for $\omega h/U_c \gg 1$, for turbulent eddies

smaller than the serration geometry. This leads to the conclusion that the dimensions of serrations should be at least on the order of the boundary layer thickness, δ, as this is on the order of the largest turbulent length scales in a conventional boundary layer. At lower frequencies, Howe predicted that noise would be largely unaffected by the serrations, but high frequency noise reduction would be substantial.

Oerlemans et al. (2009) published an experimental paper showing both that trailing edge noise was the dominant source of wind turbine noise for an observer near the ground and that serrations were an effective mechanism for reducing the overall noise at the considered observer location on the ground in front of the turbine. However, contrary to Howe's prediction, the modified serrated blade actually increased noise at the highest frequencies. Regardless, the overall noise level of the serrated blade was about 3 dB lower than that of the unmodified blade.

Gruber et al. (2011) performed experiments in an open-jet aeroacoustic wind tunnel on an NACA 65(12)-10 cambered airfoil with a series of 0.8 mm-thick serrated trailing edge inserts ranging from $h/\lambda = 0.167$ to 10. They observed that between 400 and 7000 Hz and with the airfoil at an angle of attack of 5°, the serrations were capable of reducing noise by up to 5 dB for an amplitude of $h = 10$ mm and up to 7 dB for an amplitude of $h = 15$ mm. The noise reduction tended to increase as λ became smaller and the serrations became sharper and narrower. Above 8 kHz, the noise was increased for all serration shapes, with a greater noise increase for wider serrations. They found that Howe's theory far overpredicted the amount of potential noise reduction and confirmed the high-frequency noise increase observed by Oerlemans et al. (2009). Nonetheless, an overall reduction in sound level was achieved. The general transition point from noise reduction to noise increase was at the δ-based Strouhal number, $St_\delta = f\delta/U_\infty \sim 1$. They theorized that the cause of the high-frequency noise increase is the rushing of flow between serrations. They confirmed this by releasing smoke on the pressure side of the airfoil and observing its convection past a straight trailing edge and a sawtooth trailing edge. Naturally, this implies that at higher angle of attack, more high-frequency noise will be produced, reducing the effectiveness of the serrations. The group also confirmed Howe's prediction that a serrated trailing edge would be ineffective if the

sawtooth amplitude was smaller than the eddies. Additionally, they observed that the reduction in noise was sensitive to both changes in h and λ, but they could not conclude that this relationship was distinct from dependence on the ratio h/λ as suggested by Howe (1991b). They concluded that the turbulence at the roots and tips of the teeth was largely uncorrelated, and that there were three conditions upon which noise reduction would be dependent: $f\delta/U_\infty < 1$, $h/\lambda \geq 0.5$, and that the serrations are sufficiently narrow as discussed in Howe (1991b).

In the dissertation of Gruber (2012), surface pressure fluctuations are presented for serrations in a one-sided flow. Remote microphone probes were installed on two adjacent serrations, with dimensions $\lambda = 9$ mm and $2h = 30$ mm. The surface pressure coherence for microphone pairs along the edge of the serrations were analyzed as well as spanwise microphone pairs on the same serration. These were compared with similarly spaced microphone pairs in proximity to a straight trailing edge. Gruber observed an increase in the coherence below a frequency dependent on the microphone pair's proximity to the tip of the serration. This was attributed to acoustic backscatter from the serration edges. An edgewise reduction of the coherence up to 15% in the frequency range for which trailing edge noise was reduced was also observed. The coherence reduction along the edge indicates that the correlation length along the edge is decreased contributing to the observed noise reduction.

Moreau and Doolan (2013) performed experiments on sawtooth trailing edge serrations, and measured velocity fluctuations with a hotwire probe in the near-trailing edge wakes. They used a flat plate with two different geometries, $h/\lambda = 5$ and 1.1. The wake measurements showed differences between the serrated geometries and the flat plate. The serrations altered the behavior of the flow field around the trailing edge quite significantly, and the observed noise reduction and increases corresponded directly with changes in the turbulent energy distribution close to the trailing edge. Their narrower serration produced increases in turbulent velocity fluctuations at mid-frequencies for which noise increases were observed. Reductions in the turbulent velocity spectra occurred at frequencies with observed noise reduction. Therefore, they concluded that modifications to the hydrodynamic field were responsible for the acoustic performance of the serrations rather than the

scattering efficiency of the edge geometry. Also, they suggested that disagreement between theory and experiment may be attributed to the assumption that the trailing edge does not modify the turbulence near the trailing edge.

Although there is evidence that serrations modify the structure of the turbulent boundary layer near the trailing edge, current analytical methods do not consider these changes. This is in part due to a lack of experimental data and understanding of these flow modifications. Impact on the surface pressure spectrum near the trailing edge is of interest, particularly since it is the source component used in many calculation procedures. To analyze these effects, a study of wall pressure fluctuations on serrations in an anechoic wall-jet tunnel was completed. In this study, surface pressure fluctuations were measured with embedded microphones on multiple serrations. The objective of this work is to evaluate the variation of the surface pressure spectrum and coherence between points on a single serration and, importantly, between adjacent serrations on an undercut step in a wall jet flow, which has not been directly evaluated previously. Results will aid in the development of methods to assess the performance of serrations by exposing changes to the wall pressure spectrum along the serrated edge. Note that accompanying noise measurements are presented in Letica (2020). For the considered separation distances and serration geometry, it was found that the spanwise coherence across a single serration was elevated at lower frequencies and that the coherence across the root produced no definitive change to the spanwise coherence. More importantly, the measured wall pressure spectra were shown to vary over the serration and were shown to increase from the base to the tip of the serration.

APPARATUS AND INSTRUMENTATION

Virginia Tech Anechoic Wall Jet Facility

All experiments were performed in the Virginia Tech anechoic wall jet wind tunnel shown in Figure 2. In this tunnel, flow exhausts out of a horizontal slit nozzle over a large aluminum plate 3048 mm long and 1524 mm wide. The nozzle measures 12.7 mm high by 1207 mm wide. Details of the design are given by Kleinfelter et al. (2019). The tunnel is designed to produce a quiet, spanwise uniform flow up to a nozzle jet velocity U_j = 70 m/s. A wall jet boundary layer

is different from a conventional boundary layer. In a wall jet flow, there are two primary regions: the inner boundary layer, which forms much like a conventional boundary layer along the plate, and a turbulent mixing layer between the stagnant air in the anechoic chamber and the top of the inner layer. Kleinfelter et al. (2019) show that the wall-jet profile is fully-developed for streamwise positions greater than 0.98 m from the nozzle exit and at all nozzle velocities. These inner and outer layers were shown by Yegna Narayan and Narasimha (1973) to be self-similar when normalized on the local maximum velocity, U_m, and half-height, $y_{1/2}$, which is the height at which the mean velocity in the outer layer is half of U_m. Using the equations of Wygnanski et al. (1992) and the constants for this facility measured by Kleinfelter et al. (2019), estimates of the local boundary layer parameters at the chosen location of the trailing edge location 1.283 m from the nozzle are presented in Table 1. δ is defined as the inner layer thickness from the wall to the height of the maximum velocity U_m. The boundary layer conditions reported in Table 1 were computed based on ambient conditions of 94.3 kPa and 295.2 K. Day to day changes in ambient conditions produced negligible changes in these parameters over the course of the experiment, and thus, they were assumed constant. The coordinate system for which all microphone locations will be defined is shown in Figure 1 where the origin is located at the spanwise center of the edge. The origin is located on the edge for the straight trailing edge and at the serration half height for the serrated configurations.

Surface Pressure Microphones

Two different types of surface pressure microphones were used in this study: Brüel and Kjær (B&K) 1/8" Type 4138 and Knowles FG-23329-P07 microphones. Type 4138 microphones have a wide dynamic range (43-168 dB) and a flat frequency response up to 140 kHz. This makes them ideal reference sensors for calibration and validation of measurements with the cheaper Knowles microphones. For all surface pressure measurements, the Bruel and Kjaer microphones were fitted with 0.5 mm pinhole caps to reduce the effects of spatial averaging. Due to the large outer diameter of the microphones and their cost, the B&K microphones were only used to measure surface pressure fluctuations on the flat plate of the wall jet for comparison with the Knowles microphones.

The Knowles FG-23329-P07 microphones were chosen for their small size, relatively flat response (up to 10 kHz), and low cost. They have a pinhole diameter of 0.8 mm and an outer diameter of 3 mm. These microphones were used for all surface pressure measurements along the straight and serrated trailing edges and were mounted flush with the surrounding surface. The microphones were wired in two groups of 10 with power and output signals arranged through a single supply box.

The Knowles and 1/8" B&K microphones were used for both power spectral density and coherence measurements, and thus needed to be calibrated for both frequency response and phase response. The phase and frequency response were determined by comparing the response of each microphone with that of a microphone with known response characteristics. The reference microphone in this case was a B&K 4138 microphone with the factory supplied grid cap. This microphone was individually calibrated prior to each measurement with a B&K 4228 pistonphone calibrator. The microphones were positioned in an anechoic chamber across from a speaker emitting white noise. The output of the white noise signal generator was measured so that the cross-spectrum with each microphone's response could be determined. Each microphone's calibration is calculated as a ratio of the cross-spectrum of its response and the white noise signal to the cross-spectrum of the reference microphone's calibrated response and white noise signal. The phase of the resultant frequency spectrum is the phase calibration and the magnitude is the frequency response. To ensure the quality of the data from the Knowles microphone was adequate, surface pressure measurements were completed on the flat plate of the wall jet at the approximate streamwise location that the trailing edge models would be located with both the B&K microphones employing the pinhole caps and a Knowles microphone. The Knowles microphone was mounted at the exact distance from the nozzle that the trailing edge would be positioned, and the two B&K microphones were mounted flush in a streamwise configuration and then in a spanwise configuration. All microphones were spaced 6.15 mm apart center to center. The tunnel was run at all nozzle exit speeds listed in Table 1, and the spectra and coherence between microphones were compared. Frequencies at which the Knowles response deviated from the B&K response were used to define the response limits of

Knowles microphones. An example of these results is shown in Figure 3.

At low jet speeds, U_j = 20 m/s, the high frequency noise floor is apparent in the spectra for both the Knowles and B&K microphones. At high speeds, U_j = 60 m/s, the Knowles microphone reached the upper limit of its dynamic range. This attenuated the low frequency response but had little effect at high frequency. The low frequency impact is more noticeable in the coherence. The observed attenuation at high frequency is attributed to the larger pinhole size of the Knowles microphones compared to the B&Ks. Thus, upper and lower limits were defined for which the data were deemed an acceptable representation of the spectra and coherence at each speed. Table 2 shows the valid frequency range for which data will be presented at each speed.

Trailing Edges

Two trailing edges were used in this study: a straight edge and serrated edge. Both take the form of an undercut step in which the trailing edge model rests atop the original wall jet plate. The top surface of the edge is located 12.7 mm above the original wall of the facility. To ensure a smooth flow transition from the wall jet to the top of the trailing edge surfaces, an aluminum ramp with a gradual curve was placed upstream of the edge. The upstream portion of this ramp was sealed to the wall jet plate using aluminum foil tape to ensure a smooth transition from the plate to the ramp. Millican (2017) used this same ramp configuration and showed that the ramp had a minimal effect on the flow speed, increasing U_m by up to 1% at the edge compared to the flat unmodified plate.

Straight Trailing Edge

The straight trailing edge used in this work is the same edge used by Millican (2017). It was designed to sit on top of the solid plate of the wall jet, creating a one-sided flow across the edge. This edge was manufactured in two pieces due to machining limitations and is milled from solid aluminum. The total span of the two pieces when assembled is 972 mm. The trailing edge itself has a thickness of 0.8 mm. All sharp corners outside of the 972 mm span were smoothed using 3D printed edge-rounding transitions. Figure 4 shows the full setup as mounted in the wall jet tunnel. Figure 5a shows the profile of the trailing edge geometry.

The Knowles microphones were mounted in a spanwise array flush with the surface of the

trailing edge 3 mm upstream of the edge. The microphones were held in place with adhesive on the underside of the edge. The microphones were distributed irregularly along the x_3 axis; this was done to construct a wavenumber filter to reject high-order spanwise wavenumbers (Letica (2020)). The spanwise locations of the surface pressure microphones across the straight trailing edge are listed in Table 3.

Serrated Trailing Edge

The serrated trailing edge was designed similarly to the straight trailing edge with the same edge height above the plate, 12.7 mm. It was also installed similarly centered across the span of the wall jet. The serrated trailing edge was fabricated by 3D printing the model in two spanwise sections each 457.2 mm in length. The serrations have a wavelength $\lambda = 1.5$ cm and an amplitude $2h = 1.5$ cm. This aspect ratio was chosen to maximize the number of surface pressure microphones that could be installed on the serrations while still remaining within the effective serration design parameter ($h/\lambda \geq 0.5$) given by Howe (1991b) and Gruber et al. (2011). This design is not optimal for noise reduction and could be improved by using current prediction methods like presented by Lyu et al. (2016), which accounts for the spanwise correlation of pressure fluctuations across the edge. This optimization is beyond the scope of the current work. For the chosen geometry, $\omega h/U_c > 1$ above 250 Hz and 400 Hz for $U_j = 40$ and 60 m/s, respectively. Thus, the expected far field noise reduction is expected at these frequencies, although the effect of the serrations at lower frequencies is still critical to assessing their overall performance and influence on the total trailing edge noise. Figure 5b shows the side profile of the serrated trailing edge.

There are a total of 60 serrations across the trailing edge, 30 on each piece. 18 microphones were mounted in the serrated edge, but only 15 microphones were found to work after installation. Only these microphones will be referred to in this work. The locations of these holes and their reference numbers are shown in Figure 6. The locations of the surface pressure microphones on the serrated edge are listed in Table 4.

Data Processing

Microphone data were sampled for 32 seconds at 65536 Hz, well above the Nyquist frequency for the presented range (20-20000 Hz). To reduce uncertainty, all microphone time series were divided into records of length $N = 8192$ and processed with 50% overlap. This gives a frequency resolution of 8 Hz for the spectral data and 511 averages per run. Hanning windows were applied to each record to reduce spectral leakage. The resultant uncertainty in the microphone data is ± 1 dB.

RESULTS

The single-point spectra of each of the individual surface pressure microphones across the straight trailing edge are shown in Figure 7. The maximum spanwise difference across the edge is approximately 3 dB within the frequency ranges defined in Table 2 for each speed. This confirms the two-dimensionality of the flow at the trailing edge location. The wall pressure spectra are increased relative to the flat plate at high frequency, as much as 7 dB for the 40 m/s case, but remain similar to the flat plate at lower frequencies. The frequency at which the spectra along the edge rise above the flat plate spectrum increases with flow velocity, approximately 180 Hz, 450 Hz, and 1000 Hz for $U_j = 20$, 40, and 60 m/s, respectively.

The coherence was observed to increase with velocity, but the limitations of the Knowles microphones shown in Table 2 severely reduced the frequency range of useful data at the highest velocity. Therefore, coherence data will only be presented at the $U_j = 40$ m/s condition. Figure 8 shows the coherence between microphone pairs for different spanwise separation distances. The coherence drops off quickly with frequency for all measured separation distances such that there is minimal spanwise coherence measured at frequencies greater than 1 kHz for separation distances greater than 3.05 mm. The coherence drops monotonically with increasing spanwise separation except for the 5.69 mm and 6.73 mm cases. The 6.73 mm distance has a coherence up to 0.1 greater than 5.69 mm below 200 Hz. The cause of this discrepancy is unknown but may be a function of small differences across the edge as different microphones were used for each separation pairing. In general, the coherence measured between the two B&K microphones on the flat plate

is approximately equal to the coherence across the trailing edge for similar separation distance.

The spanwise coherence length can be calculated as a function of frequency by fitting an exponential curve across coherence spectra from microphone pairs along the straight trailing edge. This relation is expressed in Eq. 1:

$$\gamma^2 = e^{-2|\Delta x_3|/L_{x_3}(f)} \tag{1}$$

$L_{x_3}(f)$ is the coherence length, Δx_3 is the separation distance between pairs of microphones, and γ^2 is the coherence. $L_{x_3}(f)$ was found through a least squares regression using the coherence spectra between all microphone pairs at each frequency. The results are shown in Figure 9 for U_j = 20, 40, and 60 m/s. The spanwise scale decreases with increasing frequency. Again, the valid frequency range of data at U_j = 60 m/s is limited, but for U_j = 40 m/s, the spanwise scale is shown to be smaller than the wavelength of the serrations to be applied for frequencies above 190 Hz.

Surface pressure spectra measured at streamwise locations near the base and tip of a serration are compared in Figure 10 for U_j = 60 m/s. There are five similar streamwise x_1 positions each with multiple microphones that can be used for comparison. The five groups contain microphones 1-4-9, 3-5, 10-12, 2-6-7-8, and 14-15. The streamwise trends observed in all spectra and at all jet velocities are well-represented by this comparison of the spectra measured by microphones 9 (at the tip) and 8 (near the base). The average autospectrum from the straight trailing edge is shown as well. A broadband hump appears closest to the tip, between 300 Hz and 1500 Hz. The frequency of this hump reduces with decreasing velocity but peaks near a Strouhal number of St = 0.05 based on trailing edge thickness or 0.31 based on the distance from the trailing edge to the flat plate of the wall jet at all velocities. Neither is consistent with the typical value expected for vortex shedding from blunt airfoils or backsteps. At U_j = 60 m/s, this peak is approximately 3 dB above the measurement at the base. Above 1 kHz, the spectra are both below the straight edge surface pressure spectra by as much as 3 dB before converging and rolling off at frequencies above 6.3 kHz.

These autospectra at all positions can be combined to produce contours of the magnitude of the

pressure fluctuations at specific frequencies. The surface pressure field at frequencies corresponding to characteristic streamwise hydrodynamic scales of $2h$, $3h$, $4h$, and $6h$ (1.5, 2.25, 3, 4.5 cm) are shown at 60 m/s in Figure 11. These scales were computed using the measured convection velocities $L_{x_1} = U_c/f$ and are within the frequency range described by Gruber et al. (2011) for the serrations to be effective at reducing noise. The convection velocity was determined from the cross spectrum of the streamwise flat plate measurements. Measurements at similar serration relative locations were averaged in order to reduce uncertainty further, and two-dimensional linear interpolation was used to determine the pressure at points between measurement locations. These figures show that the magnitude of the fluctuations increases over 2 dB at $L_{x_1} = 3h$ and $4h$, and just over 1 dB at $L_{x_1} = 2h$ and $6h$, from the root to the tip of the interpolated region. The trend observed here agrees with the measurements of Gruber (2012) and Chong and Vathylakis (2015), who observed this trend using remote microphone probes in a one-sided flow. However, it contrasts with the results of Avallone et al. (2018) and Ragni et al. (2019), who observed the pressure fluctuations decreasing in magnitude along serrations by about 3 dB. These experiments were performed on an NACA 0018 airfoil with two-sided flow, and used CFD and tomographic PIV to obtain their surface pressure data. The dissimilarity of these configurations and measurement methods may be responsible for the observed differences. Indeed, in a one-sided flow, a growing free shear layer will develop between the flow and still air on the other side of the serrations. For two-sided flows, the near wake is a function of the boundary layers developed on both sides of the surface. Of course, differences will also exist if there is mean loading on the serration. As observed in prior studies, this loading is responsible for the flow developing in between serrations and the resultant high frequency noise produced at the root (Oerlemans et al. (2009), Gruber et al. (2011), Ragni et al. (2019)). Additionally, Ragni et al. (2019) found that the streamwise decay of the RMS pressure fluctuations on the suction side of the serrations reduced with increasing angle of attack. These observations and differences between one-sided and two-sided flows warrant further investigation. Outside of the presented range of hydrodynamic scales, the fluctuations over the interpolated region do not vary more than the measurement uncertainty of the microphones.

The coherence across a single serration and between adjacent serrations was calculated and compared to the coherence of microphone pairs with similar separation distance along the straight trailing edge. Only 40 m/s data will be presented in the remainder of the paper as this condition produced significant coherence over the widest range within the acceptable response of the microphones. Figure 12a shows the measured coherence between microphones 14 and 15, at the center of the serration and toward the edge at the same x_1 location and separated by $\Delta x_3 = 3.40$ mm. These data are compared with the same measurements taken from the straight trailing edge for separation distances of $\Delta x_3 = 3.05$ mm and 5.69 mm. The coherence between the center and side of the serrations is up to 0.1 greater compared to the measured coherence across the straight trailing edge for frequencies below 550 Hz. Much of the displayed frequency range with measured coherence above 0.05 corresponds to streamwise hydrodynamic scales on the order of the size of the serration. For reference, at $U_j = 40$ m/s, dominant streamwise hydrodynamic scales are approximately equal to $L_{x_1} = U_c/f = 0.5h$ at 3 kHz and $5h$ at 300 Hz.

The coherence was examined for locations symmetrically across the serration centerline as well. The coherence between microphone pairs 3-5, 10-12, and 2-6 are plotted in Figure 12b, along with the coherence across the straight trailing edge. The difference between the 3.42 mm and 4.78 mm separation begins to increase above 300 Hz. The center-to-edge coherence measured near the base of the serration shown in Figure 12a is slightly greater than the similar separation distance between the microphone pair 3-5 by up to 0.1. In general, the spanwise coherence at all locations across the serration is similar to the straight trailing edge with differences increasing toward lower frequencies. The 3.42 mm coherence stays within 0.1 of the 3.05 mm straight trailing edge coherence. The 4.78 mm separation is the same as the 3.05 mm straight edge result below 300 Hz, and the 6.83 mm separation increases above the 6.73 straight edge result by up to 0.1 below 250 Hz. The large increase in coherence near the tip shown by Gruber (2012) attributed to acoustic backscatter from the edge is not observed in this case. This may be due to the relative narrowness of the serration geometry in Gruber's study, which had a serration height to wavelength ratio $h/\lambda = 1.7$ compared to 0.5 in the present work. Brooks and Hodgson (1981) suggest that

microphones be placed at least half a hydrodynamic wavelength from the edge in order for the scattered pressure to be insignificant. The microphones embedded in the serrations are within this range for all frequencies below 2 kHz and 3 kHz for U_j = 40 m/s and 60 m/s, respectively. The expected nearfield scattering effects include increases in the surface pressure spectra and coherence spectra that grow in significance with proximity to the edge. The surface pressure spectrum shown in Figure 10 does not appear to be significantly increased relative to the straight edge at the lowest measured frequencies, and the spanwise coherence does not differ between points at the base and root of the serration. Therefore, the proximity of the microphones to the additional wetted edge length along the serrations compared to the straight edge does not appear to have a significant effect on the results. Additionally, the spectral hump observed near the tip of the serration in the autospectra does not occur at frequencies aligning with the observed increase in coherence at lower frequencies. Nevertheless, even if nearfield scattering effects are significant, the relative variation in the surface pressure spectrum relative to the straight edge and across serrations can still be ascertained through direct comparison. In general, these observations suggest that predictions of serration performance may not need to consider changes to the coherence of the wall pressure fluctuations. Instead, the magnitude and inhomogeneity of the surface pressure fluctuations over the serration are more significant, since the scattered noise in the far field is directly proportional to the surface pressure spectrum at the edge. However, these results do not address the potential disruption of the serration root on the spanwise coherence.

The effect of the serration roots on the spanwise coherence between serrations is of particular interest as the influence of the mixing between serrations is still not well understood. The coherence between microphone pairs 6-7 and 1-4, corresponding to cross-root distances of 8.16 mm and 15.05 mm (the serration length scale), is compared to coherence across the straight trailing edge at separation distances of 9.40 mm and 15.09 mm in Figure 12c. Microphones 1 and 4 are located at the tip of two adjacent serrations, while microphones 6 and 7 are located on either side of the root. The root appears to have an insignificant effect on the coherence between these points distinct from the observations across a single serration. The coherence is similarly increased at

lower frequencies. The experiments of Gruber et al. (2011) show small jets channelled through the roots that were responsible for the increased high-frequency noise in serrated configurations. This increased high frequency noise was not observed in far field measurements made in the present configuration (Letica (2020)), but this may be due to a difference in experimental configuration. Gruber et al. (2011) considered a lifting airfoil with boundary layers on both the pressure and suction side, which may have promoted the formation of these jets. Note that the results presented in Figure 12c differ from those in Letica (2020) due to an error in that analysis. The coherence across the root increases toward lower frequencies similar to the observation between points on a single serration. Again, this indicates that predictions of serration performance may not need to consider changes particular to the coherence across the root at least for the separation distances considered in this study, $\Delta x_3/\lambda \geq 0.54$.

Finally, microphone pair 8-9, with a streamwise separation distance of $\Delta x_1 = 7.00$ mm, was used to examine the coherence along the centerline of the serration, Figure 12d. The result of the streamwise coherence measured on the flat plate is shown for reference. At low frequencies, below 300 Hz, the coherence along the serration is slightly lower than that of the flat plate and may be a consequence of the streamwise evolution of the near wall flow across the serration. Still, like the spanwise coherence, observed changes in the wall pressure magnitude over the serration are likely to have a greater effect on the serration performance. At higher frequencies, above 700 Hz, a modest increase is observed.

CONCLUSIONS

In this work, the unsteady surface pressure on a straight and serrated edge was examined. The surface pressure was measured by embedded microphones, which were flush with the surface in both edges. At low frequencies, the spanwise coherence across the serrated edge displayed a modest increase with a corresponding decrease in the streamwise coherence. Overall, results show that changes to the coherence for this moderately sharp serrated edge, $h/\lambda = 0.5$, for hydrodynamic scales on the order of h, even considering locations on adjacent serrations, are not as significant as changes in the spectral magnitude over the serration. The theory of Amiet (1976) shows that

trailing edge noise is proportional to the spanwise length scale. The spanwise length scale itself is a function of the spanwise coherence such that a 20% reduction in coherence amounts to only a 0.5 dB reduction in far field noise. Thus, larger reductions in coherence are necessary for significant noise reduction. The surface pressure is modified by the serrated edge with respect to the straight edge or flat plate. In particular, spectral magnitudes increased toward the tip of the serration for frequencies near a Strouhal number of 0.05 based on edge thickness.

DATA AVAILABILITY STATEMENT

Some or all data, models, or code that support the findings of this study are available from the corresponding author upon reasonable request.

ACKNOWLEDGMENTS

The authors would like to thank Drs. Matthew Szoke (Virginia Tech) and Lorna Ayton (University of Cambridge) for their collaborative discussions.

REFERENCES

Amiet, R. K. (1976). "Noise due to turbulent flow past a trailing edge." *Journal of Sound and Vibration*, 47(3), 387–393.

Avallone, F., Van Der Velden, W. C., Ragni, D., and Casalino, D. (2018). "Noise reduction mechanisms of sawtooth and combed-sawtooth trailing-edge serrations." *Journal of Fluid Mechanics*, 848, 560–591.

Brooks, T. F. and Hodgson, T. H. (1981). "Trailing edge noise prediction from measured surface pressures." *J. Sound & Vib.*, 78(1), 69–117.

Chong, T. P. and Vathylakis, A. (2015). "On the aeroacoustic and flow structures developed on a flat plate with a serrated sawtooth trailing edge." *Journal of Sound and Vibration*, 354, 65–90.

Curle, N. (1955). "The influence of solid boundaries upon aerodynamic sound." *Proceedings of the Royal Society of London. Series A. Mathematical and Physical Sciences*, 231(1187), 505–514.

Ffowcs Williams, J. E. and Hall, L. H. (1970). "Aerodynamic sound generation by turbulent flow in the vicinity of a scattering half plane." *Journal of Fluid Mechanics*, 40(4), 657–670.

Gruber, M. (2012). "Airfoil noise reduction by edge treatments." Ph.d. thesis, University of Southampton, Southampton, UK.

Gruber, M., Joseph, P. F., and Chong, T. P. (2011). "On the mechanisms of serrated airfoil trailing edge noise reduction." *17th AIAA/CEAS Aeroacoustics Conference*, AIAA 2011-2781.

Howe, M. S. (1991a). "Aerodynamic noise of a serrated trailing edge." *Journal of Fluids and Structures*, 5(1), 33–45.

Howe, M. S. (1991b). "Noise produced by a sawtooth trailing edge." *Journal of the Acoustical Society of America*, 90(1), 482–487.

Kleinfelter, A., Repasky, R., Hari, N., Letica, S., Vishwanathan, V., Organski, L., Schwaner, J., Alexander, W. N., and Devenport, W. (2019). "Development and calibration of a new anechoic wall jet wind tunnel." *AIAA Scitech 2019 Forum*, AIAA 2019-1936.

Letica, S. J. (2020). "Understanding the Impact of a Serrated Trailing Edge on the Unsteady Hydrodynamic Field." Master's thesis, Virginia Polytechnic Institute and State University, Blacksburg, VA, <https://vtechworks.lib.vt.edu/handle/10919/99965>.

Lyu, B., Azarpeyvand, M., and Sinayoko, S. (2016). "Prediction of noise from serrated trailing edges." *Journal of Fluid Mechanics*, 793, 556–588.

Millican, A. J. (2017). "Bio-Inspired Trailing Edge Noise Control: Acoustic and Flow Measurements." Master's thesis, Virginia Polytechnic Institute and State University, Blacksburg, VA, <https://vtechworks.lib.vt.edu/handle/10919/78376>.

Moreau, D. J. and Doolan, C. J. (2013). "Noise-reduction mechanism of a flat-plate serrated trailing edge." *AIAA Journal*, 51(10), 2513–2522.

Oerlemans, S., Fisher, M., Maeder, T., and Kögler, K. (2009). "Reduction of wind turbine noise using optimized airfoils and trailing-edge serrations." *AIAA Journal*, 47(6), 1470–1481.

Ragni, D., Avallone, F., van der Velden, W. C., and Casalino, D. (2019). "Measurements of near-wall pressure fluctuations for trailing-edge serrations and slits." *Experiments in Fluids*, 60(1), 1–22.

Wygnanski, I., Katz, Y., and Horev, E. (1992). "On the applicability of various scaling laws to the

turbulent wall jet." *Journal of Fluid Mechanics*, 234, 669–690.

Yegna Narayan, K. and Narasimha, R. (1973). "Parametric analysis of turbulent wall jets." *Aeronautical Quarterly*, 24(3), 207–218.

List of Tables

TABLE 1. Boundary layer parameters.

U_j (m/s)	U_m (m/s)	δ (mm)
20	6.343	16.04
40	13.25	14.42
60	20.40	13.55

TABLE 2. Validated frequency ranges of Knowles microphones.

U_j (m/s)	Autospectra	Coherence
20	$f \leq 5.5$ kHz	$f \geq 24$ Hz
40	$f \leq 16.5$ kHz	$f \geq 96$ Hz
60	$f \geq 176$ Hz	$f \geq 560$ Hz

TABLE 3. Spanwise microphone locations for the straight trailing edge.

Mic	x_3 (mm)	Mic	x_3 (mm)	Mic	x_3 (mm)	Mic	x_3 (mm)
1	304.8	5	39.40	9	-8.509	13	-50.90
2	182.8	6	23.60	10	-11.56	14	-84.91
3	109.6	7	14.20	11	-18.29	15	-141.5
4	65.71	8	8.509	12	-30.50	16	-236.0

TABLE 4. Serrated trailing edge surface pressure microphone locations.

Mic	x_1, mm	x_3, mm
1	1.26	97.45
2	-5.66	85.88
3	-2.20	84.12
4	1.31	82.40
5	-2.21	80.70
6	-5.70	79.05
7	-5.72	70.89
8	-5.75	22.42
9	1.25	22.32
10	-4.11	-20.15
11	-0.53	-23.10
12	-4.13	-24.93
13	-10.19	-29.99
14	-6.01	-67.44
15	-5.99	-70.86

List of Figures

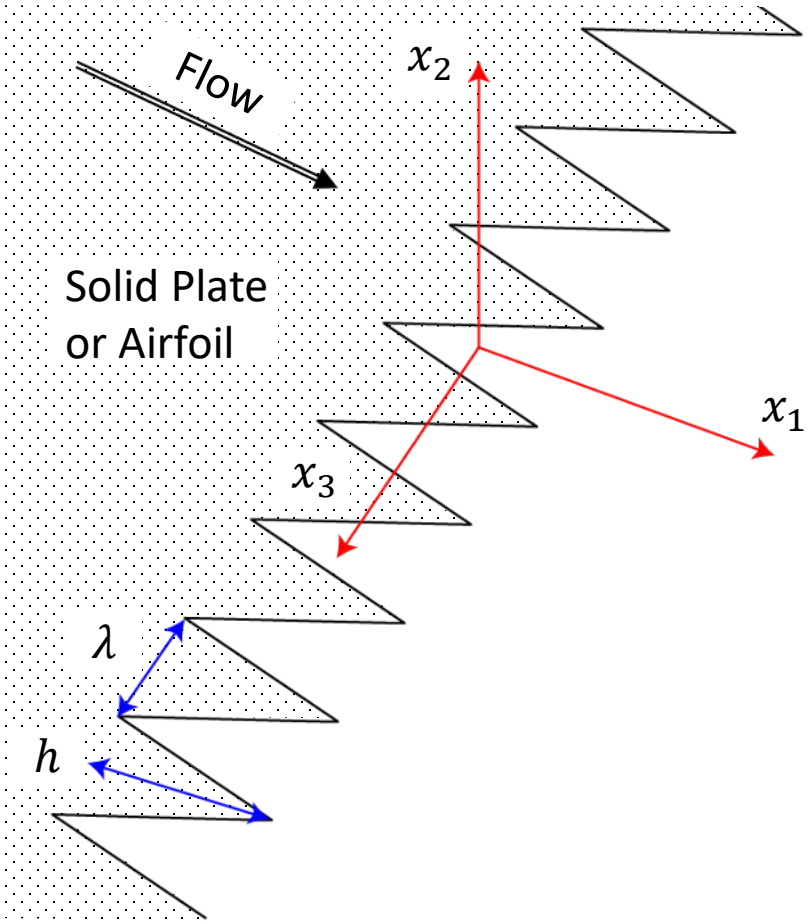

Fig. 1. Geometry and coordinate system of serrated trailing edge.

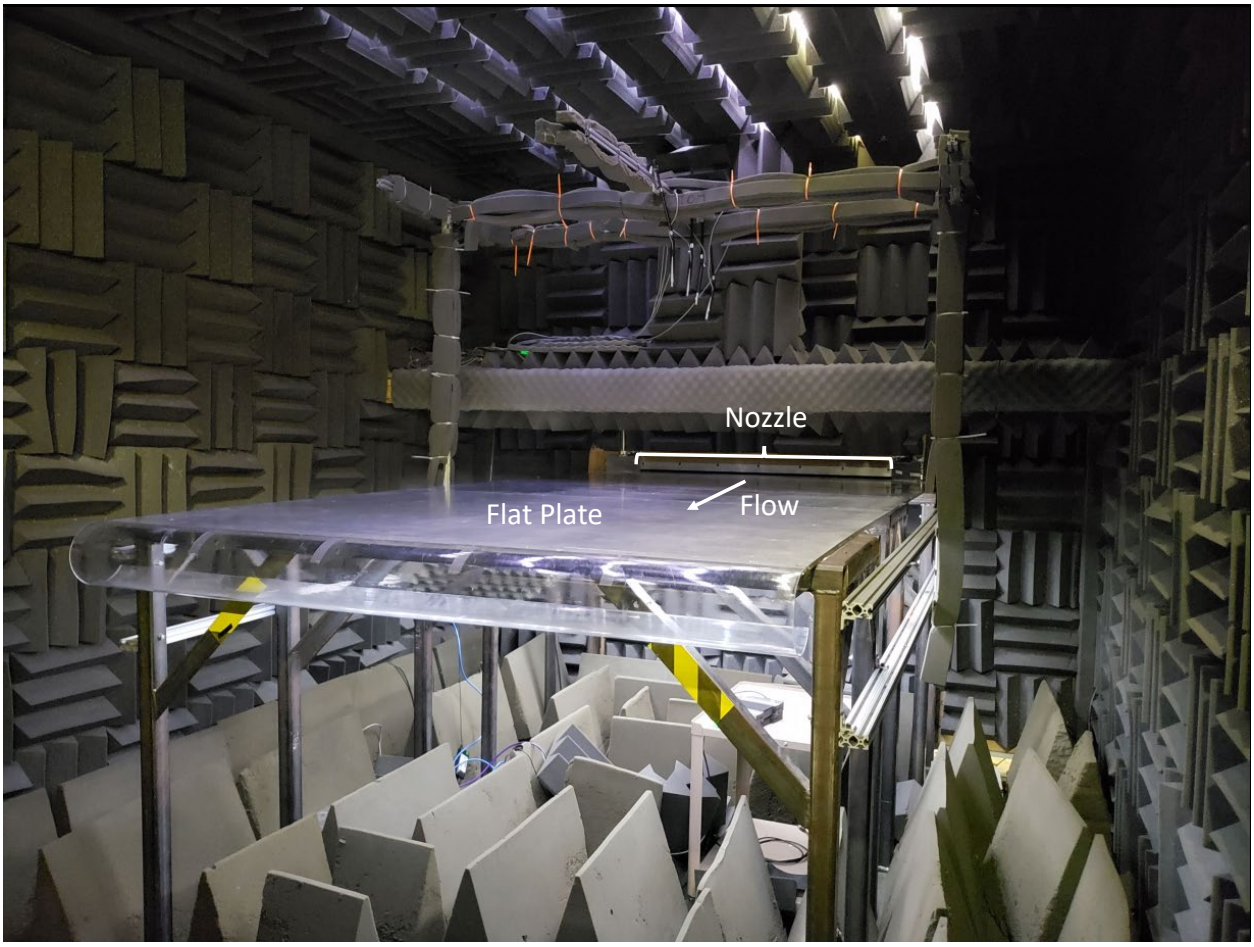

Fig. 2. Virginia Tech Anechoic Wall Jet Facility.

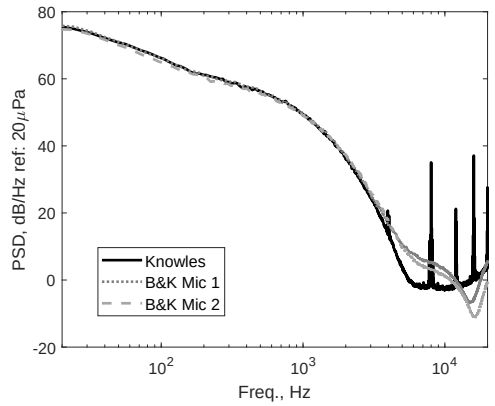

(a) $U_j = 20$ m/s

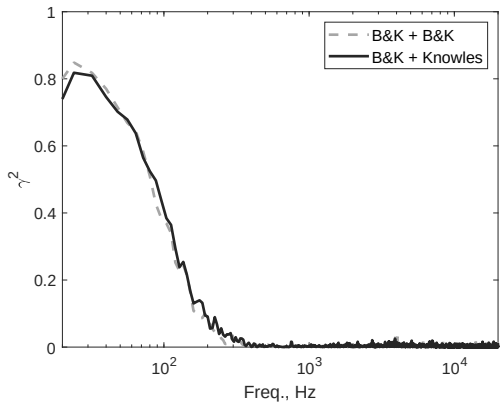

(b) $U_j = 20$ m/s

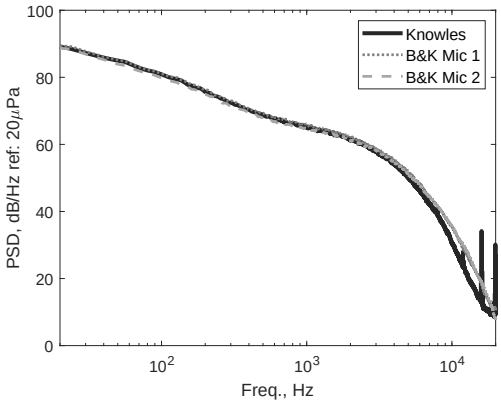

(c) $U_j = 40$ m/s

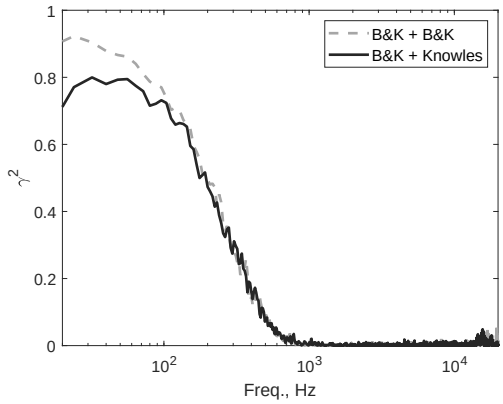

(d) $U_j = 40$ m/s

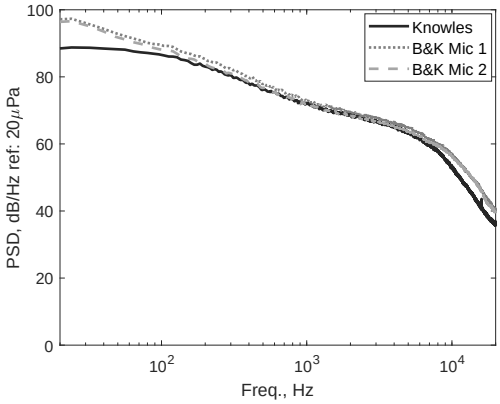

(e) $U_j = 60$ m/s

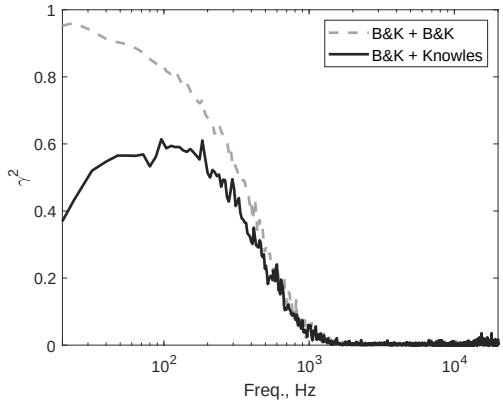

(f) $U_j = 60$ m/s

Fig. 3. Comparison of autospectra and coherence measured by Knowles and B&K microphones in the spanwise orientation on the flat plate.

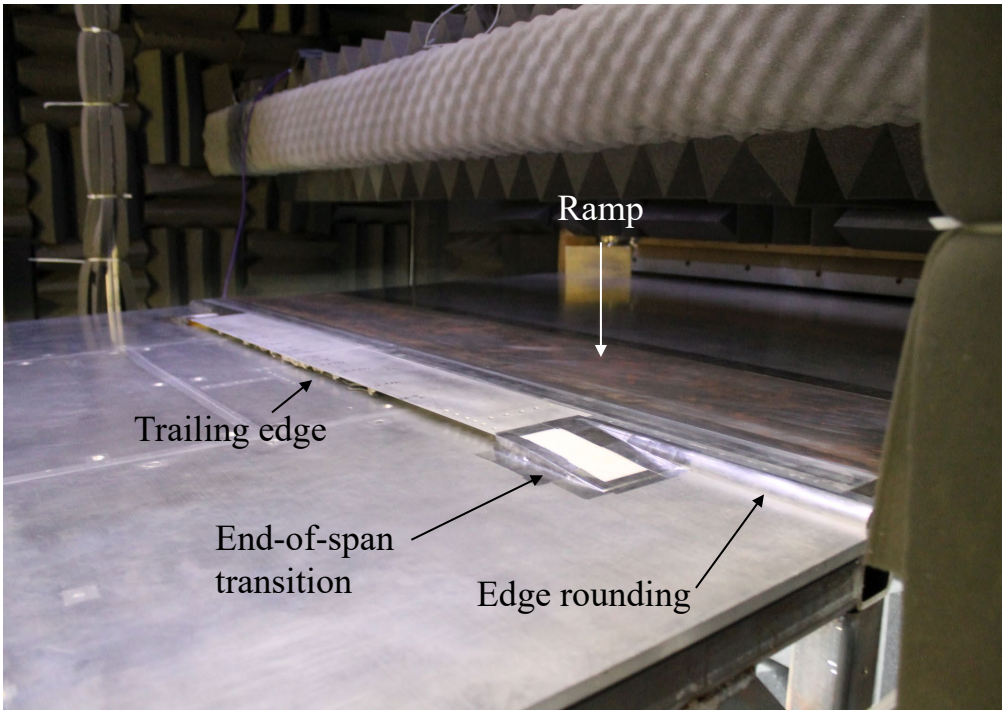

Fig. 4. Straight trailing edge in wall jet.

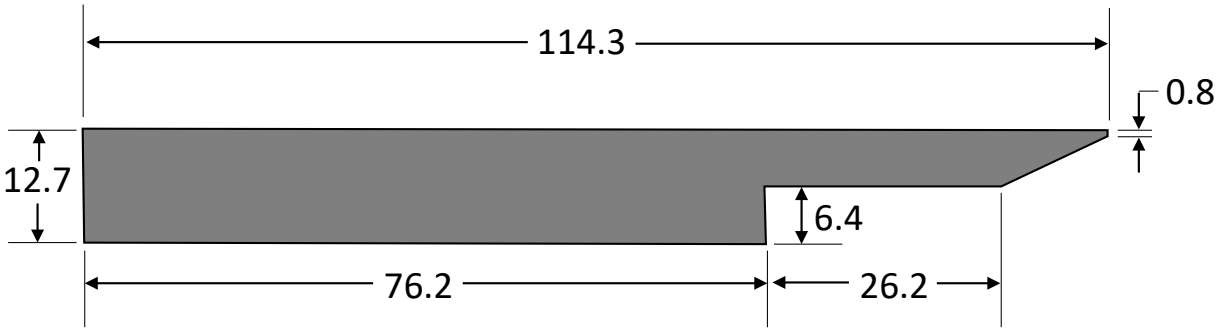

(a) Straight trailing edge

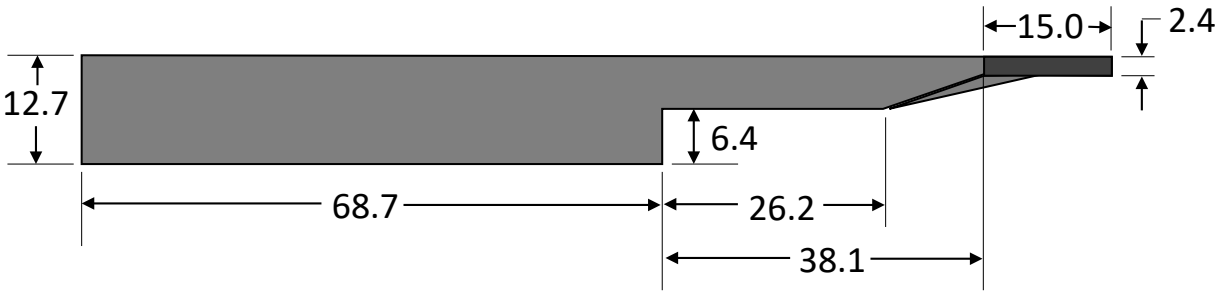

(b) Serrated trailing edge

Fig. 5. Profile geometry (all dimensions in mm).

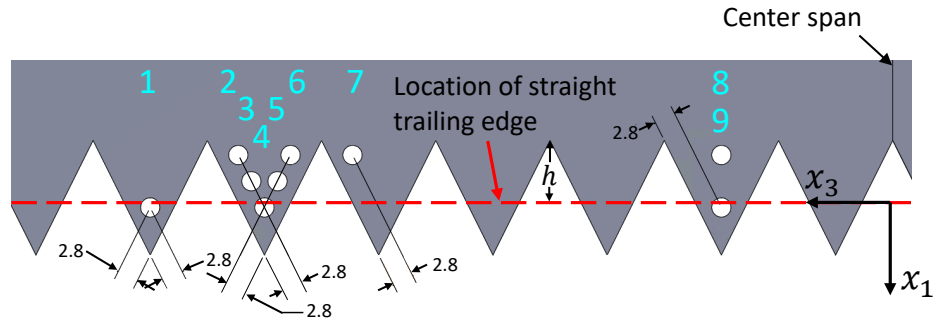

(a)

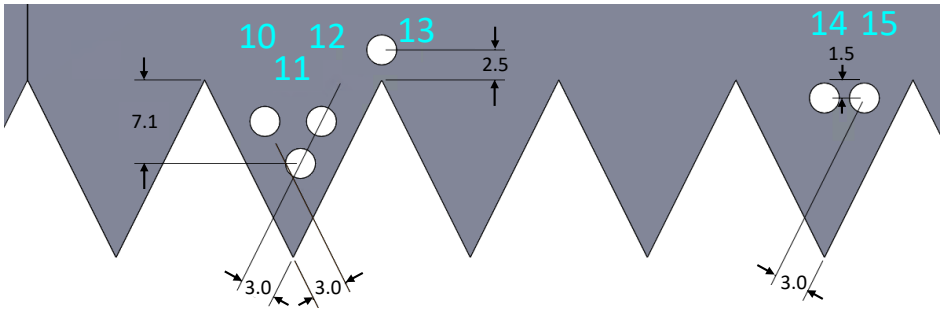

(b)

Fig. 6. Locations of microphone holes in the serrated trailing edge (all dimensions in mm).

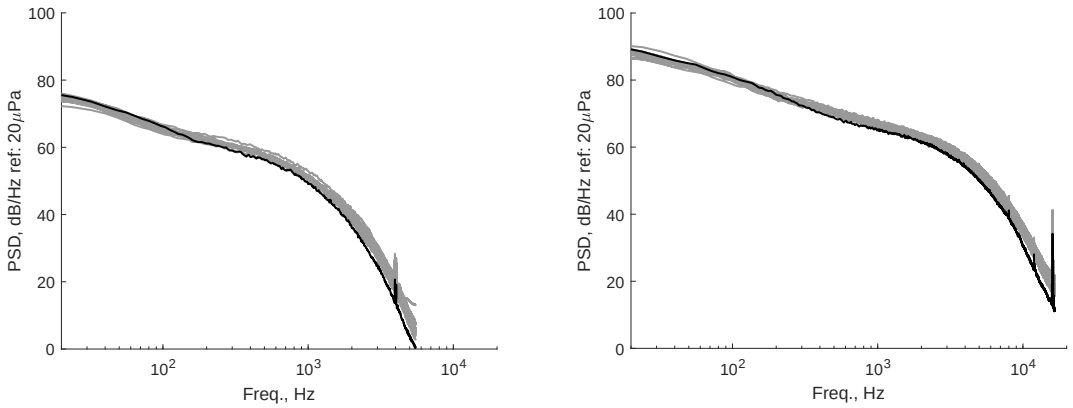

(a) $U_j = 20$ m/s

(b) $U_j = 40$ m/s

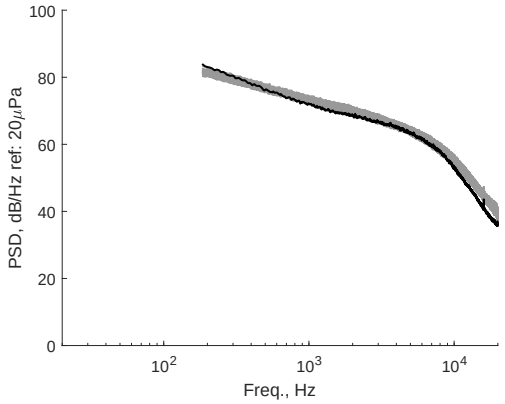

(c) $U_j = 60$ m/s

Fig. 7. Surface pressure along straight trailing edge (grey lines) compared to flat plate wall pressure spectrum (black).

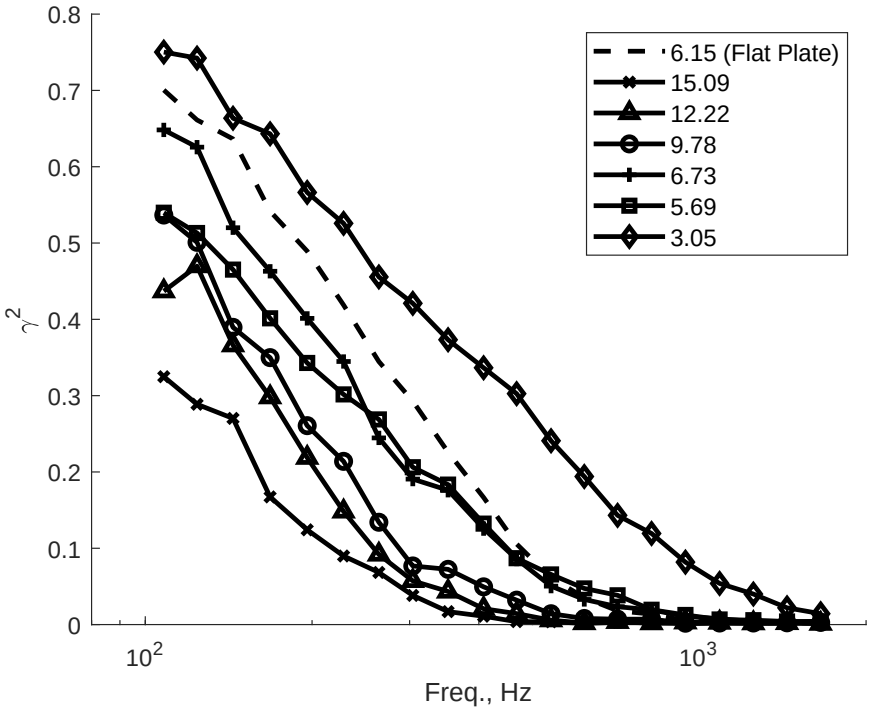

Fig. 8. Coherence of surface pressure along straight edge at U_j = 40 m/s compared to spanwise coherence on the flat plate.

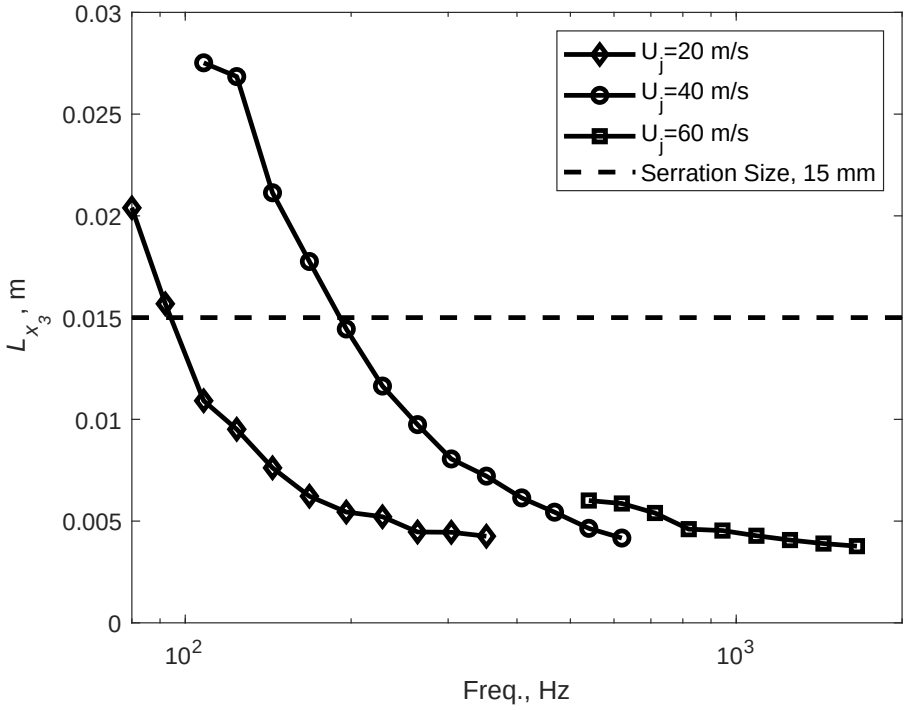

Fig. 9. Spanwise coherence length along the straight trailing edge.

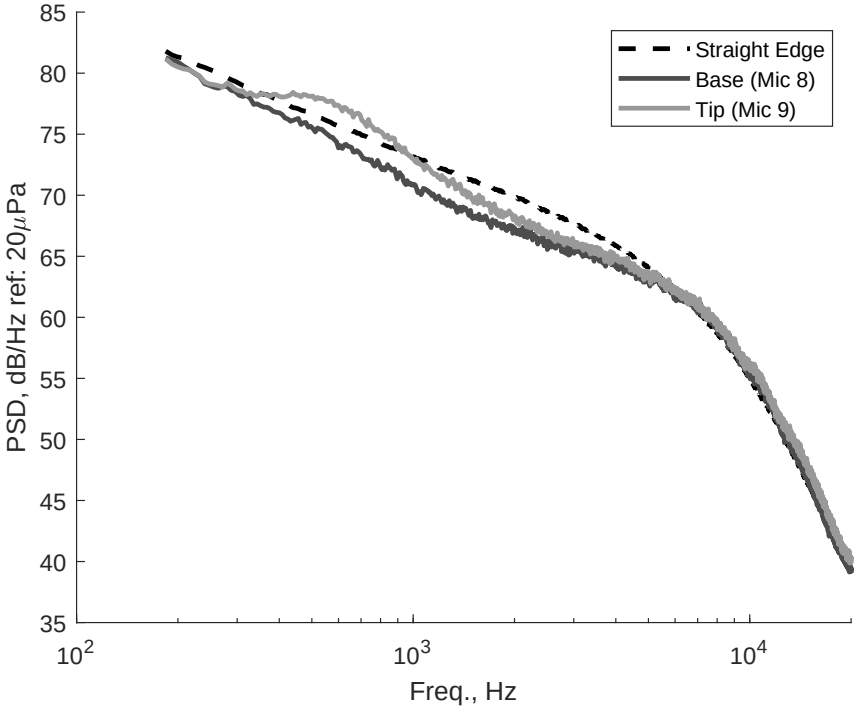

Fig. 10. Surface spectra at the base and tip of a serration compared to a straight trailing edge at $U_j = 60$ m/s.

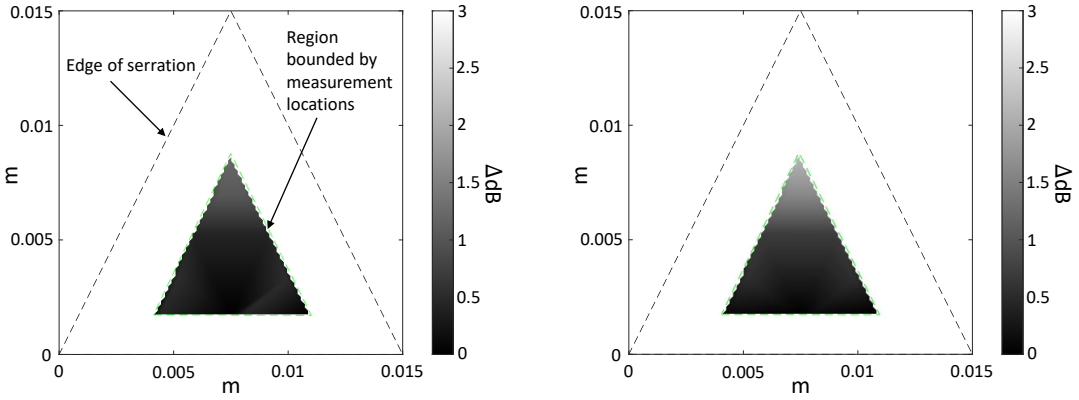

(a) $L_{x_1} = 2h$, 1210 Hz

(b) $L_{x_1} = 3h$, 807 Hz

(c) $L_{x_1} = 4h$, 605 Hz

(d) $L_{x_1} = 6h$, 403 Hz

Fig. 11. Contours of variation in surface pressure fluctuations across serrations at $U_j = 60$ m/s.

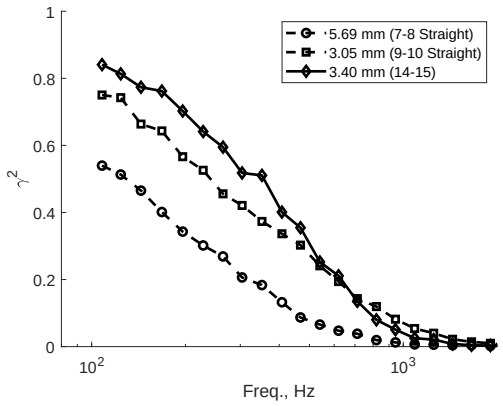

(a) Spanwise coherence between center and edge

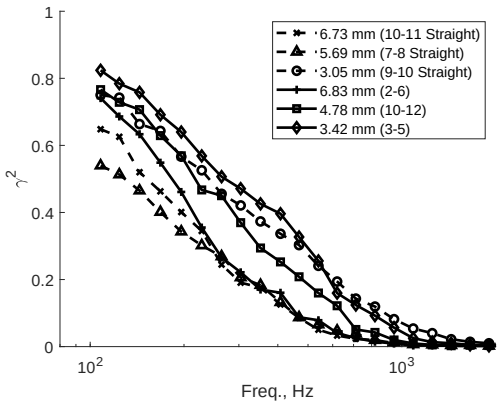

(b) Spanwise coherence across centerline

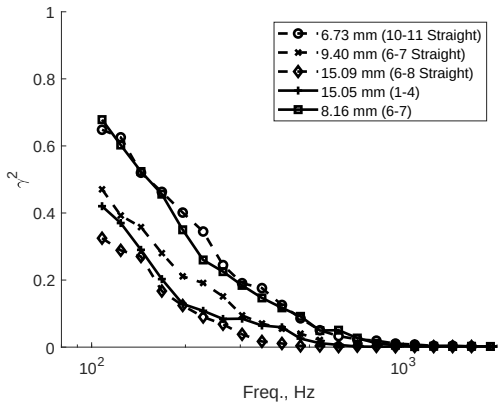

(c) Spanwise coherence across root

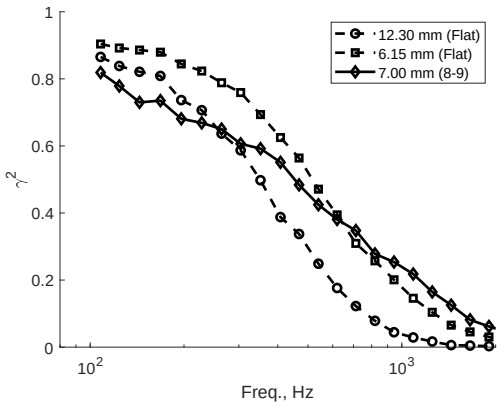

(d) Streamwise coherence along centerline

Fig. 12. Coherence between locations along the serrated edge at $U_j = 40$ m/s.

Figure 1

Click here to access/download;Figure;Figure

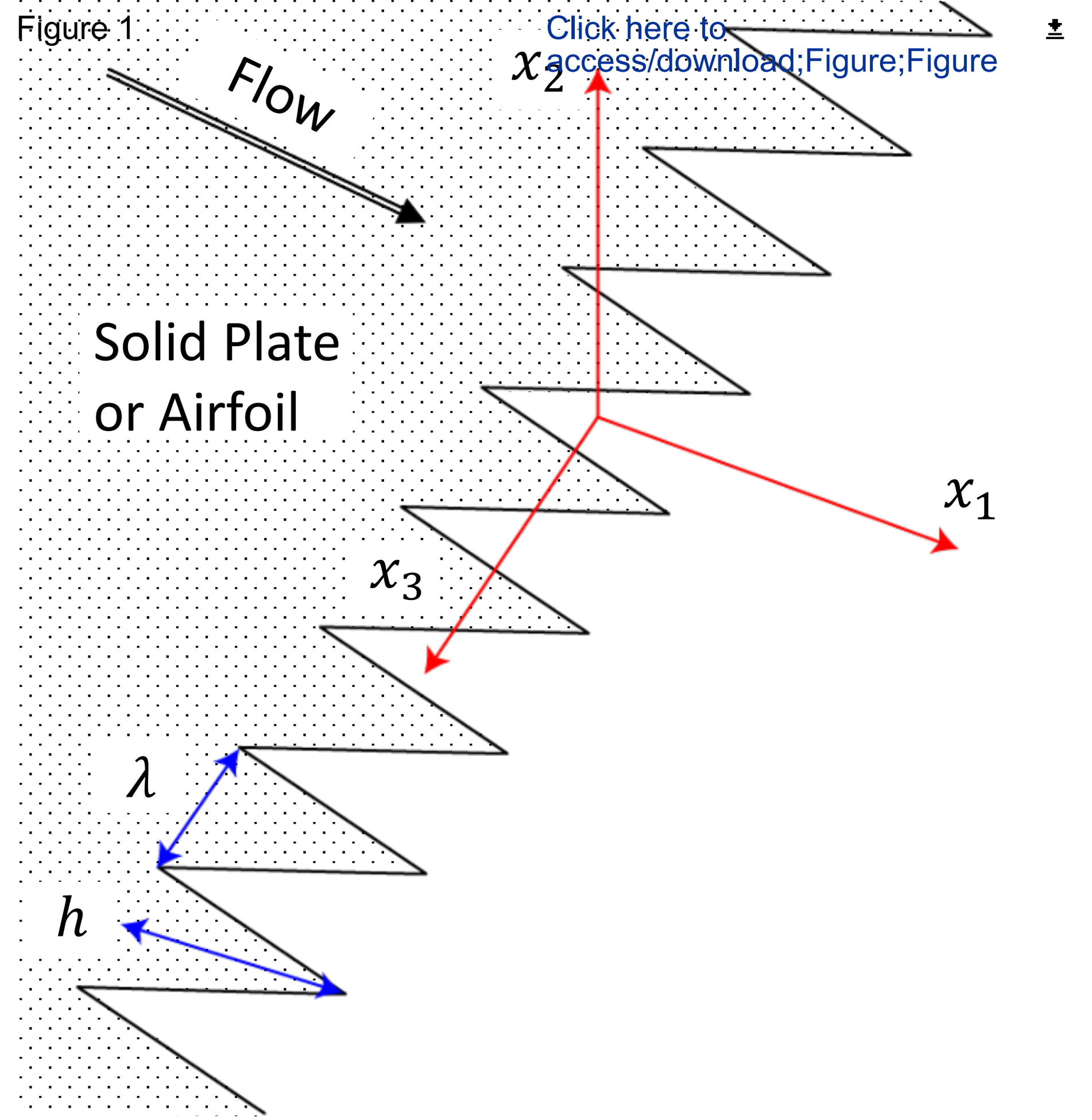

Figure 2

Click here to access/download;Figure;Figure 2.pdf

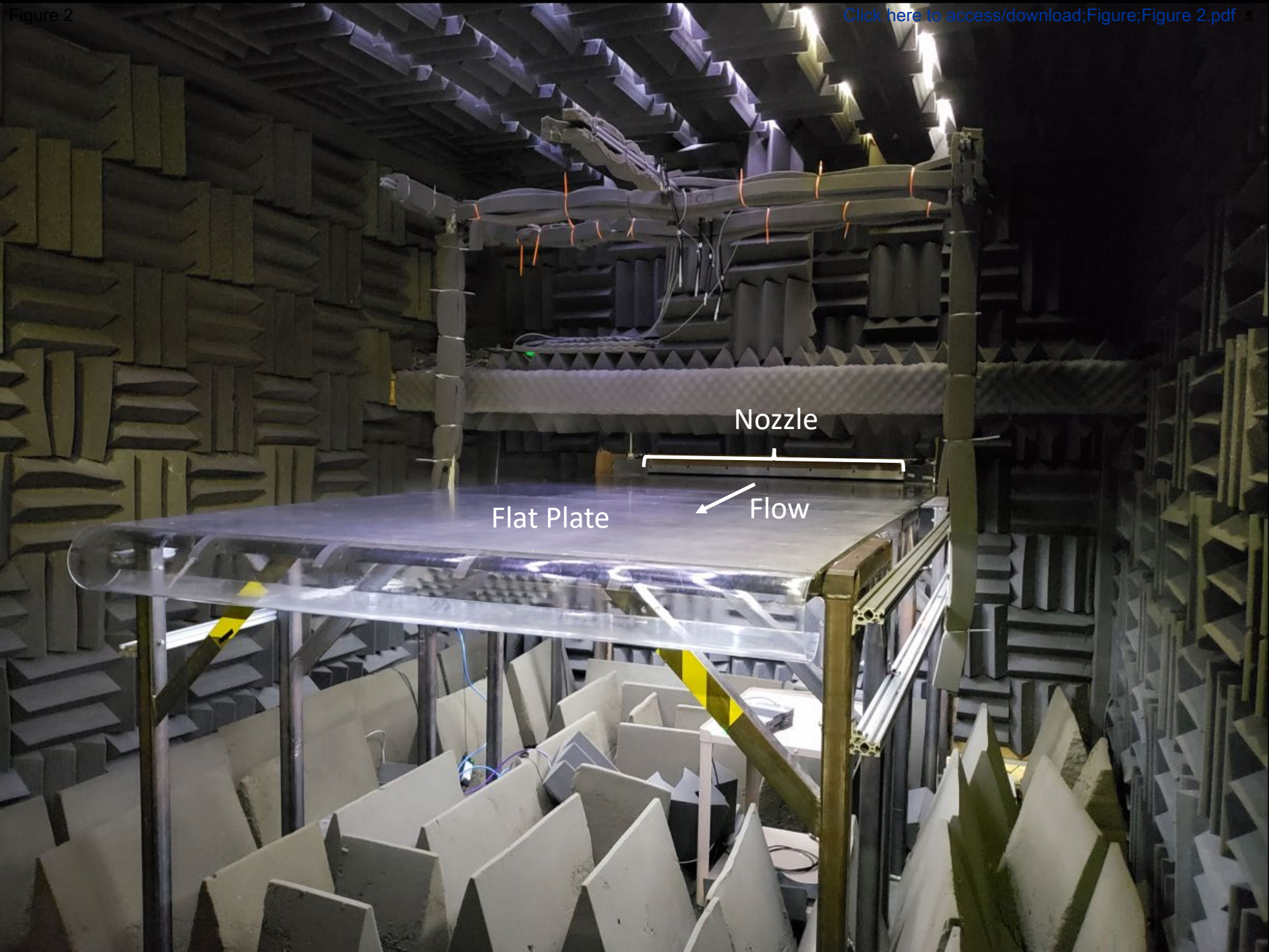

Figure 3a

Click here to access/download;Figure;Figure 3a.pdf

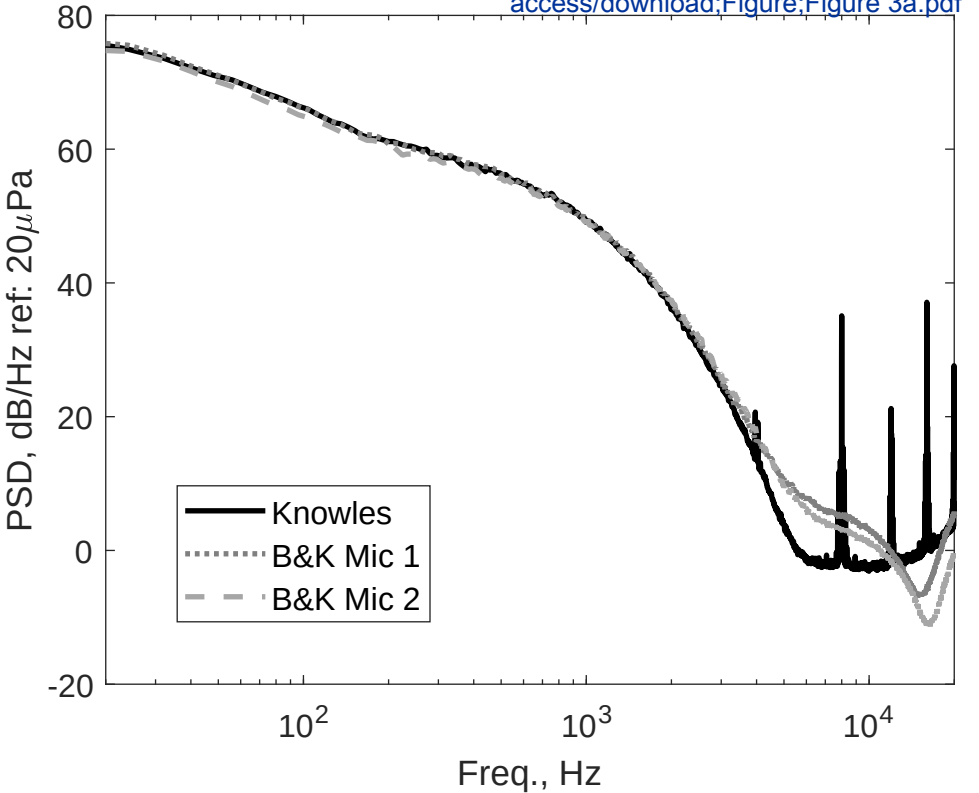

Figure 3b

Click here to access/download;Figure;Figure 3b.pdf

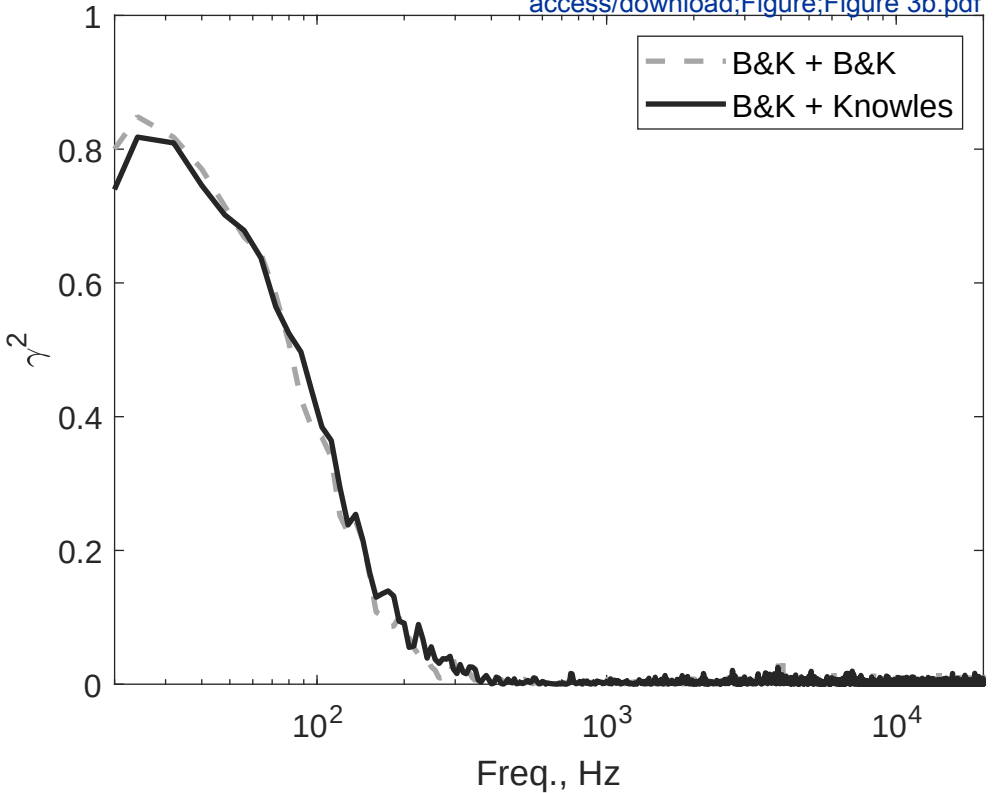

Figure 3c

Click here to access/download;Figure;Figure 3c.pdf

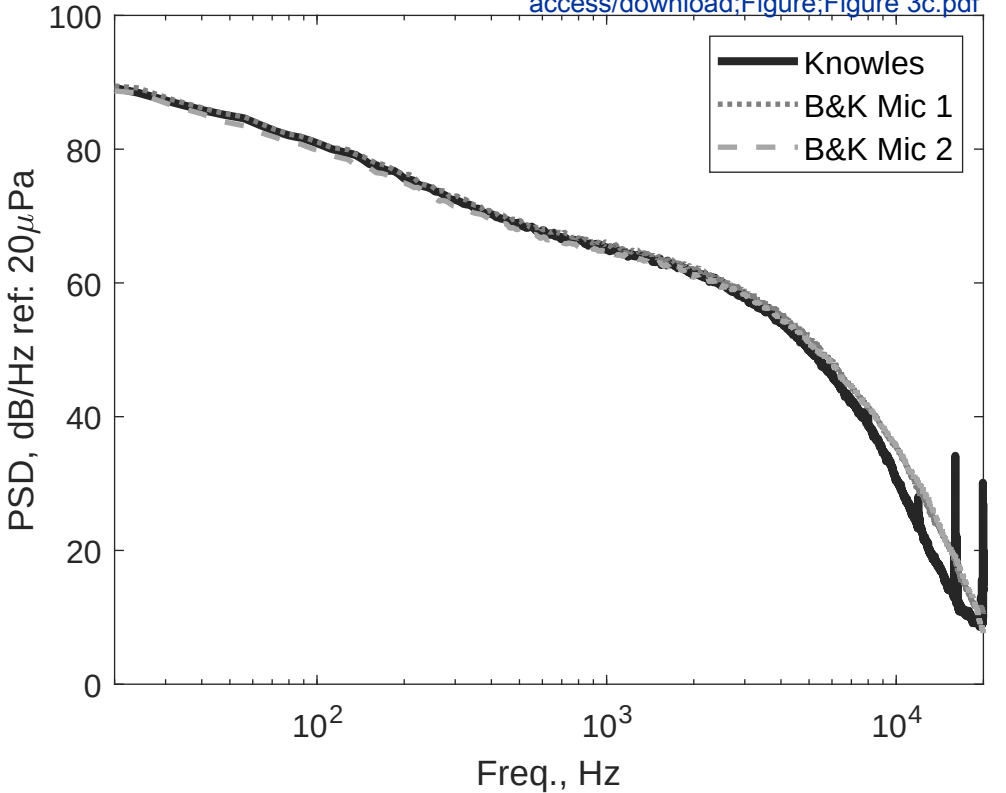

Figure 3d

Click here to access/download;Figure;Figure 3d.pdf

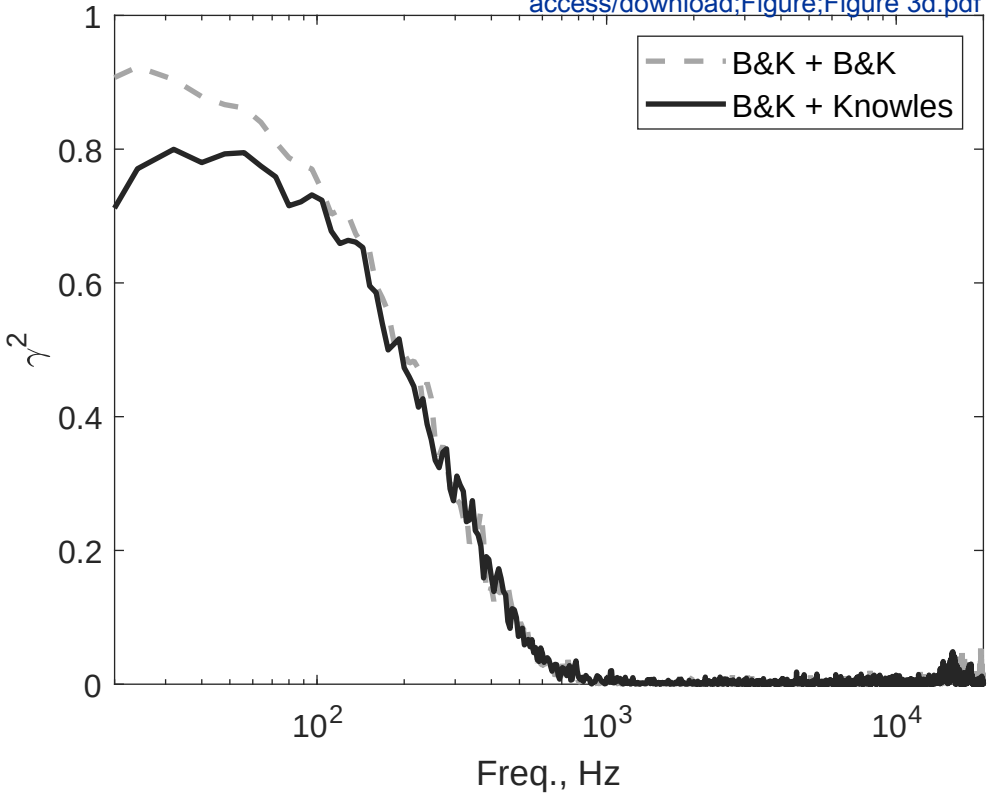

Figure 3e

Click here to access/download;Figure;Figure 3e.pdf

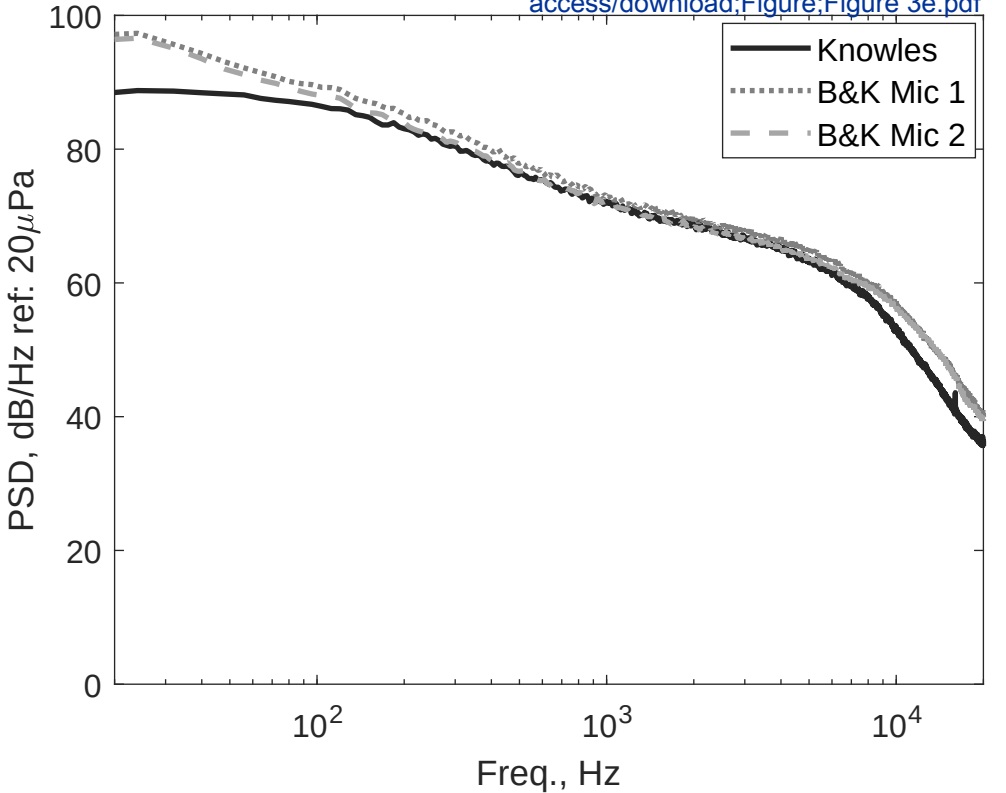

Figure 3f

Click here to access/download;Figure;Figure 3f.pdf

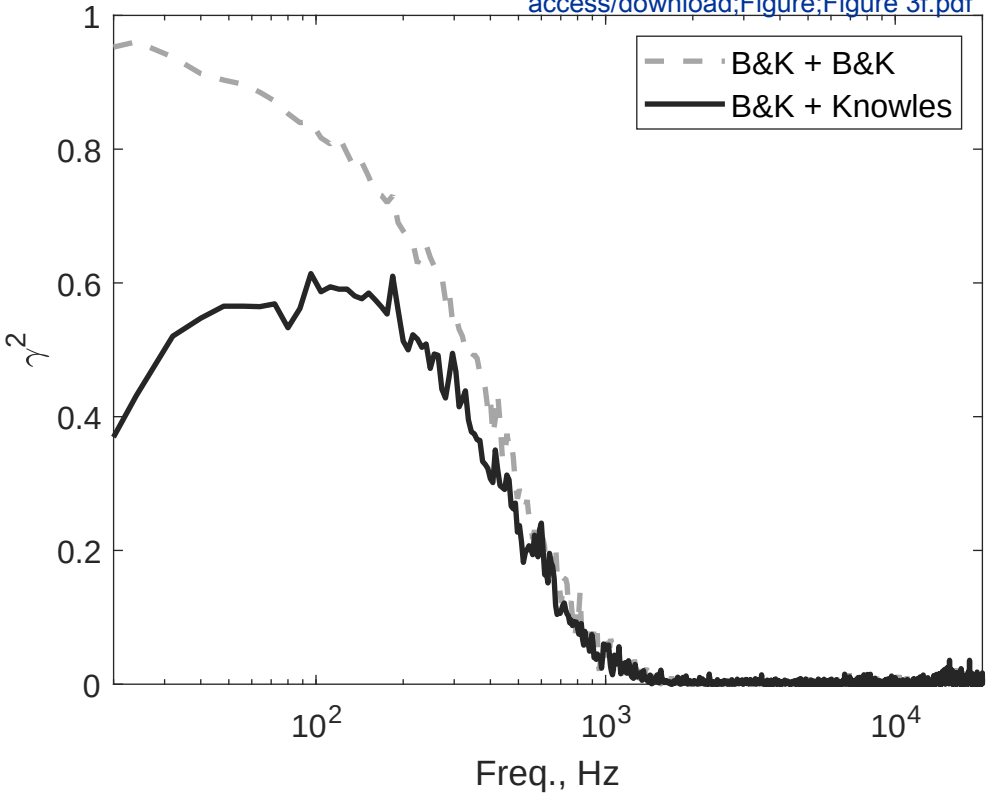

Figure 4

Click here to access/download;Figure;Figure 4.pdf

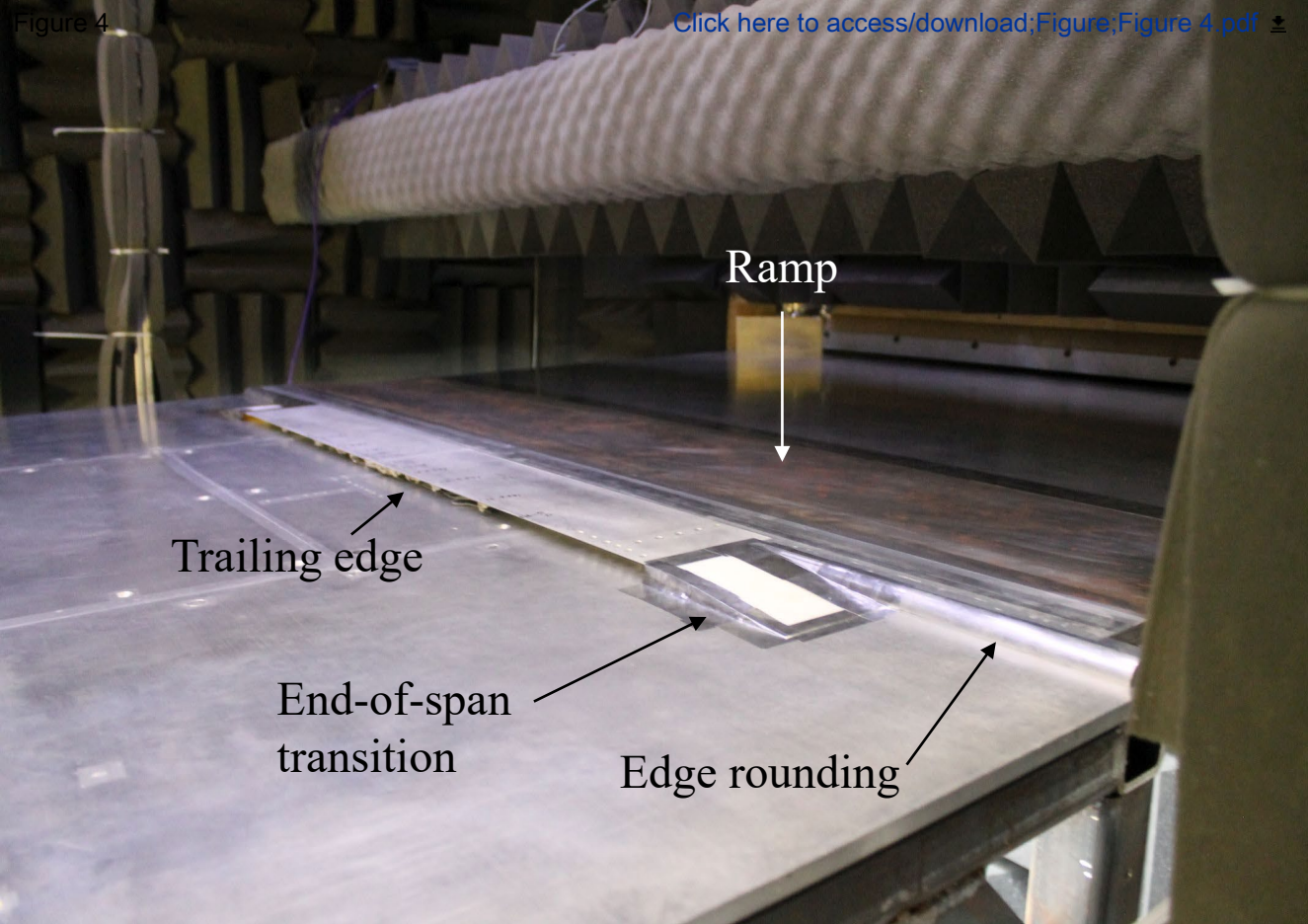

Figure 5a

Click here to access/download;Figure;Figure 5a.pdf

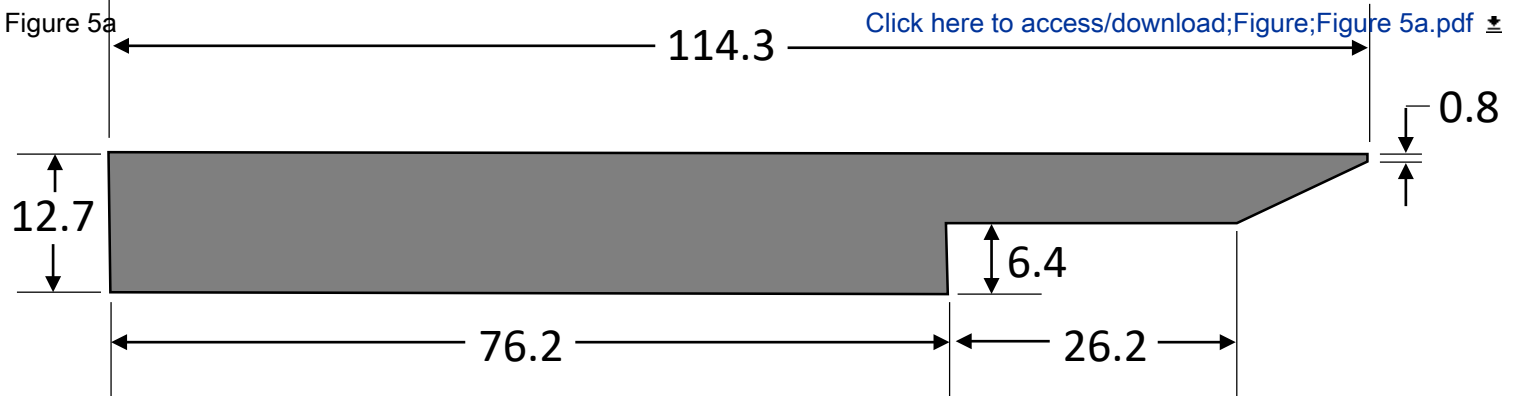

Figure 5b

Click here to access/download;Figure;Figure 5b.pdf

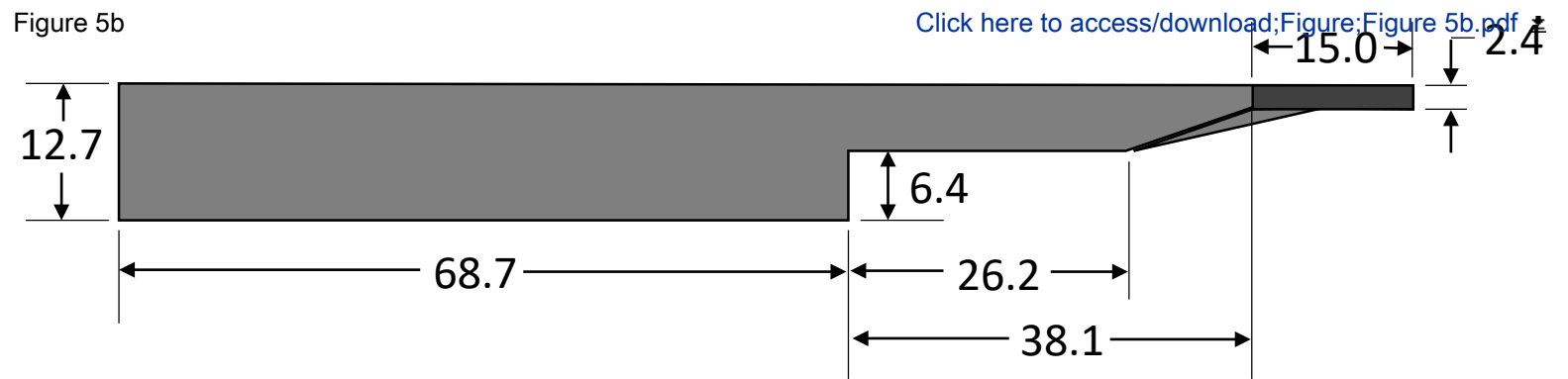

Figure 6a

Click here to access/download:Figure:Figure 6a.pdf

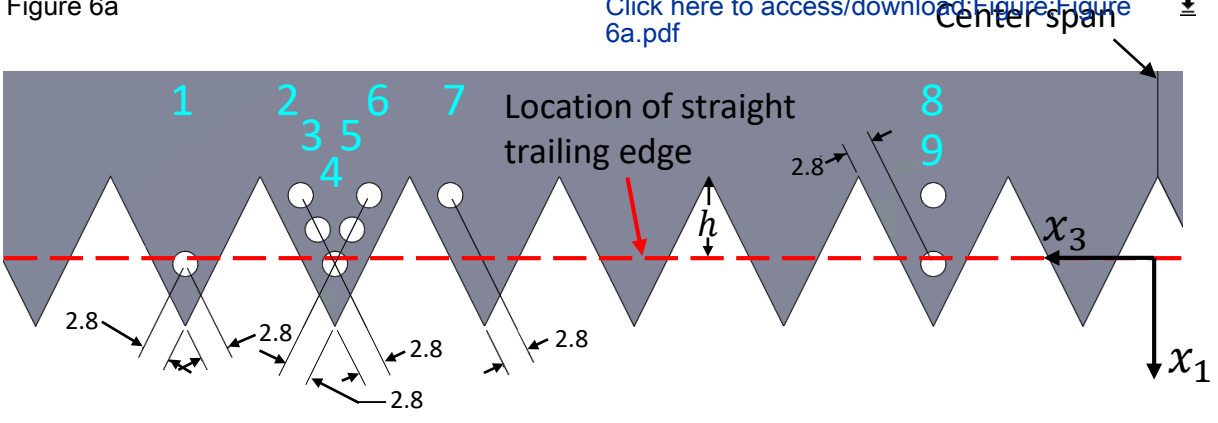

Figure 6b

Click here to access/download;Figure;Figure 6b.pdf

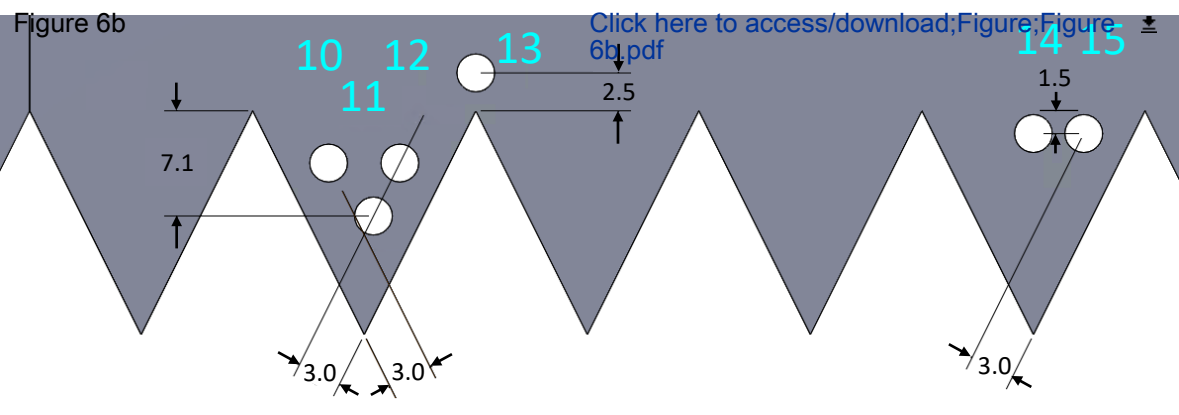

Figure 7a

Click here to access/download;Figure;Figure 7a.pdf

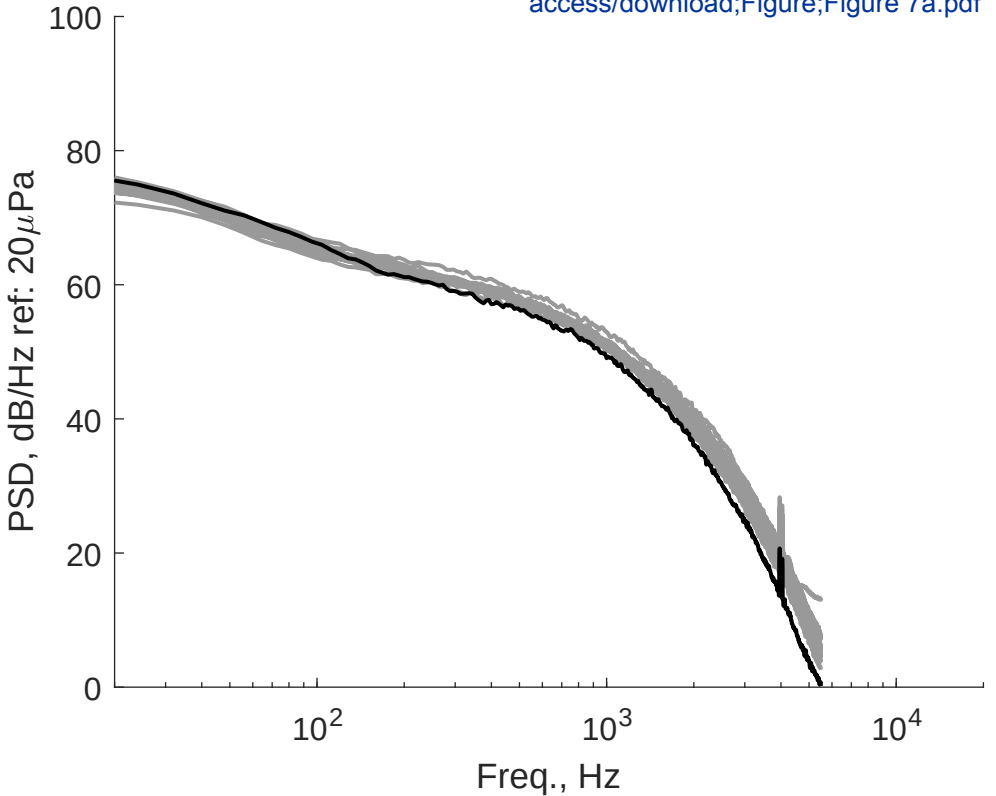

Figure 7b

Click here to access/download;Figure;Figure 7b.pdf

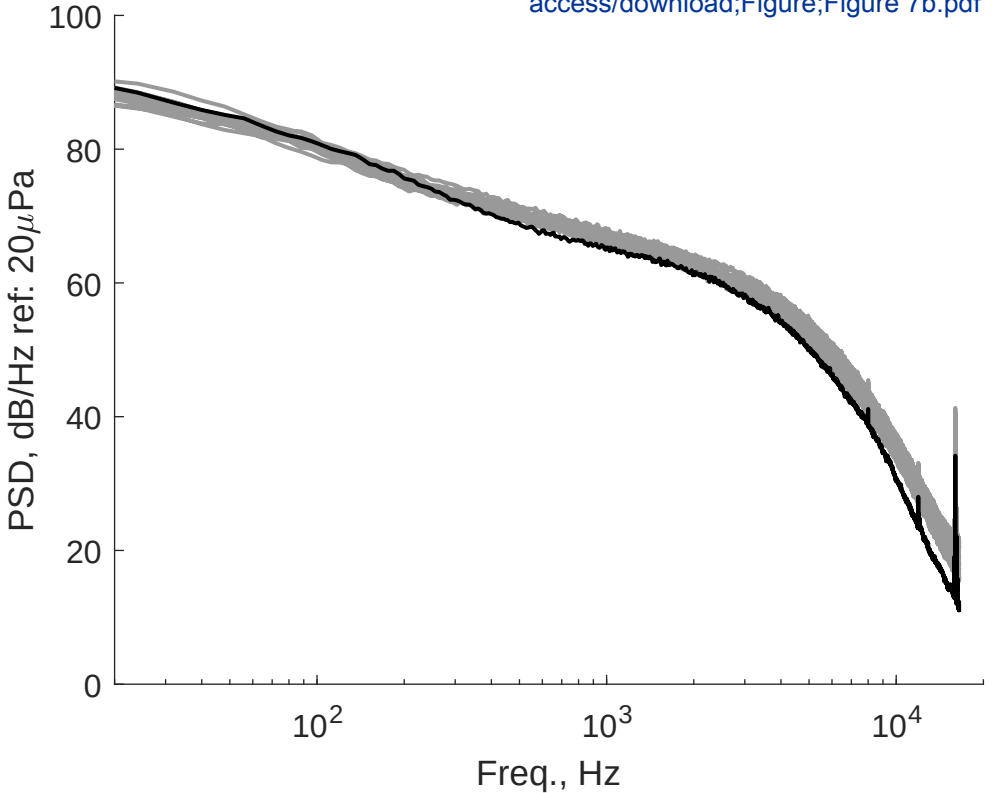

Figure 7c

Click here to access/download;Figure;Figure 7c.pdf

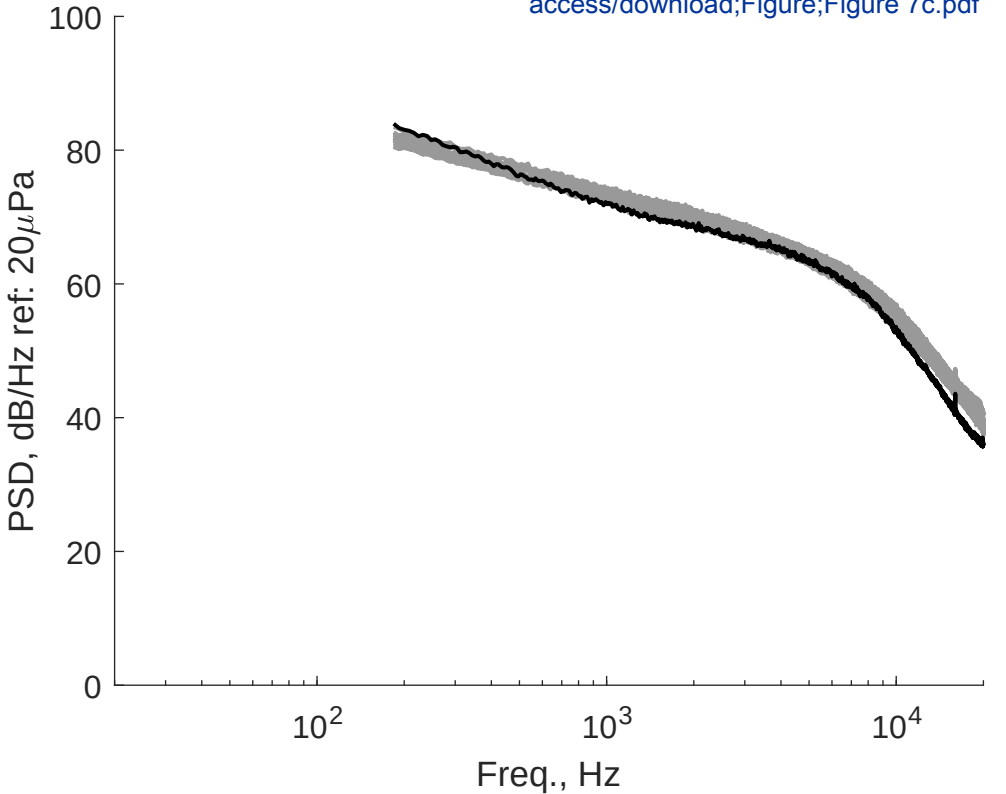

Figure 8

Click here to access/download;Figure;Figure 8.pdf

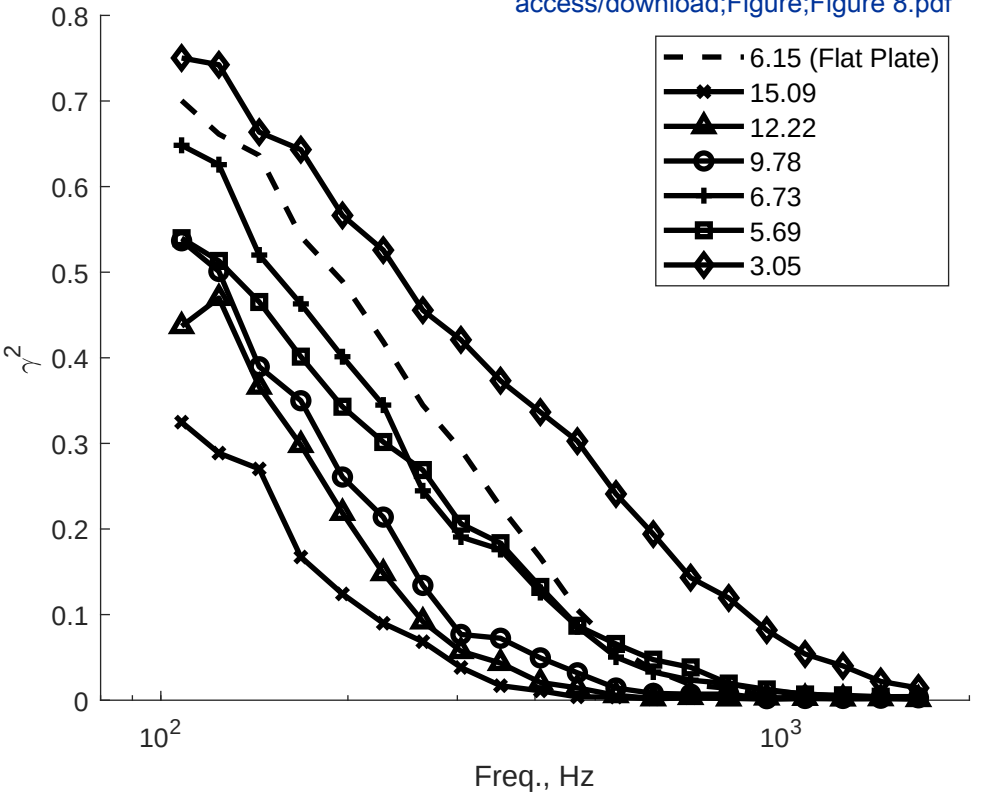

Figure 9

Click here to access/download;Figure;Figure 9.pdf

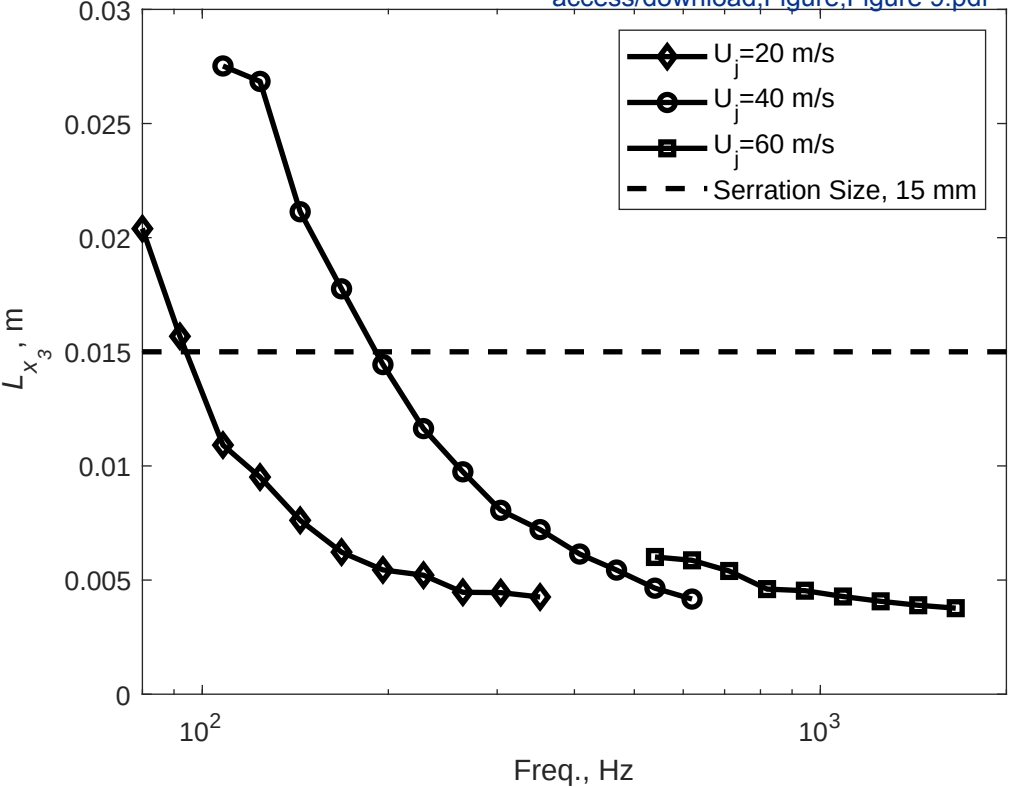

Figure 10

Click here to access/download;Figure;Figure 10.pdf

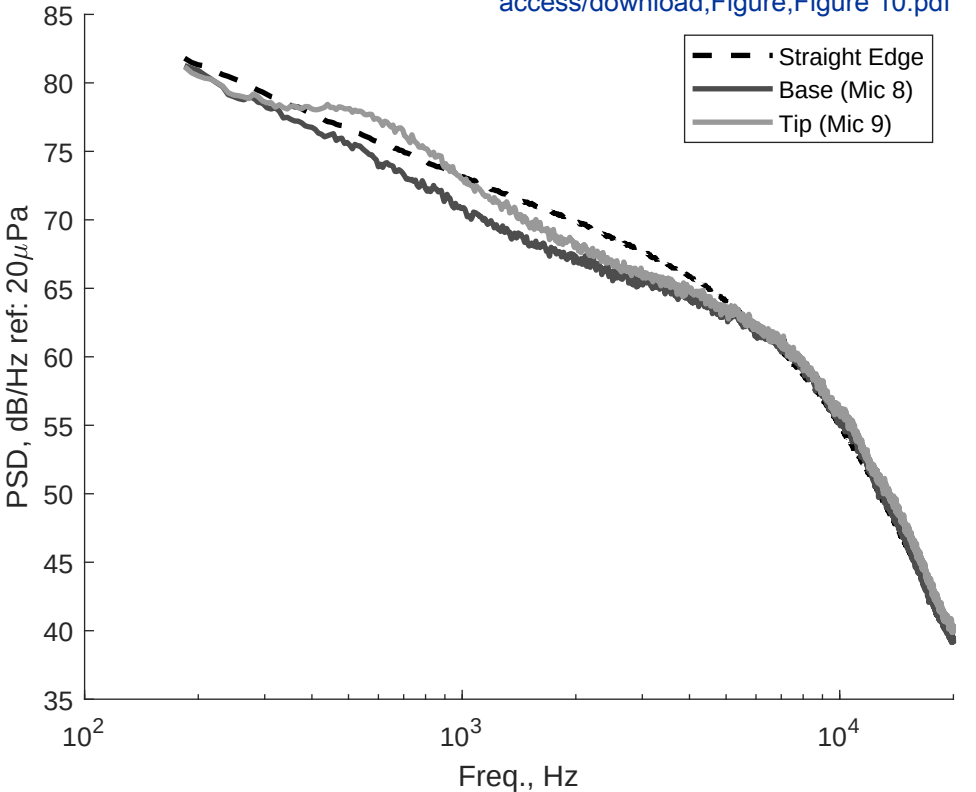

Figure 11a

Click here to access/download;Figure;Figure 11a.pdf

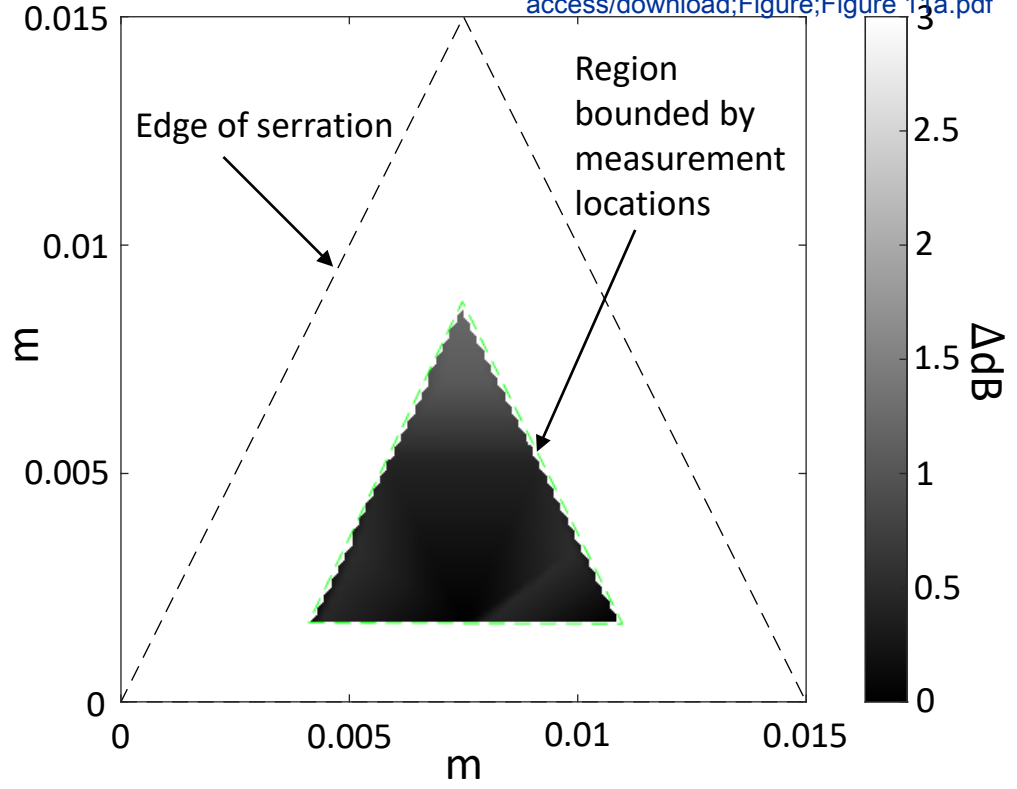

Figure 11b

Click here to access/download;Figure;Figure 11b.pdf

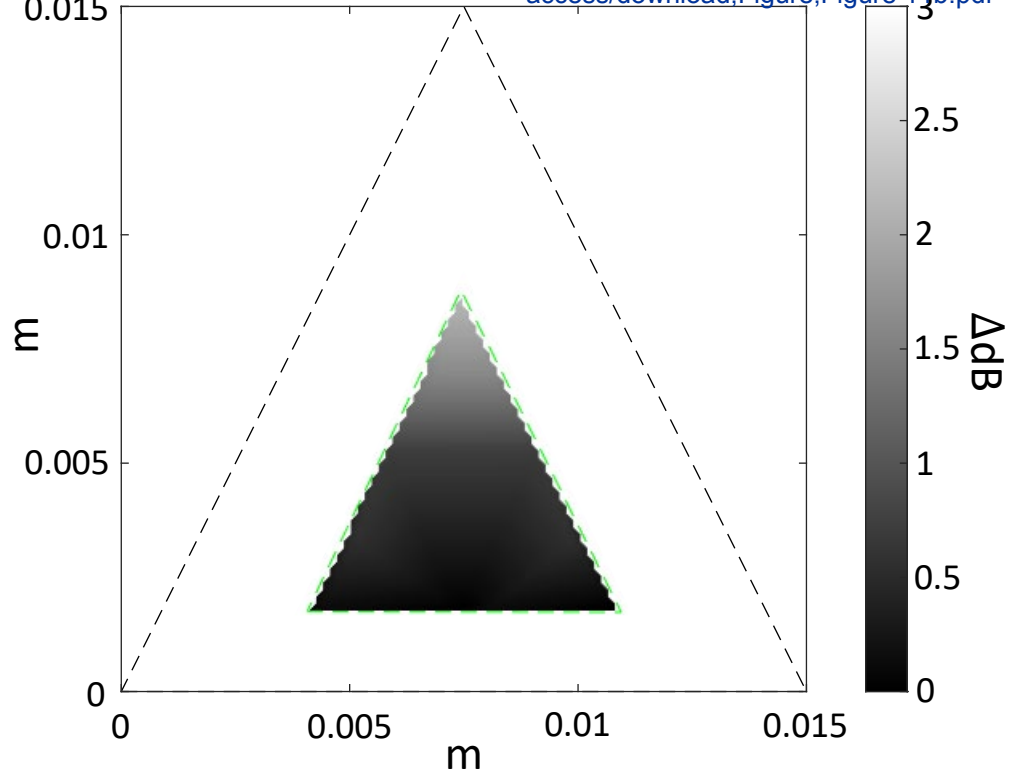

Figure 11c

Click here to
access/download;Figure;Figure 11c.pdf

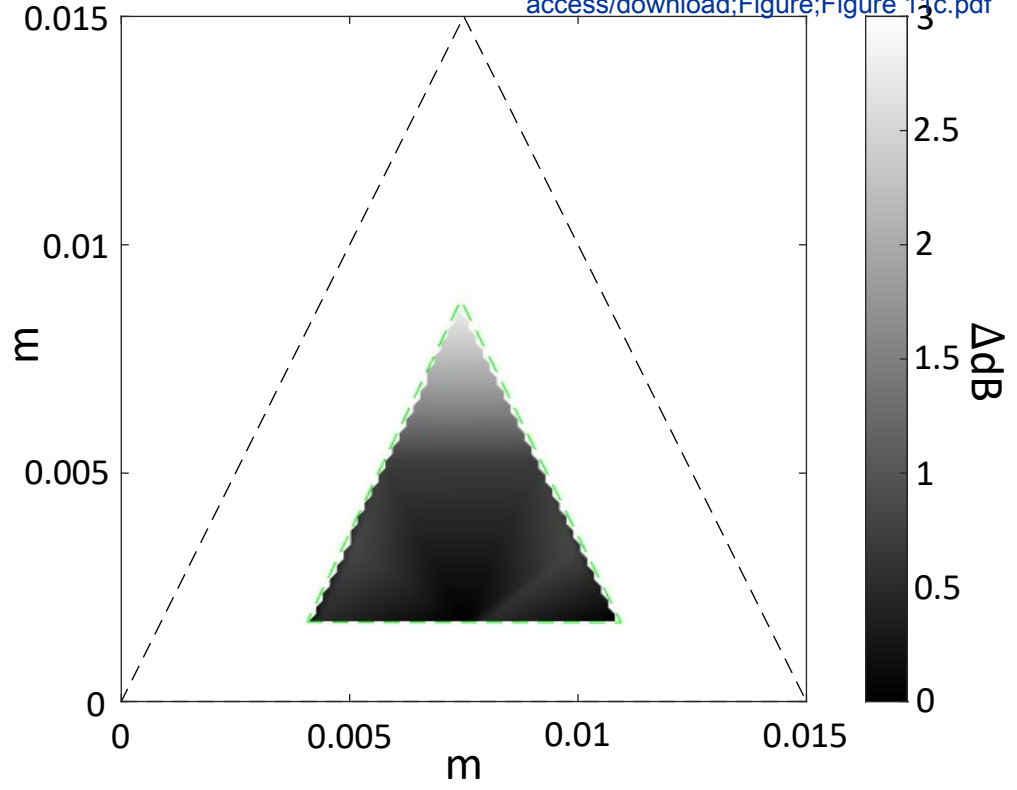

Figure 11d

Click here to access/download;Figure;Figure 11d.pdf

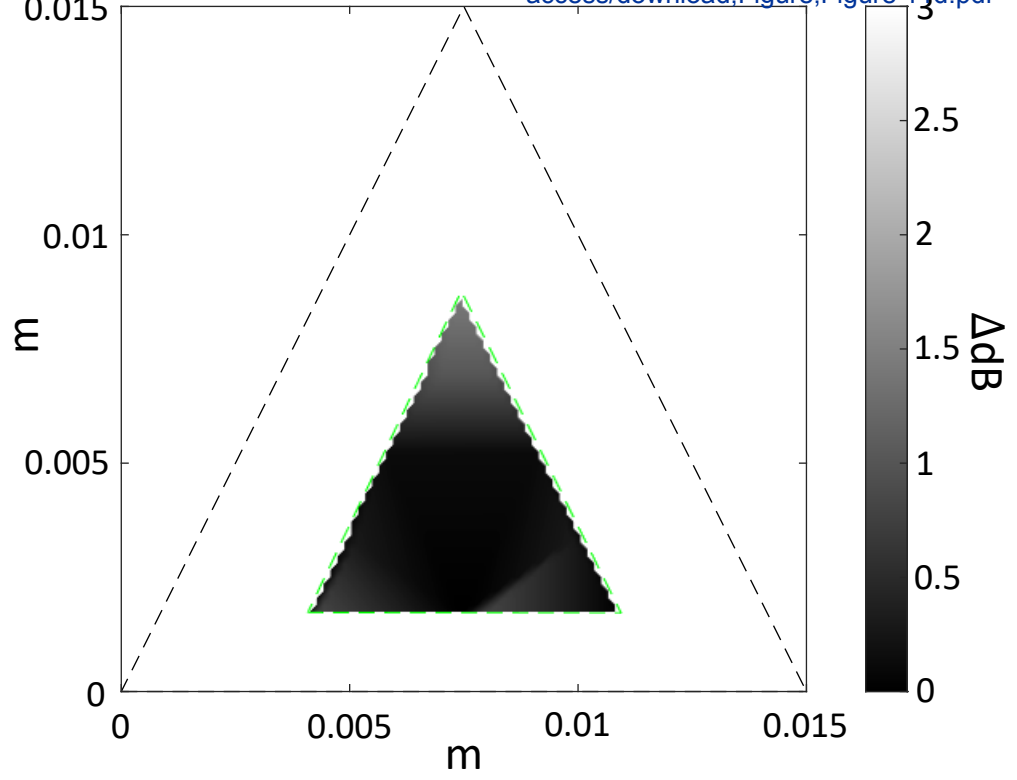

Figure 12a

Click here to access/download;Figure;Figure 12a.pdf

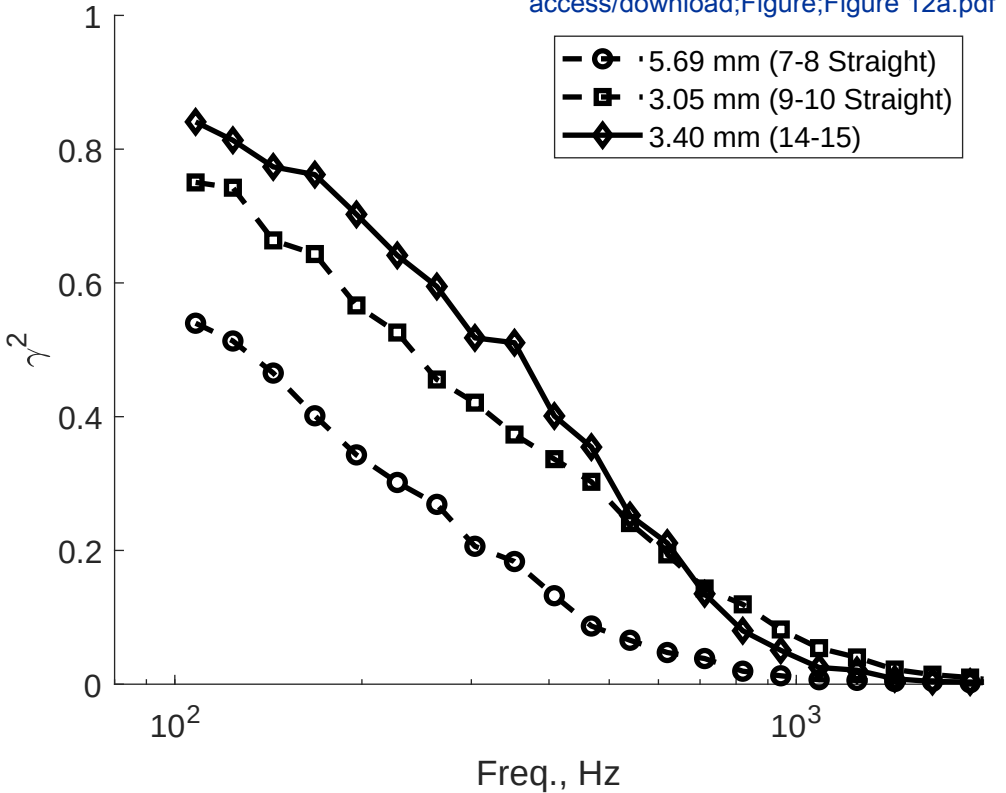

Figure 12b

Click here to access/download;Figure;Figure 12b.pdf

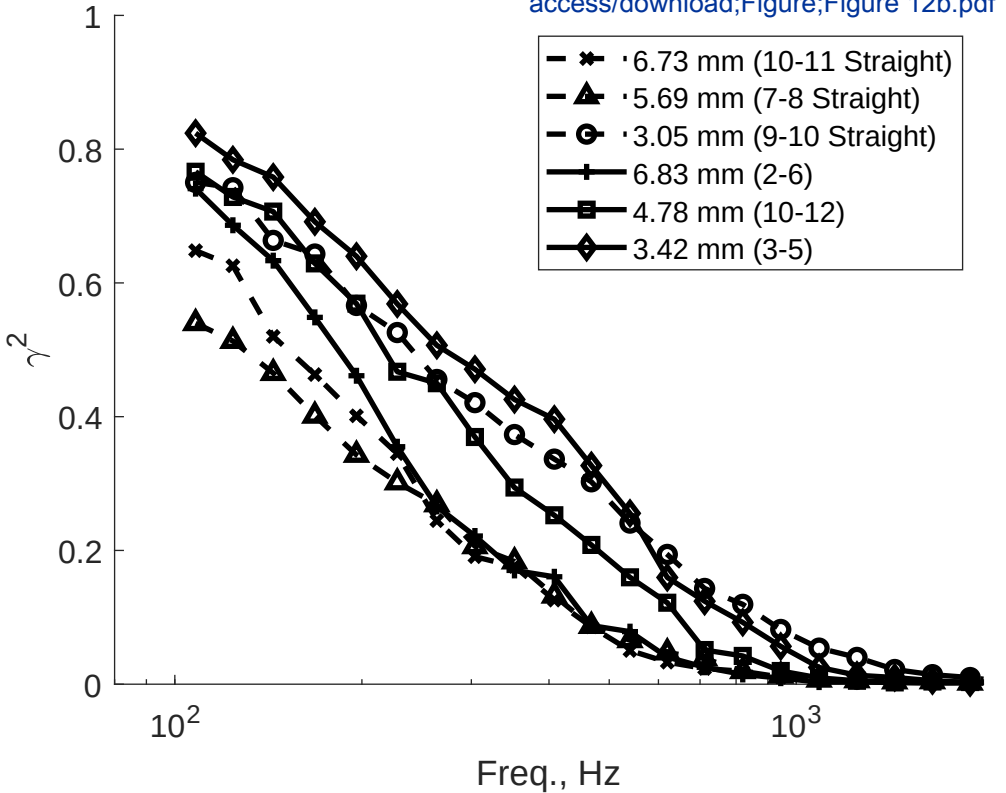

Figure 12c

Click here to access/download;Figure;Figure 12c.pdf

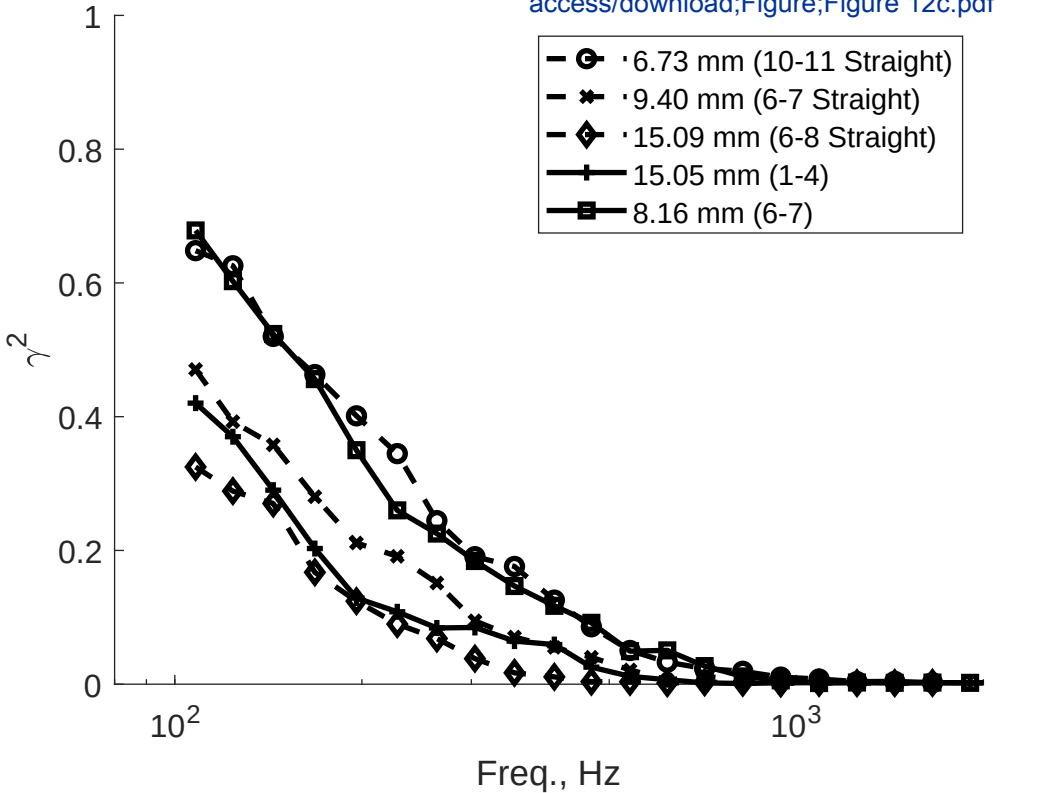

Figure 12d

Click here to access/download;Figure;Figure 12d.pdf

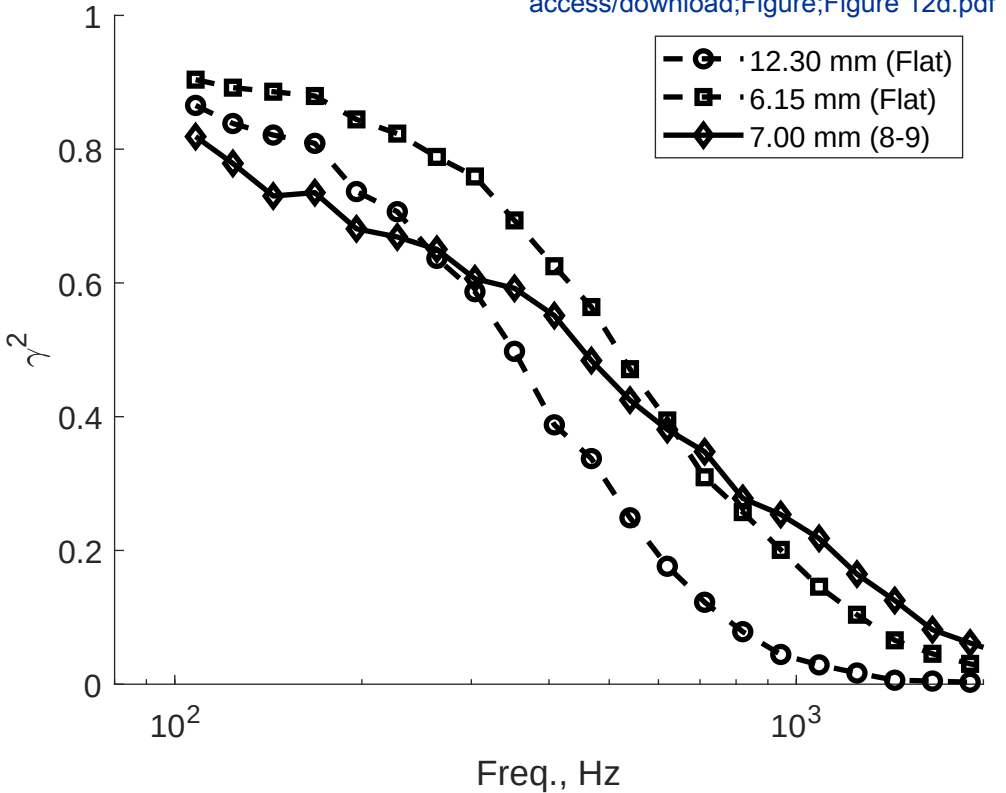

Response to Reviewers Comments
Click here to access/download;Response to Reviewers Comments;Response to Reviewers_v4.pdf

Response to Reviewers

The authors would like to thank the reviewers for their thoughtful remarks. We have addressed all comments and believe the manuscript has been improved by doing so. Direct responses to your comments are given below. Additionally, all changes have been highlighted in the manuscript.

Reviewer #1: The paper extensively uses remote microphone probes to investigate the hydrodynamic field in a serrated trailing edge. The experimental campaign in conduced in a wall-jet facility.
The paper follows a logical and well-organised structure. I couldn't find language or spelling mistakes in this paper. The discussion of the results are well supported by the experimental results. I didn't find any significant discrepancies between the results presented and the authors' analysis. I have no questions regarding the analysis and the results presented in the paper.

However, my main criticism to this paper resides in two key points: 1. the methodology; 2. placement of this research with respect to the state-of-the-art.

Regarding the methodology:
1. from the description of the experimental setup, it is reasonable to assume that the boundary layer is fully developed. However, the authors don't demonstrate this. The authors could use the already measured hot-wire anemometry data to demonstrate that the boundary layer is fully developed;

The wall-jet used in this study was shown to be fully-developed in a prior study. Rather than repeat the description of these measurements here, we have added a statement that the boundary layer is fully-developed with reference to this work. This statement located in the description of the wall-jet facility is repeated below.

“Kleinfelter et al. (2019) show that the wall-jet profile is fully-developed for streamwise positions greater than 0.98 m from the nozzle exit and at all nozzle velocities.” **(Line 134)**

2. From the hot wire anemometry data, the authors could obtain the turbulence spanwise correlation length. This information is critical to the design of a serration with aspect ratio (h/\lambda) which leads to trailing edge noise reduction.

Hotwire data were not acquired as part of this study. We do have single point hotwire profiles from the study of Kleinfelter et al. (2019), but these data do not contain two-point spanwise measurements. Thus, we cannot determine the spanwise correlation or correlation length from the hotwire measurements. Instead, the authors suggest presenting the spanwise surface pressure coherence length. We do have spanwise correlation data from surface pressure measurements along the straight trailing edge. These can be used to estimate the spanwise surface pressure coherence length as a function of frequency. This information including an additional figure has been included in the paper. It is noted that the serrations are likely to be more effective at higher frequencies, but this does not change the conclusions of the work which are focused on the surface pressure spectrum. The following (including a new figure) has been added to the manuscript in the results section.

"The spanwise coherence length can be calculated as a function of frequency by fitting an exponential curve across coherence spectra from microphone pairs along the straight trailing edge. This relation is expressed in Eq. 1:

$$\gamma^2 = e^{-2|\Delta x_3|/L_{x_3}(f)} \quad (1)$$

$L_{x_3}(f)$ is the coherence length, Δx_3 is the separation distance between pairs of microphones, and γ^2 is the coherence. $L_{x_3}(f)$ was found through a least squares regression using the coherence spectra between all microphone pairs at each frequency. The results are shown in Figure 9 for U_j=20, 40, and 60 m/s. The spanwise scale decreases with increasing frequency. Again, the valid frequency range of data at U_j=60 m/s is limited, but for U_j=40 m/s, the spanwise scale is shown to be smaller than the wavelength of the serrations to be applied for frequencies above 190 Hz." **(Line 265)**

3. The authors adopt an aspect ratio which is already used in other papers. However, the literature uses the characterized boundary layer turbulence correlation length as background information in the design of the serration aspect ratio. I recommend the authors consider the spanwise correlation length and consider the paper (classical in the field, however, not cited in the literature review of the proposed paper) for the design of the ideal serration aspect ratio: B. Lyu, M. Azarpeyvand and S. Sinayoko, Prediction of noise from serrated trailing edges, Journal of Fluid Mechanics, Volume 793, 2016. The use of an adequate geometry would lead to a more significant noise reduction which the fluid dynamic effects could be analyzed by remote microphone probes using the methodology proposed in this paper.

The studied aspect ratio was not chosen to conform with the dimensions given in prior research. The chosen scale and aspect ratio were selected in order to meet the effective parameter defined by Gruber and Howe ($\frac{h}{\lambda} \geq 0.5$) while still allowing enough area for surface microphones to be installed on the serrated edge. Thus, the minimum serration ratio, $\frac{h}{\lambda} = 0.5$, was chosen for this study. The scale of the serration was chosen so that the wavelength was similar to the boundary layer thickness. The authors agree that the chosen aspect ratio is not ideal for trailing edge noise reduction in this facility and further work could improve the design for the wall-jet, but this is beyond the scope of the current paper. The wall-jet differs from a traditional boundary layer in that the inner layer is topped by an outer mixing layer that adds to the low frequency large scale content. This is observed in the spanwise coherence decay length discussed in relation to the new figure and would tend to push an optimal solution towards very large serrations to reduce noise at lower frequencies. In addition to the statements addressing question 2, the following statement has been added to the manuscript to clarify this.

"This aspect ratio was chosen to maximize the number of surface pressure microphones that could be installed on the serrations while still remaining within the effective serration design parameter ($\frac{h}{\lambda} \geq 0.5$) given by Howe (1991b) and Gruber et al. (2011). This design is not optimal for noise reduction and could be improved by using current prediction methods like presented by Lyu et al. (2016), which accounts for the spanwise correlation of pressure fluctuations across the edge. This optimization is beyond the scope of the current work. For the chosen geometry, $\omega h/U_c > 1$ above 250 Hz and 400 Hz for $U_j = 40$ and 60 m/s, respectively. Thus, the expected far field noise reduction is expected at these frequencies, although the effect of the serrations at lower frequencies is still critical to assessing their overall performance and influence on the total trailing edge noise." **(Line 222)**

4. The authors shows a small reduction in the turbulence spanwise correlation length with expected small reduction on the trailing edge noise. However, the literature demonstrates that a well-designed serration could lead to a more significant noise reduction. I am not familiar with the wall-jet facility used in this experiment. Therefore, I don't know if this facility permits noise measurements. However, I recommend the authors demonstrate the noise reduction of the chosen geometry. I also recommend the authors investigate a serration geometry capable to produce a more significant noise reduction such to evaluate the related fluid dynamics effect.

Regarding the placement of this research in relation to the state-of-the-art, I miss some classic papers in the field. For example (to cite few):

* B. Lyu, M. Azarpeyvand and S. Sinayoko, Prediction of noise from serrated trailing edges, Journal of Fluid Mechanics, Volume 793, 2016.
* Arce Leon, C.A., A study on the near-surface flow and acoustic emissions of trailing edge serrations, PhD thesis, 2017 and the papers derived from this PhD thesis.

This research group from TUDelft has performed extensive PIV investigation of the flow on the trailing edge serrations. The proposed paper would largely benefit from its complementary approach if it performed an analysis and comparison of results available in the literature.

We have added some reference to Lyu et al. (2016) to the paper (see response to question 3). The authors agree that it would be interesting to conduct a similar study for an optimized trailing edge serration. This is beyond the scope of the paper, and we hope that the reviewer agrees that even without this optimization the presented results are significant. With the added discussion of spanwise scale (referring to Figure 9), the current manuscript shows some variation in spectral magnitude over the surface of the serration with only modest changes in the coherence spectra for frequencies with spanwise coherence scales that are less than the serration size. These results are particularly important for further advancement of wall pressure models over serrated edges and prediction of the scattered noise.

In conclusion, I recommend the authors, before publication, review the paper methodology and the placement of this research in the big picture of the existing literature in the field. If possible, I recommend the authors include noise measurements and analysis.

We do have measurements of noise, but this greatly expands the scope of the journal paper. Accompanying noise measurements are presented in Letica (2020), so we have added the following statement in the introduction.

“Note that accompanying noise measurements are presented in Letica (2020).” **(Line 118)**

Reviewer #2: This paper presents unsteady surface pressure measurements obtained on a straight and serrated trailing edge. The data presented are very interesting and insightful. Overall, the measurements are high quality and I believe the paper warrants eventual publication subject to addressing the following:

Other than a brief comment in the conclusion, very little connection is made between the surface pressure measurements and trailing edge noise generation. Please incorporate into your discussion of results, what your measurements tell us about the serration noise reduction mechanism.

We have added two additional sections describing the relation to prediction of the performance of serrations in the results section. These sections are given below.

"In general, these observations suggest that predictions of serration performance may not need to consider changes to the coherence of the wall pressure fluctuations. Instead, the magnitude and inhomogeneity of the surface pressure fluctuations over the serration are more significant, since the scattered noise in the far field is directly proportional to the surface pressure spectrum at the edge. However, these results do not address the potential disruption of the serration root on the spanwise coherence." **(Line 356)**

"The coherence across the root increases towards lower frequencies similar to the observation between points on a single serration. Again, this indicates that predictions of serration performance may not need to consider changes particular to the coherence across the root at least for the separation distances considered in this study, $\frac{\Delta x_3}{\lambda} \geq 0.54$." **(Line 376)**

"… and may be a consequence of the streamwise evolution of the near wall flow across the serration. Still, like the spanwise coherence, observed changes in the wall pressure magnitude over the serration are likely to have a greater effect on the serration performance." **(Line 384)**

The measurements are obtained for serrations in the configuration of one-sided flow. This differs from the real case in which flow occurs on both sides of the serrations. Please discuss the implications of this; how is the flow physics expected to differ between configurations of one-sided and two-sided flow and what implication will this have on the interpretation of your results?

We've added to the discussion in the results section, but we also think this is an open question and warrants further examination in future studies. One-sided flows have long been used to evaluate the performance of serrations because of the ease of instrumenting the surface, but there appears to be some difference with two-sided flows. The following has been added to the results section.

"Indeed, in a one-sided flow, a growing free shear layer will develop between the flow and still air on the other side of the serrations. For two-sided flows, the near wake is a function of the boundary layers developed on both sides of the surface. Of course, differences will also exist if there is mean loading on the serration. As observed in prior studies, this loading is responsible for the flow developing in between serrations and the resultant high frequency noise produced at the root (Oerlemans et al. (2009), Gruber et al. (2011), Ragni et al. (2019)). Additionally, Ragni et al. (2019) found that the streamwise decay of the RMS pressure fluctuations on the suction side of the serrations reduced with increasing angle of attack.

These observations and differences between one-sided and two-sided flows warrant further investigation." **(Line 305)**

Additional comments:

Introduction, page 5, after introducing the contribution of your own study, please explain briefly why the surface pressure measurements are useful and what they will be used to tell us about the noise reduction mechanism.

We have added the following text to the introduction.

"Results will aid in the development of methods to assess the performance of serrations by exposing changes to the wall pressure spectrum along the serrated edge." And "For the considered separation distances and serration geometry, it was found that the spanwise coherence across a single serration was elevated at lower frequencies and that the coherence across the root produced no definitive change to the spanwise coherence. More importantly, the measured wall pressure spectra were shown to vary over the serration and were shown to increase from the base to the tip of the serration." **(Line 116)**

Page 4, 10, 11: Incomplete citation Gruber (). – Fixed **(Line 83, 299, and 339)**

Introduction: avoid using he/she when describing the findings of authors. It can be difficult to correctly identify author gender pronouns from their surname. – Fixed **(Line 45, 52, 63, and 88)**

Figure 1, indicate that the region upstream of the serrations is the solid plate/airfoil. - Fixed

Figure 2, please label major features of the wind tunnel on the image. - Fixed

Page 6, please describe the surface pressure microphone calibration procedure and how magnitude and phase corrections were calculated.

The following text has been added.

"The phase and frequency response were determined by comparing the response of each microphone with that of a microphone with known response characteristics. The reference microphone in this case was a B&K 4138 microphone with the factory supplied grid cap. This microphone was individually calibrated prior to each measurement with a B&K 4228 pistonphone calibrator. The microphones were positioned in an anechoic chamber across from a speaker emitting white noise. The output of the white noise signal generator was measured so that the cross-spectrum with each microphone's response could be determined. Each microphone's calibration is calculated as a ratio of the cross-spectrum of its response and the white noise signal to the cross-spectrum of the reference microphone's calibrated response and white noise signal. The phase of the resultant frequency spectrum is the phase calibration and the magnitude is the frequency response." **(Line 166)**

Page 8, line 195 - 198, please explain how the geometrical parameters of the serrations (lambda and 2h) were selected. Was this serration geometry selected based on any relevant flow parameters? Are there

any expected implications of studying this serration geometry (eg. in terms of the expected frequency range of noise reduction)?

Please see response to Reviewer #1 Question 3

Page 8, line 207, please calculate and state the uncertainty (error) in the microphone measurements.

The following statement was added.

"The resultant uncertainty in the microphone data is ±1 dB." **(Line 242)**

Please revise and clarify the following statements:
Page 9, ''The 6.73 mm distance has a coherence up to 0.1 mm greater than 5.69 mm below 200 Hz.'' What do you mean by 0.1 mm greater? – The "mm" was a typo and has been deleted. **(Line 261)**
Page 9, "In general, the coherence measured between the two B&K microphones on the flat plate is near the coherence across the trailing edge for similar separation distance." What do you mean by the coherence is near to? – This has been replaced with "approximately equal to" **(Line 264)**

Page 11, line 274, define "significant measured coherence".

The passage

"The entire range of significant measured coherence corresponds to streamwise hydrodynamic scales on the order of the size of the serration."

was changed to

"Much of the displayed frequency range with measured coherence above 0.05 corresponds to streamwise hydrodynamic scales on the order of the size of the serration." **(Line 325)**

In some results figures (eg Fig 7), the axes tick labels are much smaller than the rest of the figure font. Please try to maintain consistent figure font size and style within in each figure (and ideally across all similar results figures).

We have decreased the font size on Figure 3 and corrected the figure font such that it is now consistent and scales with size of each figure.

The authors have also made a few minor additional changes as listed below to provide further clarification and correct typos.

- Deleted ", that is to say, it is statistically stationary" **(Line 33)**
- Greater than, ">", changed to "≥" in $\frac{h}{\lambda} \geq 0.5$ **(Line 81)**
- Hydrodynamic scales changed to streamwise hydrodynamic scales to clarify in "characteristic streamwise hydrodynamic scales" and "The entire range of significant measured coherence corresponds to streamwise hydrodynamic scales on the order of the size of the serration. For reference, at $U_j = 40$ m/s, dominant streamwise hydrodynamic scales are approximately equal to $L_{x_1} = U_c/f = 0.5h$ at 3 kHz and $5h$ at 300 Hz." Additionally, I added the subscript x_1 to L whenever referring to streamwise scales in the document. **(Line 325)**
- "osbserved" corrected to "observed" **(Line 372)**
- Removed the pronoun "our" from abstract **(Line 16)**
- "were" to "was" in abstract **(Line 19)**
- "From this it …" was changed to "From this conclusion, it …" in introduction **(Line 40)**
- Instances of "a NACA" were changed to "an NACA" on guidance from NASA **(Lines 61 and 303)**
- Removed hyphen in "over-predicted" **(Line 68)**
- "group confirmed" changed to "group also confirmed" **(Line 76)**
- The statement "Additionally, they observed that the reduction in noise was equally sensitive to both h and λ, rather than simply their amplitude." Was clarified to "Additionally, they observed that the reduction in noise was sensitive to both changes in h and λ, but they could not conclude that this relationship was distinct from dependence on the ratio h/λ as suggested by Howe (1991b)." **(Line 78)**
- "similar space" corrected to "similarly spaced" **(Line 87)**
- "suggest" corrected to "suggested" **(Line 104)**
- "in particular" corrected to ", particularly" **(Line 110)**
- "In this" corrected to "In this study" **(Line 112)**
- Comma added after "wall jet flow" **(Line 116)**
- Reduced significant digits on "1206.75" to "1207", "971.55" to "972", "0.794" to "0.8" **(Lines 128, 207, and 208)**
- Added the Danish symbols in the spelling of Bruel and Kjaer and defined B&K **(Line 150)**
- Added a comma after "positioned" **(Line 180)**
- "are" changed to "is" **(Line 185)**
- "50 m/s" corrected to "60 m/s" **(Line 187)**
- Comma added after "Thus" **(Line 191)**
- "full setup described above as mounted " changed to "full setup as mounted" **(Line 209)**
- "this was to" changed to "this was done to" **(Line 214)**
- Comma added after "velocity" **(Line 251)**
- "trend" modified to "trends" **(Line 278)**
- Corrected "the the" to "the" **(Line 283)**
- Comma added after "study" **(Line 341)**
- Comma added after "frequencies" **(Line 349)**

- "similar to the straight trailing edge, with a slight increase toward lower frequencies" clarified to read "similar to the straight trailing edge with differences increasing toward lower frequencies." **(Line 336)**
- "autospectra does not occur at frequencies corresponding to the observed increase in coherence" clarified to "autospectra does not occur at frequencies aligning with the observed increase in coherence at lower frequencies." **(Line 353)**
- "The root appears to have an insignificant effect on the coherence between these points on the serrations." Clarified to "The root appears to have an insignificant effect on the coherence between these points distinct from the observations across a single serration. The coherence is similarly increased at lower frequencies." **(Line 369)**
- Deleted the repetitive sentence "For this single-sided flow, the spanwise coherence of the low frequency large scale structures is not significantly influenced by the serration root." **(Line 376)**
- Comma added after "microphones" in conclusions **(Line 391)**
- "Overall, these results show that this moderately sharp serrated edge, $h/\lambda = 0.5$, in a wall jet does not significantly influence the coherence of hydrodynamic scales on the order of h even considering locations on adjacent serrations." Clarified to explain that the term significance was referring to the observed differences impact on the far field sound. "At low frequencies, the spanwise coherence across the serrated edge displayed a modest increase with a corresponding decrease in the streamwise coherence. Overall, results show that changes to the coherence for this moderately sharp serrated edge, $h/\lambda = 0.5$, for hydrodynamic scales on the order of h, even considering locations on adjacent serrations, are not as significant as changes in the spectral magnitude over the serration." **(Line 392)**
- Deleted "At low frequencies, the spanwise coherence displayed a modest increase between locations on a single serration and a decrease in the streamwise coherence." **(Line 402)**
- Deleted "Even so," **(Line 400)**
- Corrected spelling of "Acknowledgements" to "Acknowledgments" **(Line 406)**
- Added "(All dimensions in mm)" to the caption of Figure 6
- Added "at $U_j = 60$ m/s" to caption of Figure 9 (now Fig. 10)
- Improved resolution of Figure 5
- Changed all instances of "towards" to "toward"
- Added a comma after "suction side" **(Line 375)**
- Added "." at the end of all figure and table captions

Manuscript with Highlights
Click here to access/download;Response to Reviewers Comments;Letica_and_Alexander_JAE (14) with Highlights.pdf

Understanding the Impact of a Serrated Trailing Edge on the Unsteady Hydrodynamic Field

Stefan Letica[1] and W. Nathan Alexander[2]

[1]Research Aerospace Engineer, NASA Langley Research Center, Aeroacoustics Branch (Mail Stop 461), 2 North Dryden St., Building 1208, Rm. 214, Hampton, VA 23681-2199, Email: stefan.j.letica@nasa.gov

[2]Assistant Professor, Kevin T. Crofton Department of Aerospace and Ocean Engineering, Virginia Tech, Randolph Hall, Rm. 215, 460 Old Turner St., Blacksburg, VA 24061-0203, Email: alexande@vt.edu

ABSTRACT

Trailing edge noise is a common noise source in aerodynamic applications. Many prior experiments have shown that trailing edge serrations can reduce this noise, but the mechanism by which serrations reduce noise and their aerodynamic impact near the edge is not fully understood. Previous theoretical models have assumed that the turbulence convecting past a serrated trailing edge is unchanged by the presence of the serrations, but experiments have shown that this is not accurate. This work attempts to further understanding of the unsteady surface pressure fluctuations on sawtooth serrations. Experiments were performed in an anechoic wall jet wind tunnel on an undercut trailing edge with a straight and serrated edge configuration. The magnitude of unsteady surface pressure fluctuations was found to increase near the tips of the serrations for Strouhal numbers near 0.5 based on edge thickness. Spanwise coherence was increased on a single serration, while coherence across the root of adjacent serrations was similar to results across a straight trailing edge at similar spanwise separation distance.

INTRODUCTION

Trailing edge noise is produced when acoustic sources in a turbulent boundary layer are convected past a sharp trailing edge. The sharp trailing edge radiates the sound produced directly by the turbulence to the far field much more efficiently than it would in an otherwise free field environment. From the work of Curle (1955), Ffowcs Williams and Hall (1970) derived an analytical solution for the noise produced by the scattering of turbulent acoustic sources by a semi-infinite half plane with a sharp trailing edge. This method, however, requires highly resolved knowledge of the three-dimensional turbulence field, and a more practical method was desired. This was provided by Amiet (1976), who solved the scattering problem by using the surface pressure generated by the turbulent boundary layer on the plate as the input to an equation that gives the sound radiated to the far field. The turbulence is assumed to be unaffected by the presence of the trailing edge.

The most common method to reduce this noise source is through the use of trailing edge serrations. Howe (1991a) performed a theoretical study of the noise reduction produced by sinusoidal serrations showing that the edge becomes an inefficient scatterer of convected turbulent acoustic sources when it is at an angle of less than 45° to the mean flow. Like Amiet, this analysis assumed that the turbulence was unaffected by the presence of the serrations. Howe concluded that for a sinusoidal serration shape, while the total arc length along the trailing edge is increased, the effective wetted length, or the length of the edge which radiates efficiently, is reduced. From this conclusion, it was logical to assume that further reduction could be obtained by making all edges of the serrations inefficient scatterers by using a sawtooth configuration with sharp tips and roots. Howe (1991b) analyzed this configuration as well, and found that it was indeed much more effective than a sinusoidal configuration. The noise reduction was found to be heavily dependent on the serration geometry, in particular on the ratio h/λ, which is defined in Figure 1. Howe predicted that the expected noise reduction by a sawtooth trailing edge was $10\log_{10}\left(1+(4h/\lambda)^2\right)$ dB. This translates to a reduction of approximately 18 dB for $h/\lambda = 2$ and 30 dB for $h/\lambda = 8$, conditions corresponding to angles of 7.13° and 1.79° between the flow direction and edge, respectively. Additionally, Howe predicted that the sound reduction would only be effective for $\omega h/U_c \gg 1$, for turbulent eddies

smaller than the serration geometry. This leads to the conclusion that the dimensions of serrations should be at least on the order of the boundary layer thickness, δ, as this is on the order of the largest turbulent length scales in a conventional boundary layer. At lower frequencies, Howe predicted that noise would be largely unaffected by the serrations, but high frequency noise reduction would be substantial.

Oerlemans et al. (2009) published an experimental paper showing both that trailing edge noise was the dominant source of wind turbine noise for an observer near the ground and that serrations were an effective mechanism for reducing the overall noise at the considered observer location on the ground in front of the turbine. However, contrary to Howe's prediction, the modified serrated blade actually increased noise at the highest frequencies. Regardless, the overall noise level of the serrated blade was about 3 dB lower than that of the unmodified blade.

Gruber et al. (2011) performed experiments in an open-jet aeroacoustic wind tunnel on an NACA 65(12)-10 cambered airfoil with a series of 0.8 mm-thick serrated trailing edge inserts ranging from $h/\lambda = 0.167$ to 10. They observed that between 400 and 7000 Hz and with the airfoil at an angle of attack of 5°, the serrations were capable of reducing noise by up to 5 dB for an amplitude of $h = 10$ mm and up to 7 dB for an amplitude of $h = 15$ mm. The noise reduction tended to increase as λ became smaller and the serrations became sharper and narrower. Above 8 kHz, the noise was increased for all serration shapes, with a greater noise increase for wider serrations. They found that Howe's theory far overpredicted the amount of potential noise reduction and confirmed the high-frequency noise increase observed by Oerlemans et al. (2009). Nonetheless, an overall reduction in sound level was achieved. The general transition point from noise reduction to noise increase was at the δ-based Strouhal number, $St_\delta = f\delta/U_\infty \sim 1$. They theorized that the cause of the high-frequency noise increase is the rushing of flow between serrations. They confirmed this by releasing smoke on the pressure side of the airfoil and observing its convection past a straight trailing edge and a sawtooth trailing edge. Naturally, this implies that at higher angle of attack, more high-frequency noise will be produced, reducing the effectiveness of the serrations. The group also confirmed Howe's prediction that a serrated trailing edge would be ineffective if the

sawtooth amplitude was smaller than the eddies. Additionally, they observed that the reduction in noise was sensitive to both changes in h and λ, but they could not conclude that this relationship was distinct from dependence on the ratio h/λ as suggested by Howe (1991b). They concluded that the turbulence at the roots and tips of the teeth was largely uncorrelated, and that there were three conditions upon which noise reduction would be dependent: $f\delta/U_\infty < 1$, $h/\lambda \geq 0.5$, and that the serrations are sufficiently narrow as discussed in Howe (1991b).

In the dissertation of Gruber (2012), surface pressure fluctuations are presented for serrations in a one-sided flow. Remote microphone probes were installed on two adjacent serrations, with dimensions $\lambda = 9$ mm and $2h = 30$ mm. The surface pressure coherence for microphone pairs along the edge of the serrations were analyzed as well as spanwise microphone pairs on the same serration. These were compared with similarly spaced microphone pairs in proximity to a straight trailing edge. Gruber observed an increase in the coherence below a frequency dependent on the microphone pair's proximity to the tip of the serration. This was attributed to acoustic backscatter from the serration edges. An edgewise reduction of the coherence up to 15% in the frequency range for which trailing edge noise was reduced was also observed. The coherence reduction along the edge indicates that the correlation length along the edge is decreased contributing to the observed noise reduction.

Moreau and Doolan (2013) performed experiments on sawtooth trailing edge serrations, and measured velocity fluctuations with a hotwire probe in the near-trailing edge wakes. They used a flat plate with two different geometries, $h/\lambda = 5$ and 1.1. The wake measurements showed differences between the serrated geometries and the flat plate. The serrations altered the behavior of the flow field around the trailing edge quite significantly, and the observed noise reduction and increases corresponded directly with changes in the turbulent energy distribution close to the trailing edge. Their narrower serration produced increases in turbulent velocity fluctuations at mid-frequencies for which noise increases were observed. Reductions in the turbulent velocity spectra occurred at frequencies with observed noise reduction. Therefore, they concluded that modifications to the hydrodynamic field were responsible for the acoustic performance of the serrations rather than the

scattering efficiency of the edge geometry. Also, they suggested that disagreement between theory and experiment may be attributed to the assumption that the trailing edge does not modify the turbulence near the trailing edge.

Although there is evidence that serrations modify the structure of the turbulent boundary layer near the trailing edge, current analytical methods do not consider these changes. This is in part due to a lack of experimental data and understanding of these flow modifications. Impact on the surface pressure spectrum near the trailing edge is of interest, particularly since it is the source component used in many calculation procedures. To analyze these effects, a study of wall pressure fluctuations on serrations in an anechoic wall-jet tunnel was completed. In this study, surface pressure fluctuations were measured with embedded microphones on multiple serrations. The objective of this work is to evaluate the variation of the surface pressure spectrum and coherence between points on a single serration and, importantly, between adjacent serrations on an undercut step in a wall jet flow, which has not been directly evaluated previously. Results will aid in the development of methods to assess the performance of serrations by exposing changes to the wall pressure spectrum along the serrated edge. Note that accompanying noise measurements are presented in Letica (2020). For the considered separation distances and serration geometry, it was found that the spanwise coherence across a single serration was elevated at lower frequencies and that the coherence across the root produced no definitive change to the spanwise coherence. More importantly, the measured wall pressure spectra were shown to vary over the serration and were shown to increase from the base to the tip of the serration.

APPARATUS AND INSTRUMENTATION

Virginia Tech Anechoic Wall Jet Facility

All experiments were performed in the Virginia Tech anechoic wall jet wind tunnel shown in Figure 2. In this tunnel, flow exhausts out of a horizontal slit nozzle over a large aluminum plate 3048 mm long and 1524 mm wide. The nozzle measures 12.7 mm high by 1207 mm wide. Details of the design are given by Kleinfelter et al. (2019). The tunnel is designed to produce a quiet, spanwise uniform flow up to a nozzle jet velocity U_j = 70 m/s. A wall jet boundary layer

is different from a conventional boundary layer. In a wall jet flow, there are two primary regions: the inner boundary layer, which forms much like a conventional boundary layer along the plate, and a turbulent mixing layer between the stagnant air in the anechoic chamber and the top of the inner layer. Kleinfelter et al. (2019) show that the wall-jet profile is fully-developed for streamwise positions greater than 0.98 m from the nozzle exit and at all nozzle velocities. These inner and outer layers were shown by Yegna Narayan and Narasimha (1973) to be self-similar when normalized on the local maximum velocity, U_m, and half-height, $y_{1/2}$, which is the height at which the mean velocity in the outer layer is half of U_m. Using the equations of Wygnanski et al. (1992) and the constants for this facility measured by Kleinfelter et al. (2019), estimates of the local boundary layer parameters at the chosen location of the trailing edge location 1.283 m from the nozzle are presented in Table 1. δ is defined as the inner layer thickness from the wall to the height of the maximum velocity U_m. The boundary layer conditions reported in Table 1 were computed based on ambient conditions of 94.3 kPa and 295.2 K. Day to day changes in ambient conditions produced negligible changes in these parameters over the course of the experiment, and thus, they were assumed constant. The coordinate system for which all microphone locations will be defined is shown in Figure 1 where the origin is located at the spanwise center of the edge. The origin is located on the edge for the straight trailing edge and at the serration half height for the serrated configurations.

Surface Pressure Microphones

Two different types of surface pressure microphones were used in this study: Brüel and Kjær (B&K) 1/8" Type 4138 and Knowles FG-23329-P07 microphones. Type 4138 microphones have a wide dynamic range (43-168 dB) and a flat frequency response up to 140 kHz. This makes them ideal reference sensors for calibration and validation of measurements with the cheaper Knowles microphones. For all surface pressure measurements, the Bruel and Kjaer microphones were fitted with 0.5 mm pinhole caps to reduce the effects of spatial averaging. Due to the large outer diameter of the microphones and their cost, the B&K microphones were only used to measure surface pressure fluctuations on the flat plate of the wall jet for comparison with the Knowles microphones.

The Knowles FG-23329-P07 microphones were chosen for their small size, relatively flat response (up to 10 kHz), and low cost. They have a pinhole diameter of 0.8 mm and an outer diameter of 3 mm. These microphones were used for all surface pressure measurements along the straight and serrated trailing edges and were mounted flush with the surrounding surface. The microphones were wired in two groups of 10 with power and output signals arranged through a single supply box.

The Knowles and 1/8" B&K microphones were used for both power spectral density and coherence measurements, and thus needed to be calibrated for both frequency response and phase response. The phase and frequency response were determined by comparing the response of each microphone with that of a microphone with known response characteristics. The reference microphone in this case was a B&K 4138 microphone with the factory supplied grid cap. This microphone was individually calibrated prior to each measurement with a B&K 4228 pistonphone calibrator. The microphones were positioned in an anechoic chamber across from a speaker emitting white noise. The output of the white noise signal generator was measured so that the cross-spectrum with each microphone's response could be determined. Each microphone's calibration is calculated as a ratio of the cross-spectrum of its response and the white noise signal to the cross-spectrum of the reference microphone's calibrated response and white noise signal. The phase of the resultant frequency spectrum is the phase calibration and the magnitude is the frequency response. To ensure the quality of the data from the Knowles microphone was adequate, surface pressure measurements were completed on the flat plate of the wall jet at the approximate streamwise location that the trailing edge models would be located with both the B&K microphones employing the pinhole caps and a Knowles microphone. The Knowles microphone was mounted at the exact distance from the nozzle that the trailing edge would be positioned, and the two B&K microphones were mounted flush in a streamwise configuration and then in a spanwise configuration. All microphones were spaced 6.15 mm apart center to center. The tunnel was run at all nozzle exit speeds listed in Table 1, and the spectra and coherence between microphones were compared. Frequencies at which the Knowles response deviated from the B&K response were used to define the response limits of

Knowles microphones. An example of these results is shown in Figure 3.

At low jet speeds, $U_j = 20$ m/s, the high frequency noise floor is apparent in the spectra for both the Knowles and B&K microphones. At high speeds, $U_j = 60$ m/s, the Knowles microphone reached the upper limit of its dynamic range. This attenuated the low frequency response but had little effect at high frequency. The low frequency impact is more noticeable in the coherence. The observed attenuation at high frequency is attributed to the larger pinhole size of the Knowles microphones compared to the B&Ks. Thus, upper and lower limits were defined for which the data were deemed an acceptable representation of the spectra and coherence at each speed. Table 2 shows the valid frequency range for which data will be presented at each speed.

Trailing Edges

Two trailing edges were used in this study: a straight edge and serrated edge. Both take the form of an undercut step in which the trailing edge model rests atop the original wall jet plate. The top surface of the edge is located 12.7 mm above the original wall of the facility. To ensure a smooth flow transition from the wall jet to the top of the trailing edge surfaces, an aluminum ramp with a gradual curve was placed upstream of the edge. The upstream portion of this ramp was sealed to the wall jet plate using aluminum foil tape to ensure a smooth transition from the plate to the ramp. Millican (2017) used this same ramp configuration and showed that the ramp had a minimal effect on the flow speed, increasing U_m by up to 1% at the edge compared to the flat unmodified plate.

Straight Trailing Edge

The straight trailing edge used in this work is the same edge used by Millican (2017). It was designed to sit on top of the solid plate of the wall jet, creating a one-sided flow across the edge. This edge was manufactured in two pieces due to machining limitations and is milled from solid aluminum. The total span of the two pieces when assembled is 972 mm. The trailing edge itself has a thickness of 0.8 mm. All sharp corners outside of the 972 mm span were smoothed using 3D printed edge-rounding transitions. Figure 4 shows the full setup as mounted in the wall jet tunnel. Figure 5a shows the profile of the trailing edge geometry.

The Knowles microphones were mounted in a spanwise array flush with the surface of the

trailing edge 3 mm upstream of the edge. The microphones were held in place with adhesive on the underside of the edge. The microphones were distributed irregularly along the x_3 axis; this was done to construct a wavenumber filter to reject high-order spanwise wavenumbers (Letica (2020)). The spanwise locations of the surface pressure microphones across the straight trailing edge are listed in Table 3.

Serrated Trailing Edge

The serrated trailing edge was designed similarly to the straight trailing edge with the same edge height above the plate, 12.7 mm. It was also installed similarly centered across the span of the wall jet. The serrated trailing edge was fabricated by 3D printing the model in two spanwise sections each 457.2 mm in length. The serrations have a wavelength $\lambda = 1.5$ cm and an amplitude $2h = 1.5$ cm. This aspect ratio was chosen to maximize the number of surface pressure microphones that could be installed on the serrations while still remaining within the effective serration design parameter ($h/\lambda \geq 0.5$) given by Howe (1991b) and Gruber et al. (2011). This design is not optimal for noise reduction and could be improved by using current prediction methods like presented by Lyu et al. (2016), which accounts for the spanwise correlation of pressure fluctuations across the edge. This optimization is beyond the scope of the current work. For the chosen geometry, $\omega h/U_c >$ 1 above 250 Hz and 400 Hz for $U_j =$ 40 and 60 m/s, respectively. Thus, the expected far field noise reduction is expected at these frequencies, although the effect of the serrations at lower frequencies is still critical to assessing their overall performance and influence on the total trailing edge noise. Figure 5b shows the side profile of the serrated trailing edge.

There are a total of 60 serrations across the trailing edge, 30 on each piece. 18 microphones were mounted in the serrated edge, but only 15 microphones were found to work after installation. Only these microphones will be referred to in this work. The locations of these holes and their reference numbers are shown in Figure 6. The locations of the surface pressure microphones on the serrated edge are listed in Table 4.

Data Processing

Microphone data were sampled for 32 seconds at 65536 Hz, well above the Nyquist frequency for the presented range (20-20000 Hz). To reduce uncertainty, all microphone time series were divided into records of length $N = 8192$ and processed with 50% overlap. This gives a frequency resolution of 8 Hz for the spectral data and 511 averages per run. Hanning windows were applied to each record to reduce spectral leakage. The resultant uncertainty in the microphone data is ± 1 dB.

RESULTS

The single-point spectra of each of the individual surface pressure microphones across the straight trailing edge are shown in Figure 7. The maximum spanwise difference across the edge is approximately 3 dB within the frequency ranges defined in Table 2 for each speed. This confirms the two-dimensionality of the flow at the trailing edge location. The wall pressure spectra are increased relative to the flat plate at high frequency, as much as 7 dB for the 40 m/s case, but remain similar to the flat plate at lower frequencies. The frequency at which the spectra along the edge rise above the flat plate spectrum increases with flow velocity, approximately 180 Hz, 450 Hz, and 1000 Hz for $U_j = 20$, 40, and 60 m/s, respectively.

The coherence was observed to increase with velocity, but the limitations of the Knowles microphones shown in Table 2 severely reduced the frequency range of useful data at the highest velocity. Therefore, coherence data will only be presented at the $U_j = 40$ m/s condition. Figure 8 shows the coherence between microphone pairs for different spanwise separation distances. The coherence drops off quickly with frequency for all measured separation distances such that there is minimal spanwise coherence measured at frequencies greater than 1 kHz for separation distances greater than 3.05 mm. The coherence drops monotonically with increasing spanwise separation except for the 5.69 mm and 6.73 mm cases. The 6.73 mm distance has a coherence up to 0.1 greater than 5.69 mm below 200 Hz. The cause of this discrepancy is unknown but may be a function of small differences across the edge as different microphones were used for each separation pairing. In general, the coherence measured between the two B&K microphones on the flat plate

is approximately equal to the coherence across the trailing edge for similar separation distance.

The spanwise coherence length can be calculated as a function of frequency by fitting an exponential curve across coherence spectra from microphone pairs along the straight trailing edge. This relation is expressed in Eq. 1:

$$\gamma^2 = e^{-2|\Delta x_3|/L_{x_3}(f)} \tag{1}$$

$L_{x_3}(f)$ is the coherence length, Δx_3 is the separation distance between pairs of microphones, and γ^2 is the coherence. $L_{x_3}(f)$ was found through a least squares regression using the coherence spectra between all microphone pairs at each frequency. The results are shown in Figure 9 for U_j = 20, 40, and 60 m/s. The spanwise scale decreases with increasing frequency. Again, the valid frequency range of data at U_j = 60 m/s is limited, but for U_j = 40 m/s, the spanwise scale is shown to be smaller than the wavelength of the serrations to be applied for frequencies above 190 Hz.

Surface pressure spectra measured at streamwise locations near the base and tip of a serration are compared in Figure 10 for U_j = 60 m/s. There are five similar streamwise x_1 positions each with multiple microphones that can be used for comparison. The five groups contain microphones 1-4-9, 3-5, 10-12, 2-6-7-8, and 14-15. The streamwise trends observed in all spectra and at all jet velocities are well-represented by this comparison of the spectra measured by microphones 9 (at the tip) and 8 (near the base). The average autospectrum from the straight trailing edge is shown as well. A broadband hump appears closest to the tip, between 300 Hz and 1500 Hz. The frequency of this hump reduces with decreasing velocity but peaks near a Strouhal number of St = 0.05 based on trailing edge thickness or 0.31 based on the distance from the trailing edge to the flat plate of the wall jet at all velocities. Neither is consistent with the typical value expected for vortex shedding from blunt airfoils or backsteps. At U_j = 60 m/s, this peak is approximately 3 dB above the measurement at the base. Above 1 kHz, the spectra are both below the straight edge surface pressure spectra by as much as 3 dB before converging and rolling off at frequencies above 6.3 kHz.

These autospectra at all positions can be combined to produce contours of the magnitude of the

pressure fluctuations at specific frequencies. The surface pressure field at frequencies corresponding to characteristic streamwise hydrodynamic scales of $2h$, $3h$, $4h$, and $6h$ (1.5, 2.25, 3, 4.5 cm) are shown at 60 m/s in Figure 11. These scales were computed using the measured convection velocities $L_{x_1} = U_c/f$ and are within the frequency range described by Gruber et al. (2011) for the serrations to be effective at reducing noise. The convection velocity was determined from the cross spectrum of the streamwise flat plate measurements. Measurements at similar serration relative locations were averaged in order to reduce uncertainty further, and two-dimensional linear interpolation was used to determine the pressure at points between measurement locations. These figures show that the magnitude of the fluctuations increases over 2 dB at $L_{x_1} = 3h$ and $4h$, and just over 1 dB at $L_{x_1} = 2h$ and $6h$, from the root to the tip of the interpolated region. The trend observed here agrees with the measurements of Gruber (2012) and Chong and Vathylakis (2015), who observed this trend using remote microphone probes in a one-sided flow. However, it contrasts with the results of Avallone et al. (2018) and Ragni et al. (2019), who observed the pressure fluctuations decreasing in magnitude along serrations by about 3 dB. These experiments were performed on an NACA 0018 airfoil with two-sided flow, and used CFD and tomographic PIV to obtain their surface pressure data. The dissimilarity of these configurations and measurement methods may be responsible for the observed differences. Indeed, in a one-sided flow, a growing free shear layer will develop between the flow and still air on the other side of the serrations. For two-sided flows, the near wake is a function of the boundary layers developed on both sides of the surface. Of course, differences will also exist if there is mean loading on the serration. As observed in prior studies, this loading is responsible for the flow developing in between serrations and the resultant high frequency noise produced at the root (Oerlemans et al. (2009), Gruber et al. (2011), Ragni et al. (2019)). Additionally, Ragni et al. (2019) found that the streamwise decay of the RMS pressure fluctuations on the suction side of the serrations reduced with increasing angle of attack. These observations and differences between one-sided and two-sided flows warrant further investigation. Outside of the presented range of hydrodynamic scales, the fluctuations over the interpolated region do not vary more than the measurement uncertainty of the microphones.

The coherence across a single serration and between adjacent serrations was calculated and compared to the coherence of microphone pairs with similar separation distance along the straight trailing edge. Only 40 m/s data will be presented in the remainder of the paper as this condition produced significant coherence over the widest range within the acceptable response of the microphones. Figure 12a shows the measured coherence between microphones 14 and 15, at the center of the serration and toward the edge at the same x_1 location and separated by $\Delta x_3 = 3.40$ mm. These data are compared with the same measurements taken from the straight trailing edge for separation distances of $\Delta x_3 = 3.05$ mm and 5.69 mm. The coherence between the center and side of the serrations is up to 0.1 greater compared to the measured coherence across the straight trailing edge for frequencies below 550 Hz. Much of the displayed frequency range with measured coherence above 0.05 corresponds to streamwise hydrodynamic scales on the order of the size of the serration. For reference, at $U_j = 40$ m/s, dominant streamwise hydrodynamic scales are approximately equal to $L_{x_1} = U_c/f = 0.5h$ at 3 kHz and $5h$ at 300 Hz.

The coherence was examined for locations symmetrically across the serration centerline as well. The coherence between microphone pairs 3-5, 10-12, and 2-6 are plotted in Figure 12b, along with the coherence across the straight trailing edge. The difference between the 3.42 mm and 4.78 mm separation begins to increase above 300 Hz. The center-to-edge coherence measured near the base of the serration shown in Figure 12a is slightly greater than the similar separation distance between the microphone pair 3-5 by up to 0.1. In general, the spanwise coherence at all locations across the serration is similar to the straight trailing edge with differences increasing toward lower frequencies. The 3.42 mm coherence stays within 0.1 of the 3.05 mm straight trailing edge coherence. The 4.78 mm separation is the same as the 3.05 mm straight edge result below 300 Hz, and the 6.83 mm separation increases above the 6.73 straight edge result by up to 0.1 below 250 Hz. The large increase in coherence near the tip shown by Gruber (2012) attributed to acoustic backscatter from the edge is not observed in this case. This may be due to the relative narrowness of the serration geometry in Gruber's study, which had a serration height to wavelength ratio $h/\lambda = 1.7$ compared to 0.5 in the present work. Brooks and Hodgson (1981) suggest that

microphones be placed at least half a hydrodynamic wavelength from the edge in order for the scattered pressure to be insignificant. The microphones embedded in the serrations are within this range for all frequencies below 2 kHz and 3 kHz for U_j = 40 m/s and 60 m/s, respectively. The expected nearfield scattering effects include increases in the surface pressure spectra and coherence spectra that grow in significance with proximity to the edge. The surface pressure spectrum shown in Figure 10 does not appear to be significantly increased relative to the straight edge at the lowest measured frequencies, and the spanwise coherence does not differ between points at the base and root of the serration. Therefore, the proximity of the microphones to the additional wetted edge length along the serrations compared to the straight edge does not appear to have a significant effect on the results. Additionally, the spectral hump observed near the tip of the serration in the autospectra does not occur at frequencies aligning with the observed increase in coherence at lower frequencies. Nevertheless, even if nearfield scattering effects are significant, the relative variation in the surface pressure spectrum relative to the straight edge and across serrations can still be ascertained through direct comparison. In general, these observations suggest that predictions of serration performance may not need to consider changes to the coherence of the wall pressure fluctuations. Instead, the magnitude and inhomogeneity of the surface pressure fluctuations over the serration are more significant, since the scattered noise in the far field is directly proportional to the surface pressure spectrum at the edge. However, these results do not address the potential disruption of the serration root on the spanwise coherence.

The effect of the serration roots on the spanwise coherence between serrations is of particular interest as the influence of the mixing between serrations is still not well understood. The coherence between microphone pairs 6-7 and 1-4, corresponding to cross-root distances of 8.16 mm and 15.05 mm (the serration length scale), is compared to coherence across the straight trailing edge at separation distances of 9.40 mm and 15.09 mm in Figure 12c. Microphones 1 and 4 are located at the tip of two adjacent serrations, while microphones 6 and 7 are located on either side of the root. The root appears to have an insignificant effect on the coherence between these points distinct from the observations across a single serration. The coherence is similarly increased at

lower frequencies. The experiments of Gruber et al. (2011) show small jets channelled through the roots that were responsible for the increased high-frequency noise in serrated configurations. This increased high frequency noise was not observed in far field measurements made in the present configuration (Letica (2020)), but this may be due to a difference in experimental configuration. Gruber et al. (2011) considered a lifting airfoil with boundary layers on both the pressure and suction side, which may have promoted the formation of these jets. Note that the results presented in Figure 12c differ from those in Letica (2020) due to an error in that analysis. The coherence across the root increases toward lower frequencies similar to the observation between points on a single serration. Again, this indicates that predictions of serration performance may not need to consider changes particular to the coherence across the root at least for the separation distances considered in this study, $\Delta x_3/\lambda \geq 0.54$.

Finally, microphone pair 8-9, with a streamwise separation distance of $\Delta x_1 = 7.00$ mm, was used to examine the coherence along the centerline of the serration, Figure 12d. The result of the streamwise coherence measured on the flat plate is shown for reference. At low frequencies, below 300 Hz, the coherence along the serration is slightly lower than that of the flat plate and may be a consequence of the streamwise evolution of the near wall flow across the serration. Still, like the spanwise coherence, observed changes in the wall pressure magnitude over the serration are likely to have a greater effect on the serration performance. At higher frequencies, above 700 Hz, a modest increase is observed.

CONCLUSIONS

In this work, the unsteady surface pressure on a straight and serrated edge was examined. The surface pressure was measured by embedded microphones, which were flush with the surface in both edges. At low frequencies, the spanwise coherence across the serrated edge displayed a modest increase with a corresponding decrease in the streamwise coherence. Overall, results show that changes to the coherence for this moderately sharp serrated edge, $h/\lambda = 0.5$, for hydrodynamic scales on the order of h, even considering locations on adjacent serrations, are not as significant as changes in the spectral magnitude over the serration. The theory of Amiet (1976) shows that

trailing edge noise is proportional to the spanwise length scale. The spanwise length scale itself is a function of the spanwise coherence such that a 20% reduction in coherence amounts to only a 0.5 dB reduction in far field noise. Thus, larger reductions in coherence are necessary for significant noise reduction. The surface pressure is modified by the serrated edge with respect to the straight edge or flat plate. In particular, spectral magnitudes increased toward the tip of the serration for frequencies near a Strouhal number of 0.05 based on edge thickness.

DATA AVAILABILITY STATEMENT

Some or all data, models, or code that support the findings of this study are available from the corresponding author upon reasonable request.

ACKNOWLEDGMENTS

The authors would like to thank Drs. Matthew Szoke (Virginia Tech) and Lorna Ayton (University of Cambridge) for their collaborative discussions.

REFERENCES

Amiet, R. K. (1976). "Noise due to turbulent flow past a trailing edge." *Journal of Sound and Vibration*, 47(3), 387–393.

Avallone, F., Van Der Velden, W. C., Ragni, D., and Casalino, D. (2018). "Noise reduction mechanisms of sawtooth and combed-sawtooth trailing-edge serrations." *Journal of Fluid Mechanics*, 848, 560–591.

Brooks, T. F. and Hodgson, T. H. (1981). "Trailing edge noise prediction from measured surface pressures." *J. Sound & Vib.*, 78(1), 69–117.

Chong, T. P. and Vathylakis, A. (2015). "On the aeroacoustic and flow structures developed on a flat plate with a serrated sawtooth trailing edge." *Journal of Sound and Vibration*, 354, 65–90.

Curle, N. (1955). "The influence of solid boundaries upon aerodynamic sound." *Proceedings of the Royal Society of London. Series A. Mathematical and Physical Sciences*, 231(1187), 505–514.

Ffowcs Williams, J. E. and Hall, L. H. (1970). "Aerodynamic sound generation by turbulent flow in the vicinity of a scattering half plane." *Journal of Fluid Mechanics*, 40(4), 657–670.

Gruber, M. (2012). "Airfoil noise reduction by edge treatments." Ph.d. thesis, University of Southampton, Southampton, UK.

Gruber, M., Joseph, P. F., and Chong, T. P. (2011). "On the mechanisms of serrated airfoil trailing edge noise reduction." *17th AIAA/CEAS Aeroacoustics Conference*, AIAA 2011-2781.

Howe, M. S. (1991a). "Aerodynamic noise of a serrated trailing edge." *Journal of Fluids and Structures*, 5(1), 33–45.

Howe, M. S. (1991b). "Noise produced by a sawtooth trailing edge." *Journal of the Acoustical Society of America*, 90(1), 482–487.

Kleinfelter, A., Repasky, R., Hari, N., Letica, S., Vishwanathan, V., Organski, L., Schwaner, J., Alexander, W. N., and Devenport, W. (2019). "Development and calibration of a new anechoic wall jet wind tunnel." *AIAA Scitech 2019 Forum*, AIAA 2019-1936.

Letica, S. J. (2020). "Understanding the Impact of a Serrated Trailing Edge on the Unsteady Hydrodynamic Field." Master's thesis, Virginia Polytechnic Institute and State University, Blacksburg, VA, <https://vtechworks.lib.vt.edu/handle/10919/99965>.

Lyu, B., Azarpeyvand, M., and Sinayoko, S. (2016). "Prediction of noise from serrated trailing edges." *Journal of Fluid Mechanics*, 793, 556–588.

Millican, A. J. (2017). "Bio-Inspired Trailing Edge Noise Control: Acoustic and Flow Measurements." Master's thesis, Virginia Polytechnic Institute and State University, Blacksburg, VA, <https://vtechworks.lib.vt.edu/handle/10919/78376>.

Moreau, D. J. and Doolan, C. J. (2013). "Noise-reduction mechanism of a flat-plate serrated trailing edge." *AIAA Journal*, 51(10), 2513–2522.

Oerlemans, S., Fisher, M., Maeder, T., and Kögler, K. (2009). "Reduction of wind turbine noise using optimized airfoils and trailing-edge serrations." *AIAA Journal*, 47(6), 1470–1481.

Ragni, D., Avallone, F., van der Velden, W. C., and Casalino, D. (2019). "Measurements of near-wall pressure fluctuations for trailing-edge serrations and slits." *Experiments in Fluids*, 60(1), 1–22.

Wygnanski, I., Katz, Y., and Horev, E. (1992). "On the applicability of various scaling laws to the

turbulent wall jet." *Journal of Fluid Mechanics*, 234, 669–690.

Yegna Narayan, K. and Narasimha, R. (1973). "Parametric analysis of turbulent wall jets." *Aeronautical Quarterly*, 24(3), 207–218.

List of Tables

TABLE 1. Boundary layer parameters.

U_j (m/s)	U_m (m/s)	δ (mm)
20	6.343	16.04
40	13.25	14.42
60	20.40	13.55

TABLE 2. Validated frequency ranges of Knowles microphones.

U_j (m/s)	Autospectra	Coherence
20	$f \leq 5.5$ kHz	$f \geq 24$ Hz
40	$f \leq 16.5$ kHz	$f \geq 96$ Hz
60	$f \geq 176$ Hz	$f \geq 560$ Hz

TABLE 3. Spanwise microphone locations for the straight trailing edge.

Mic	x_3 (mm)	Mic	x_3 (mm)	Mic	x_3 (mm)	Mic	x_3 (mm)
1	304.8	5	39.40	9	-8.509	13	-50.90
2	182.8	6	23.60	10	-11.56	14	-84.91
3	109.6	7	14.20	11	-18.29	15	-141.5
4	65.71	8	8.509	12	-30.50	16	-236.0

TABLE 4. Serrated trailing edge surface pressure microphone locations.

Mic	x_1, mm	x_3, mm
1	1.26	97.45
2	-5.66	85.88
3	-2.20	84.12
4	1.31	82.40
5	-2.21	80.70
6	-5.70	79.05
7	-5.72	70.89
8	-5.75	22.42
9	1.25	22.32
10	-4.11	-20.15
11	-0.53	-23.10
12	-4.13	-24.93
13	-10.19	-29.99
14	-6.01	-67.44
15	-5.99	-70.86

List of Figures

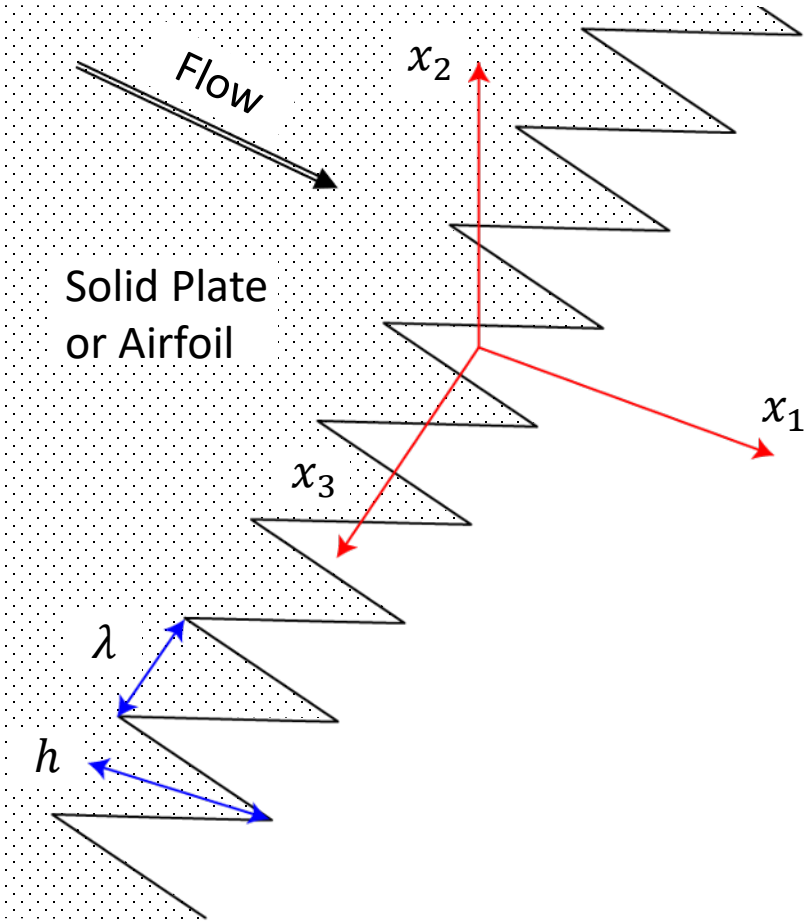

Fig. 1. Geometry and coordinate system of serrated trailing edge.

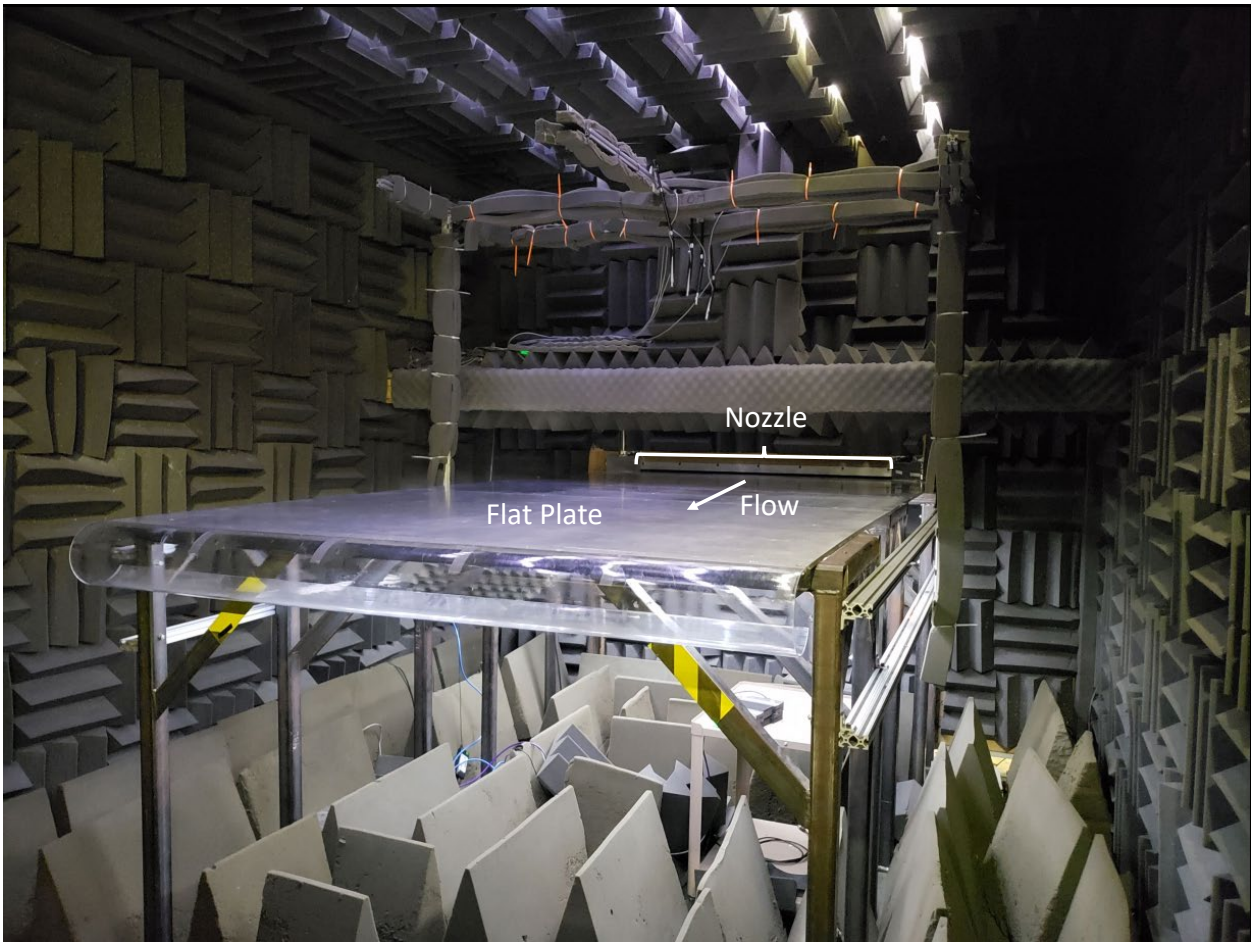

Fig. 2. Virginia Tech Anechoic Wall Jet Facility.

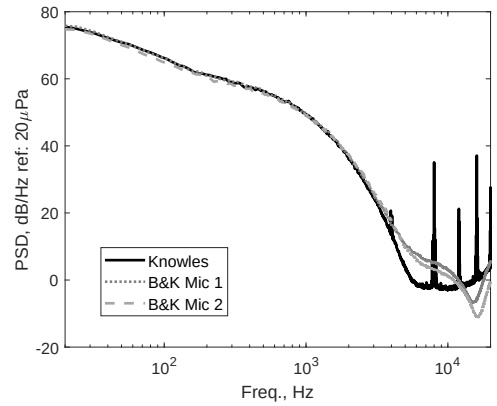

(a) $U_j = 20$ m/s

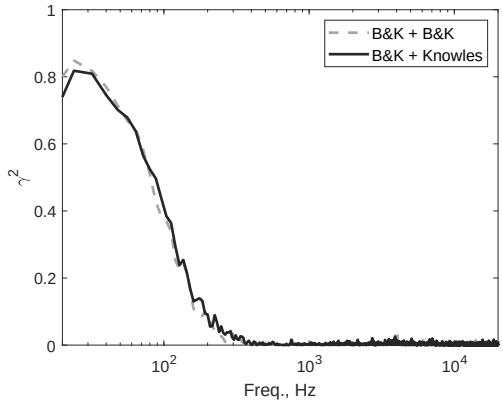

(b) $U_j = 20$ m/s

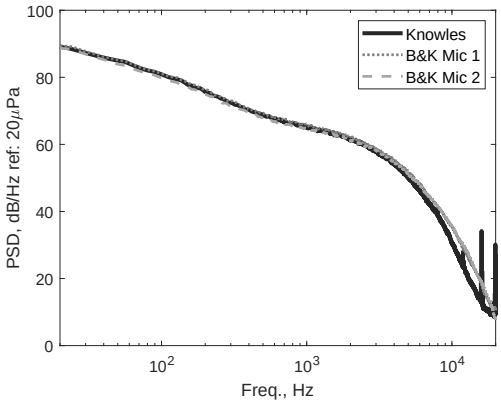

(c) $U_j = 40$ m/s

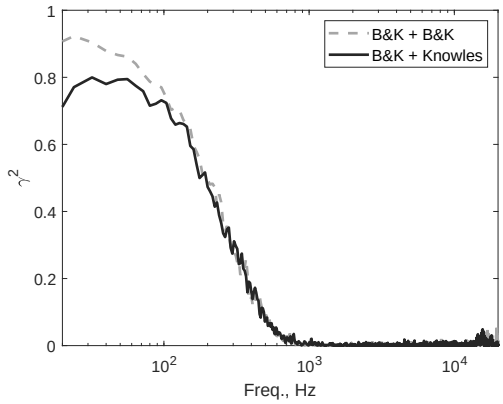

(d) $U_j = 40$ m/s

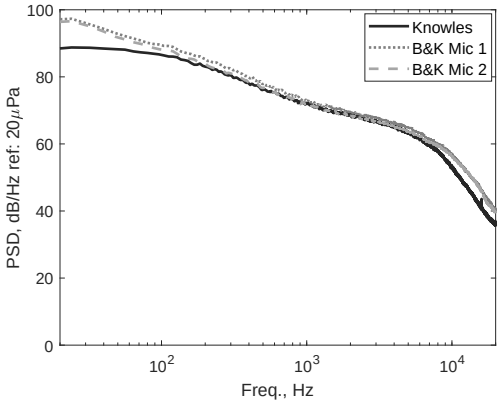

(e) $U_j = 60$ m/s

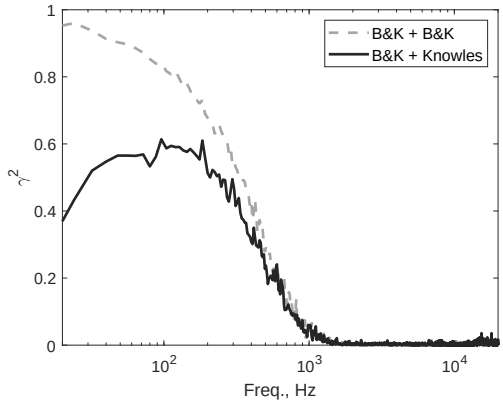

(f) $U_j = 60$ m/s

Fig. 3. Comparison of autospectra and coherence measured by Knowles and B&K microphones in the spanwise orientation on the flat plate.

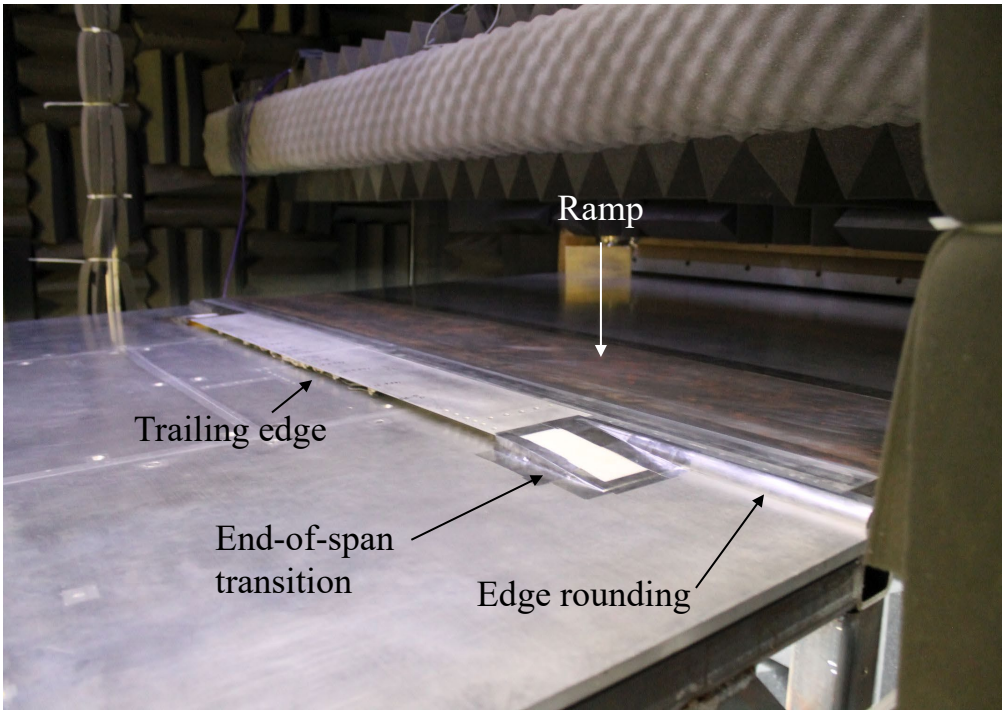

Fig. 4. Straight trailing edge in wall jet.

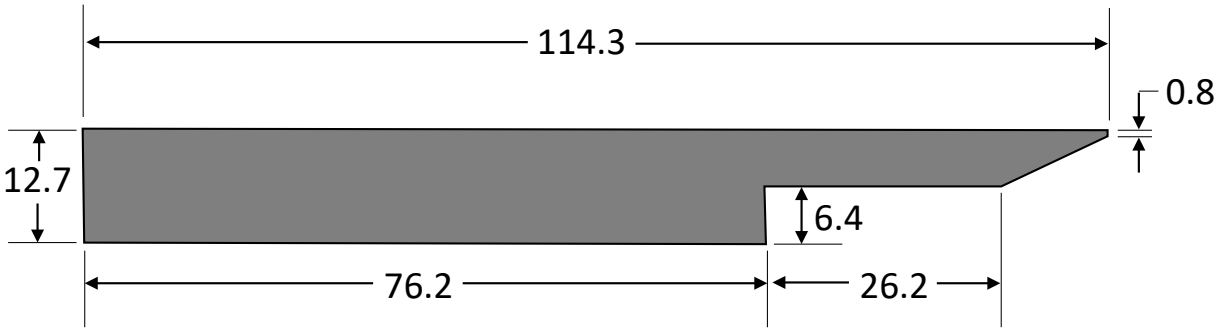

(a) Straight trailing edge

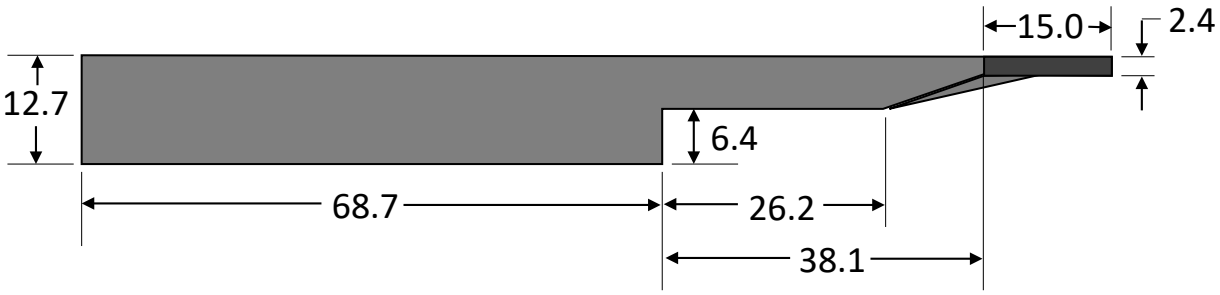

(b) Serrated trailing edge

Fig. 5. Profile geometry (all dimensions in mm).

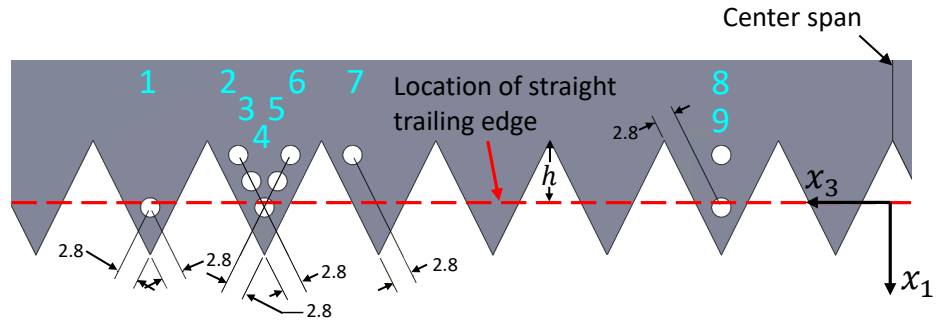

(a)

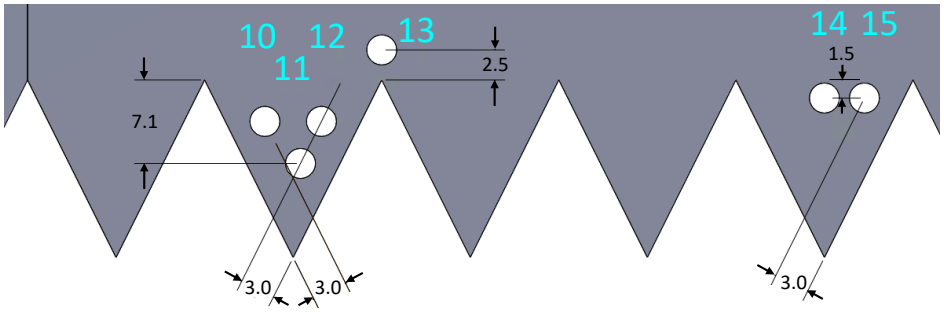

(b)

Fig. 6. Locations of microphone holes in the serrated trailing edge (all dimensions in mm).

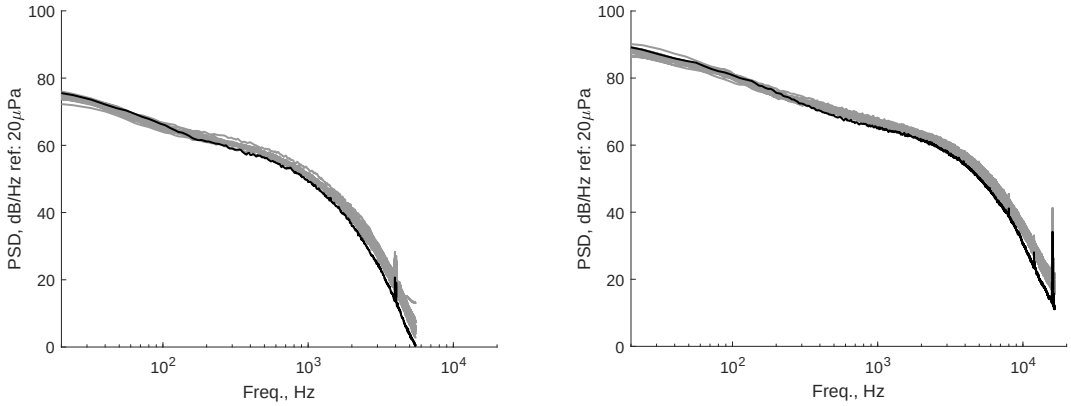

(a) $U_j = 20$ m/s

(b) $U_j = 40$ m/s

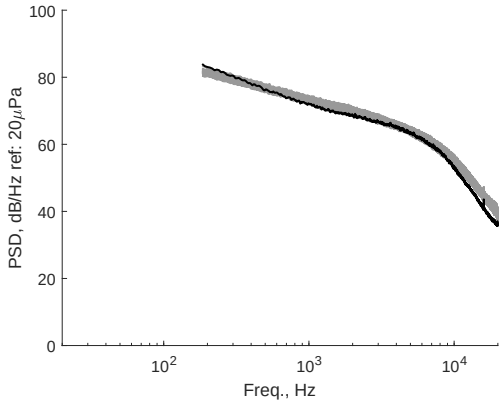

(c) $U_j = 60$ m/s

Fig. 7. Surface pressure along straight trailing edge (grey lines) compared to flat plate wall pressure spectrum (black).

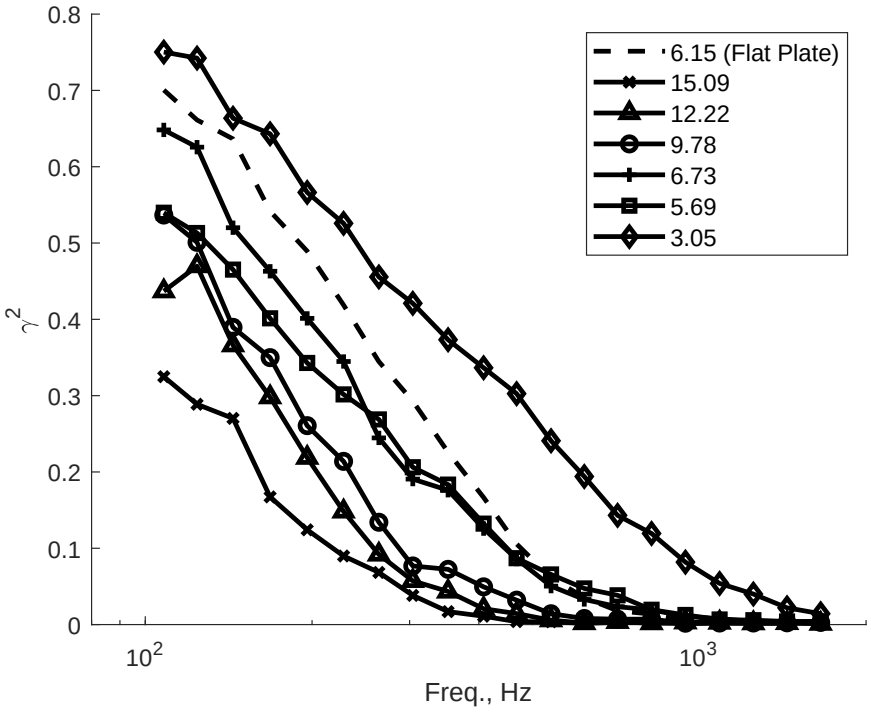

Fig. 8. Coherence of surface pressure along straight edge at U_j = 40 m/s compared to spanwise coherence on the flat plate.

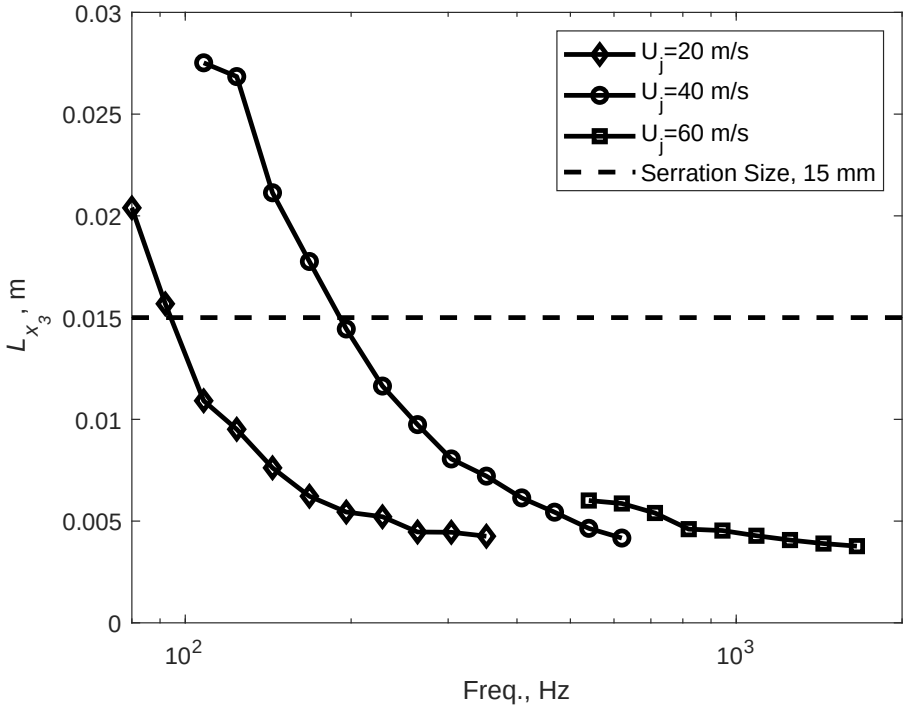

Fig. 9. Spanwise coherence length along the straight trailing edge.

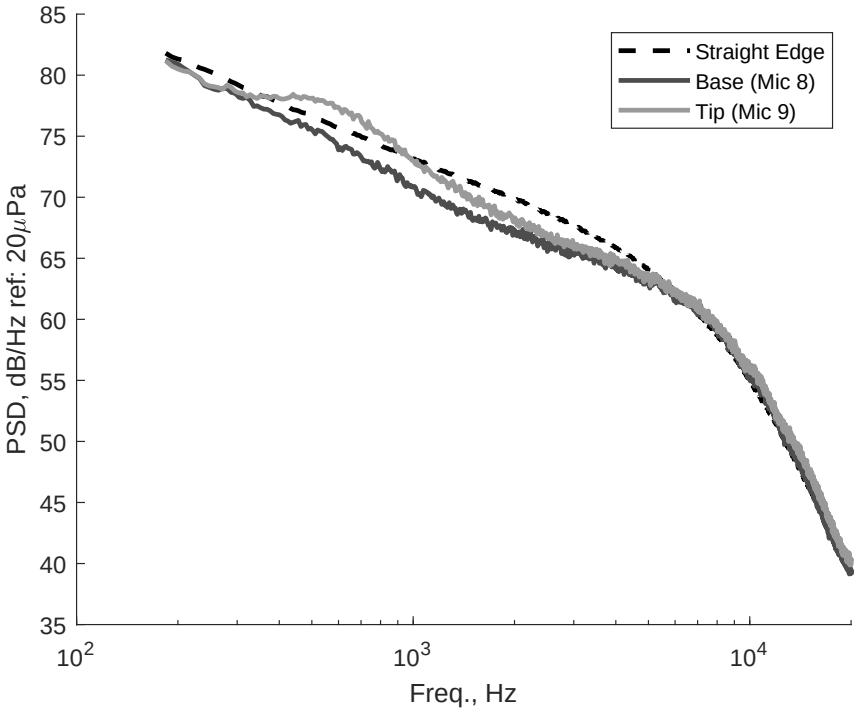

Fig. 10. Surface spectra at the base and tip of a serration compared to a straight trailing edge at $U_j = 60$ m/s.

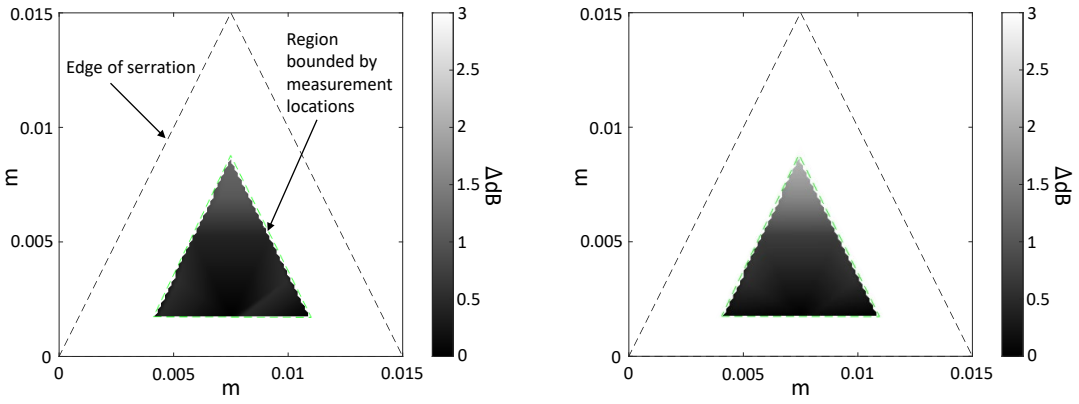

(a) $L_{x_1} = 2h$, 1210 Hz

(b) $L_{x_1} = 3h$, 807 Hz

(c) $L_{x_1} = 4h$, 605 Hz

(d) $L_{x_1} = 6h$, 403 Hz

Fig. 11. Contours of variation in surface pressure fluctuations across serrations at $U_j = 60$ m/s.

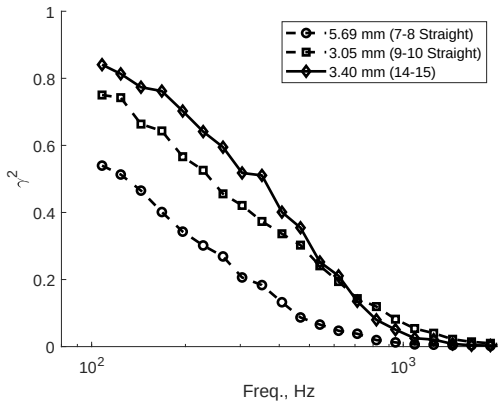

(a) Spanwise coherence between center and edge

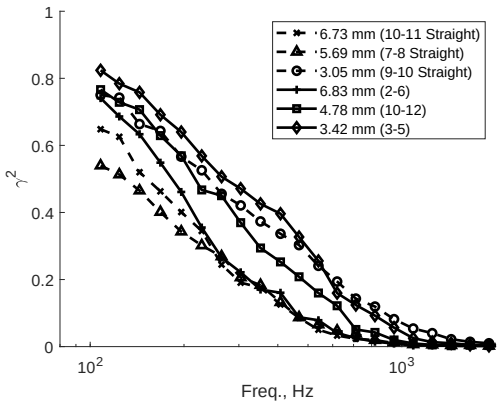

(b) Spanwise coherence across centerline

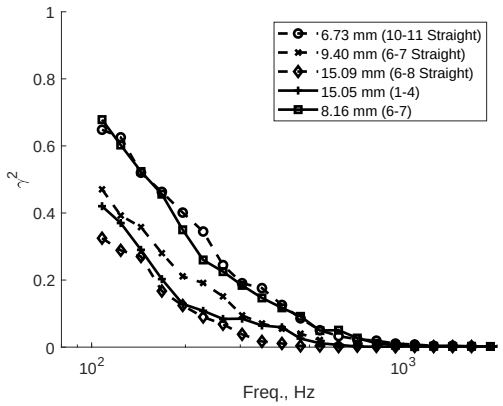

(c) Spanwise coherence across root

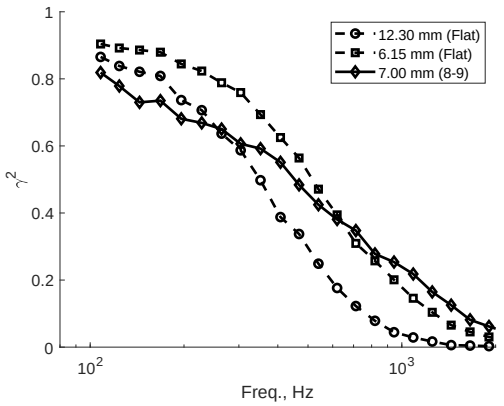

(d) Streamwise coherence along centerline

Fig. 12. Coherence between locations along the serrated edge at $U_j = 40$ m/s.